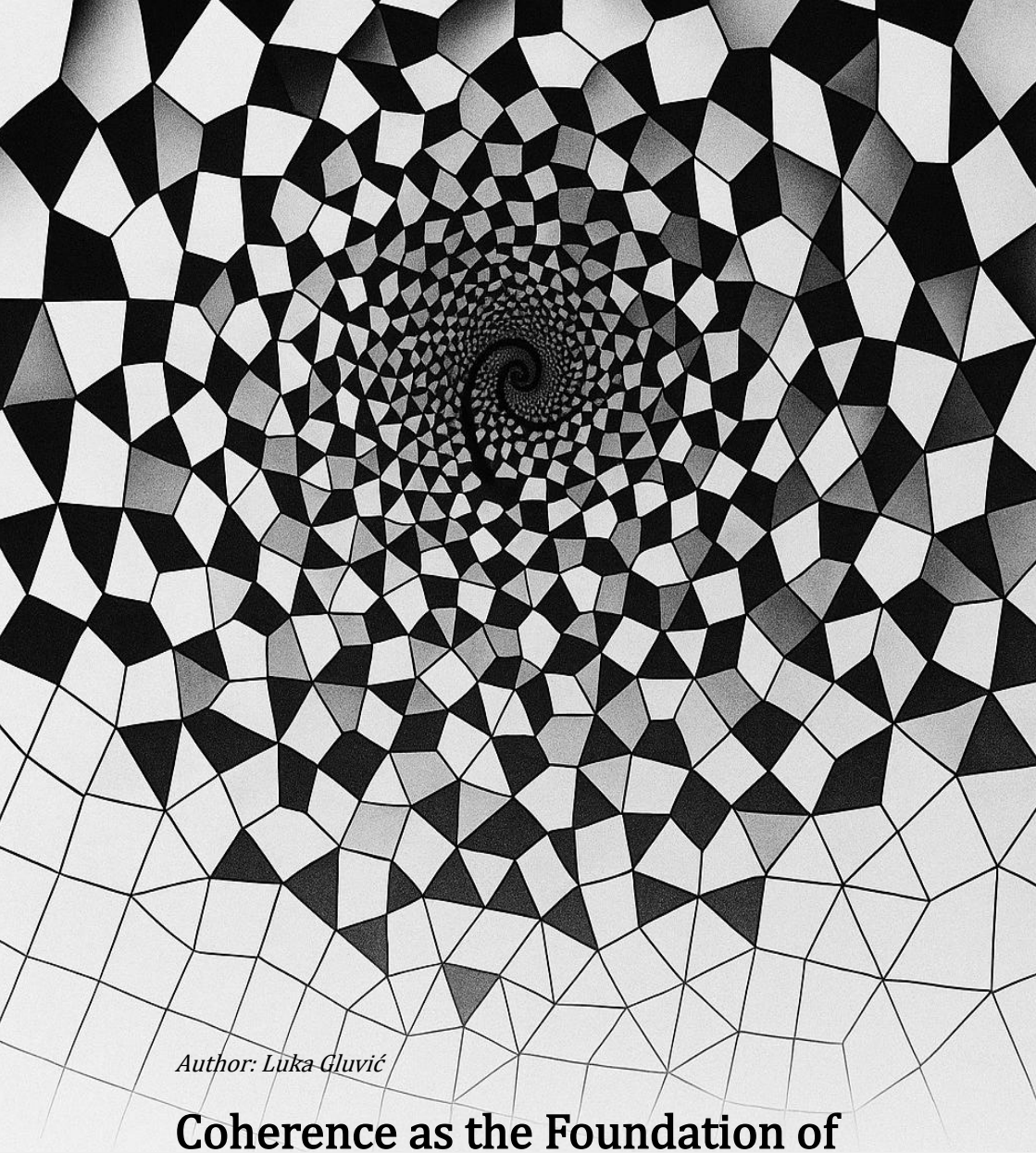

Author: Luka Gluvić

Coherence as the Foundation of Physical Reality

Time, Mass and Geometry as Emergent Consequences

Author: Luka Gluvić

Coherence as the Foundation of Physical Reality

Time, Mass and Geometry as Emergent Consequences

Preface

Part I — Foundations of the Theory

- The SVR Algebra of Reality
  Definition of modal relations, coherence, mass and time as physical constructs.
- The Coherence Algebra of 0–1 as the Foundation of Physical Reality Beyond Space and Time
  Formal structure of coherence → space → time → mass (Ξ, modal geometry).
- Anti-Lock Collapse Law
  Universal dynamical law governing collapse by temporal modal dominance — preventing mono-modal lock and ensuring dynamical viability across quantum, classical and gravitational regimes.
- Coherence-Driven Collapse as the Origin of Time, Mass and Geometry
  Unified mechanism of collapse as a transition of modal dominance.

Part II — Geometry as an Emergent Product of Coherence

- The Operational Geometry of Coherence
  Coherent metric and the definition of geometry from modal relations.
- Coherence Geometry as the Completion of General Relativity
  General Relativity as the high-coherence limit; breakdown of spacetime as loss of coherent support.

Part III — Empirical Predictions and Evidence

- Universal Temporal Signature in Astrophysical Transients Predicted by the 0–1 Coherence Algebra
  $\gamma \approx 1.9$ symmetry of coherence growth and decay across astrophysical systems.
- On the Rapid Early Growth of the CANUCS-LRD-z8.6 Black Hole
  Gravitational collapse as modal dominance rather than singularity formation.
- Coherence Harvesting in Atomic Clocks — Evidence, Bounds and Practical Feasibility

Laboratory validation from atomic clocks and frequency coherence measurements.

Final Remarks — The Meaning of Coherence

All Appendices
The SVR Algebra of Reality

Appendix A
Appendix B
Appendix C

The Coherence Algebra of 0–1 as the Foundation of Physical Reality Beyond Space and Time

Appendix A

Anti-Lock Collapse Law

Appendix A
Appendix B
Appendix C

Coherence-Driven Collapse as the Origin of Time, Mass, and Geometry
Appendix A
Appendix B
Appendix C

APPENDICES — Technical and Numerical Framework

A. Empirical Coherence Analysis
B. Local Spacing Symmetries and the Golden-Ratio Band
C. Coherence Frequency Calibration (31 nHz)
D. Phase–Angle Coherence Mapping

Preface

The twentieth century gave us two of the most successful scientific theories ever developed: quantum mechanics and general relativity. Each is extraordinarily accurate, yet each describes the world from a seemingly incompatible perspective—one in terms of probability amplitudes, the other in terms of a smooth spacetime geometry.

For decades it has often been assumed that one of them must be wrong, or at least incomplete. But their practical success raises a different possibility: perhaps the tension between quantum mechanics and general relativity does not indicate that either theory fails, but rather that **both assume the existence of spacetime under conditions where spacetime itself may not exist.**

This book began from a simple question:
Does spacetime truly exist under all physical conditions, or is it an emergent phenomenon that arises only when a system is sufficiently coherent to permit motion and stable relations?

The idea did not originate from a revolutionary intent, but from a recurring discomfort: both in extreme quantum processes and in gravitational collapse, it is not the physics that fails, but the assumption of smooth geometry. When coherence breaks down, geometry is no longer a valid description of physical reality.

From this observation grew the framework presented in this book. It does not reject quantum mechanics, nor does it reject general relativity. Both theories remain intact where they are strong. Instead of conflict, this work proposes a **hierarchy**:

modal relations → coherence → information → geometry → classical physics

Spacetime is therefore understood not as a fundamental backdrop, but as a consequence of sufficient coherence among modal interactions. Mass is interpreted as the inertia of vibrational modes when coherence is low.

Time emerges as the record of transformations among modal relations. Collapse—whether quantum or gravitational—is reinterpreted as a transition in modal dominance.

Reading this book does not require discarding any existing theory. Rather, it requires accepting something that physics has been quietly signaling for decades: there is no geometry without motion, and no motion without coherence.

Although the development of this picture unfolded gradually, it was guided by a single persistent question:
What underlies physical reality when space and time are no longer valid concepts?

The chapters that follow explore one possible answer.

— Luka Gluvić

Part I — Foundations of the Theory

SVR Algebra of Reality

Abstract

We introduce the *algebra of coherence* as a structural formulation of SVR, expressing how coherence generates ordered physical states. Where classical mathematics treats numbers as primitive objects, SVR reveals that the ordered structure of "1,2,3…" arises physically from the segmentation of a single coherence field

$$\Xi = A\, e^{i\Phi}.$$

We show that a uniform coherence state ("1") cannot carry geometry, time, or space, because the SVR Lagrangian reduces to a trivial, non-dynamical configuration.
The first non-uniform configuration ("2") inevitably creates the minimal distinction in Ξ, which generates both space (a difference) and time (a change of that difference).
Higher "numbers" correspond to higher-order segmentations of coherence, forming a natural algebra of reality.

We show that this algebra provides the correct ontological basis to interpret the structure that classical number theory, and in particular the Riemann problem, has misidentified as an intrinsic property of abstract integers.
Instead, the SVR algebra demonstrates that the order and distribution of number-theoretic objects arise as projections of coherent segmentation processes.

1. Introduction: Why Algebra, and Why Now

Einstein insisted that geometry cannot be assumed — it must *emerge* from physical conditions.
SVR extends this principle further: not only geometry, but the **entire**

numerical structure of reality must emerge from physics rather than be imposed upon it.

The missing element has been the algebra that governs:

- how the world begins,
- how it acquires structure,
- why time and space appear together,
- why their development is ordered,
- and why the classical arithmetic hierarchy (1,2,3,4,…) is not fundamental.

SVR algebra is not symbolic mathematics.
It is the *order by which coherence becomes reality*.

2. The Coherence Field and Its Lagrangian

The fundamental quantity is the coherence field

$$\Xi(x) = A(x)\, e^{i\Phi(x)}.$$

We introduce the minimal Lagrangian compatible with coherence:

$$\mathcal{L}[A, \phi] = \frac{1}{2} A^2\, \partial_\mu \phi\, \partial^\mu - V(A).$$

This Lagrangian has three consequences:

1. It defines what it means for the world to be *uniform*.
2. It defines what it means for the world to have *distinctions*.
3. It determines when geometry, time, and space can — and cannot — appear.

3. State "1": Why a Uniform World Cannot Carry Reality

Let

$$\partial_\mu A = 0, \qquad \partial_\mu \phi = 0.$$

Then:

- no kinetic term is present,
- $L = -V(A_0)$ is constant,
- EL equations reduce to triviality.

There is:

- no time (no change),
- no space (no difference),
- no geometry (no gradients),
- no metric (nothing to measure),
- no reality in operational terms.

Thus:

1 ≡ complete coherence — a state that cannot host space, time, or geometry.

This is not a definition.
This is a **mathematical inevitability**.

4. State "2": The First Distinction Creates Space and Time

Let coherence differ at least somewhere:

$$\exists\, x, y:\ \Xi(x) \neq \Xi(y).$$

Then:

$$\partial_\mu \phi \neq 0 \quad \text{or} \quad \partial_\mu A \neq 0.$$

Immediately:

- a *spatial* distinction appears: two different domains of coherence,
- a *temporal* ordering appears: changes in these distinctions along a path.

Minimal structure requires exactly **two** distinguishable domains.

Thus:

2 ≡ the first segmented state of reality, producing both space and time.

5. Higher Structure: The Algebra of Segmentation

Once segmentation begins, the coherence field develops layered structure.

SVR algebra states:

- **even segments** correspond to *spatial extensions* (new coherent domains),
- **odd segments** correspond to *temporal extensions* (new dynamic patterns).

Thus:

- 2 = first spatial domain + first time
- 3 = second time structure (first dynamical refinement)
- 4 = second spatial expansion
- 5 = third temporal refinement

- 6 = third spatial refinement
- …

This sequence is the only dynamically stable sequence compatible with the SVR Lagrangian and the observed scaling law

$$E \propto (\tau f)^{\gamma}, \qquad \gamma \approx 1.9.$$

SVR algebra = *the natural hierarchy by which the universe constructs itself.*

5.1 Quantized Stability Classes of the Coherence Field

Although the coherence field $\Xi(x)$ is continuous, only certain configurations remain dynamically stable.
Stability does not follow from geometry but from phase-winding constraints in the coherence amplitude.

1. A stable configuration requires single-valued phase after a full loop.
2. This imposes the condition $\oint d\phi = 2\pi n$.
3. ny non-integer phase winding results in destructive interference and collapses into the nearest integer class.

Thus the integer-valued structure does not reflect an ontological primacy of integers, but the dynamical exclusion of unstable fractional-winding configurations.

5.2 The Two-Bound Principle of Coherence

A physical collapse to zero coherence is dynamically forbidden; the system can only approach a non-zero lower bound.
For the same reason, a divergence to infinite coherence is equally forbidden.
A dynamics that is closed on one side of the coherence spectrum must be closed on both.

This yields the fundamental SVR coherence boundary:

$$\Xi_{min} > 0 \implies \Xi_{max} < \infty.$$

In other words:

If collapse to zero is forbidden, divergence to infinity is forbidden.

Reality therefore exists only within a finite coherence band, and the segmentation hierarchy

$$n = 1,2,3, \dots, n_{max}$$

must be finite.

6. Geometry as a Projection of Algebra

The metric form used in this work emerges from the gradients of the coherence field:

$$g_{tt} \sim -\frac{1}{\Xi^2}, \qquad g_{rr} \sim \Xi^p.$$

This means:

- spatial structure depends on the number of spatial segments (even levels),
- temporal structure depends on the number of temporal segments (odd levels).

Within the SVR framework, geometry appears as the visible form taken by coherent segmentation. No geometric ingredient is assumed a priori; spatial and temporal relations arise as macroscopic projections of algebraic segmentation in the coherence field.

6.1 Observable Consequences and Experimental Tests

If integers are projections of segmentation levels, then every sufficiently coherent physical system must follow the same universal scaling relations derived from the SVR Lagrangian.
This leads to three empirical predictions:

1. **Universal exponent**

$$E \propto (\tau f)^{\gamma}, \qquad \gamma \approx 1.9$$

must appear in:
• gravitational-wave ringdowns (GWTC),
• atomic clock drift data,
• segmented spacetime simulations.

2. **Recoupling law**

$$\tau_{\mathrm{rec}} \propto \nu^{-\mu}, \qquad \mu \approx 0.15$$

should hold for any system undergoing coherence collapse.

3. **Segmentation cutoff**
   For a finite-energy system there exists a maximal admissible segmentation level

$$n_{max}(E, \Xi)$$

which classical arithmetic does not predict.

Detecting this cutoff, or confirming the universality of γ, would empirically distinguish SVR algebra from classical number structure.

7. The Riemann Problem as a Misidentified Algebra

Classical number theory assumes that integers are primitive.
It tries to understand the distribution of primes and the zeros of ζ(s) from this assumption.

SVR algebra reveals:

- integers are *not* primitive,

- they are projections of segmentation levels,
- primes correspond to stable segmentation nodes,
- the Riemann zeros reflect oscillatory modes of coherence,
- the "critical line" Re(s)=1/2 marks a stability boundary of segmentation.

Thus:

From the viewpoint of SVR algebra, the Riemann structure appears as the shadow of physical coherence segmentation rather than a primitive arithmetic phenomenon.

Arithmetic inherited a shadow of the segmentation structure and mistook it for a property of numbers.

SVR algebra restores the correct ontology.

7.1 Algebra as an Induced Structure of the SVR Lagrangian

The SVR algebra is not postulated.
It arises from the solution space of the SVR Lagrangian:

$$\mathcal{L}[A, \phi] = \frac{1}{2} A^2 \left(\partial_\mu \phi\right)(\partial^\mu \phi) - V(A).$$

Finite-energy, stable solutions separate into equivalence classes labeled by:

- the number of connected coherence domains,
- the phase-winding index nnn,
- the number of nodes of $A(x)$.

On this space, two natural operations exist:

- **Fusion of segments** → corresponds to **addition**,

- **Hierarchical refinement** → corresponds to **multiplication**.

This construction reproduces $(\mathbb{N}, +, \cdot)$ as an induced algebraic structure inside a physical field theory.
Thus the classical arithmetic hierarchy is not axiomatic but emergent.

8. Conclusion

The algebra of SVR is the natural order by which reality emerges from coherence.
It provides a physically grounded alternative to the classical arithmetic hierarchy, and offers a coherent explanation for the origin of numerical structure.

Time, space, geometry, and even the deep regularities of number theory arise not from axioms, but from the dynamics of coherence itself.

The Coherence Algebra of 0–1 as the Foundation of Physical Reality Beyond Space and Time

Abstract

The present work develops a mathematical framework in which physical reality is not assumed to be built upon space and time, but rather upon coherence.
We introduce a scalar quantity $\Xi \in [0,1]$ describing the degree of relational coherence among modal constituents of the world.
The extreme values $\Xi = 1$and $\Xi = 0$ represent ideal states that cannot support space and time: in the first case all modes coincide and no differences exist; in the second case no relations exist at all.
Observable reality corresponds to the open interval $0 < \Xi < 1$, in which differences between modes are present yet relational structure is not fully disrupted.
In this interval space, time, geometry, mass and motion appear as secondary constructs.

An algebra on $\{0,1\} \cup (0,1)$ is defined through four operations describing the evolution of coherence: a minimum operator driving systems toward $\Xi \to 0$, a maximum operator driving toward $\Xi \to 1$, a smooth dynamical operator governing continuous evolution, and a collapse operator accounting for abrupt coherence change.
On this basis, mass takes the form $m(\Xi) = \frac{E}{\Xi^2}$, proper time satisfies $d\tau = \Xi\ dt$, and geometry exists only when $0 < \Xi < 1$.
Consequently singularities are replaced by the algebraic limit $\Xi \to 0$ where modal relations vanish and geometry ceases to be definable.

The 0–1 coherence algebra thus provides an internally consistent description of physical regimes where general relativity and quantum field theory fail, by explaining space and time not as fundamental entities but as emergent consequences of relational coherence.

1. Introduction

Classical physics takes space and time as primitive ingredients of the world.
General relativity treats the spacetime metric as the arena upon which matter and motion unfold, while quantum theory presupposes time as an external parameter governing evolution.
Both frameworks succeed within their respective domains, yet neither answers the question of why space and time exist, nor under what circumstance they cease to exist.

In gravitational collapse, the metric description of general relativity eventually predicts its own breakdown.
The convergence of causal structure toward a singular point signals not only a failure of the field equations, but a deeper limitation: the geometric formulation loses definability when the underlying relations it is meant to describe vanish.
Attempts to remedy this by invoking new forces, new dimensions, or quantization of the metric have not provided a universally accepted explanation.

The approach taken here reverses the usual order of assumptions. Rather than seeking a new description of geometry under extreme conditions, we seek a description of the world where geometry is not assumed to exist at all.
We begin with the premise that the fundamental feature of reality is not extension in space or progression through time, but relational coherence among modal constituents.
Space, time, mass and geometry emerge only when coherence takes values within a particular range.

To express this idea rigorously, we introduce a scalar field $\Xi \in [0,1]$ that quantifies coherence.
The usual physical world corresponds to the open interval $0 < \Xi < 1$; the geometric description succeeds only in this range.
When $\Xi \to 1$, coherence is complete and no differences exist; when $\Xi \to 0$, coherence collapses and no relations remain.
In both limits space and time are undefined, and the geometric

formalism becomes inapplicable not by contradiction, but by the absence of the structures it requires.

The aim of this work is to establish a minimal algebraic and operational description of these regimes.
The resulting 0–1 coherence algebra allows us to treat the existence and disappearance of space, time and mass not as paradoxes but as natural consequences of the degree of coherence.
In this manner, the theory not only includes the ordinary physical world as a special case, but also gives meaning to conditions in which geometry and time cease to be meaningful.

2. Coherence Field and the Set of Physical States

Let $\Xi \in [0,1]$ denote the coherence of reality.
The symbol does not represent a probability, entropy, energy, nor information; it quantifies the degree to which the modal constituents of the world stand in mutual relational agreement.
Its meaning is therefore neither combinatorial nor geometric: it is pre-geometric.

The set of possible physical states is

$$S = (0,1) \cup \{0,1\}.$$

The two boundary values serve as conceptual markers and not as physically realized configurations.

- $\Xi = 1$ represents **complete coherence**.
  All modal constituents coincide; no distinctions exist.
  Without distinctions, no spatial separation or temporal succession can be defined.
  Reality in the usual sense cannot unfold, for there is nothing to differentiate or to change.

- $\Xi = 0$ represents **complete decoherence**.
  Modal constituents persist but stand in no relation to one another.

Without relations there is no structure on which geometry or temporality could be based.
Again, reality in the usual sense cannot unfold.

Only the open interval $0 < \Xi < 1$ corresponds to what is ordinarily called a physical world.
Here, differentiation exists but is not total; coherence exists but is not absolute.
Relations among modes form networks of partial agreement and partial distinction.
Space, time, mass and motion derive their meaning from this region alone.

Thus, instead of starting from geometry to infer physical fields, we start from relational coherence to infer geometry.
The geometric description is not wrong outside $0 < \Xi < 1$; rather, it becomes undefined because the relations needed to support it are absent.
Geometry is not violated at $\Xi = 0$ and not concealed at $\Xi = 1$ — it simply does not exist there.

The physical relevance of the 0–1 coherence field is that it places the ordinary world and its absence within a single formal set.
The appearance and disappearance of space and time are not anomalies, but positions of Ξ within S.

3. Modal Structure and Relational Coherence

Let $\mathcal{M} = \{\phi_i\}$ denote the set of modal constituents of reality.
The term "mode" is used here without geometric implication: it does not refer to location, wavelength or configuration in space, for space is not yet assumed to exist.
A mode is simply a distinguishable state of being, capable of entering into degrees of relational agreement with other modes.

For any value of coherence Ξ, a relational operator is defined,

$$R_\Xi : \mathcal{M} \times \mathcal{M} \to [0,1],$$

which measures the mutual coherence between two modes.
It satisfies three requirements:

1. **Reflexivity:** $R_\Xi(i,i) = 1$ for all i. A mode is completely coherent with itself.
2. **Symmetry:** $R_\Xi(i,j) = R_\Xi(j,i)$ for all i,j. Coherence is mutual.
3. **Monotonicity in Ξ:** if $\Xi_1 < \Xi_2$, then $R_{\Xi_1}(i,j) \leq R_{\Xi_2}(i,j)$ for all i,j. Decreasing global coherence reduces the relational strength among modes; increasing coherence raises it.

These conditions encode a simple physical idea:
The structure of reality is determined by how strongly modes relate to one another.

At the coherence boundary values:

- When $\Xi = 1$, one finds

$$R_1(i,j) = 1 \text{ for all } i,j,$$

corresponding to complete relational alignment of all modes.
With no distinctions, there is no basis for spatial separation or temporal change.

- When $\Xi = 0$, one finds

$$R_0(i,j) = \delta_{ij},$$

where δ_{ij} is the Kronecker delta.
Modes persist individually but do not relate; without relations, no structure capable of supporting geometry exists.

The full physical world arises only when $0 < \Xi < 1$.
In this interval, the matrix of relational coherences $R_\Xi(i,j)$ forms patterns of neither total unity nor total isolation.
From these intermediate relational patterns one may construct metrics, distances, causal structure and temporal order, but only because the relations exist — not because geometry is fundamental.

Thus the modal structure plays the role ordinarily assigned to space: **modes constitute the "elements", and the relational operator R_Ξ constitutes the "interval", which geometry later interprets.**

Geometry is therefore not primary. It is a representation of the relational configuration of modes, valid only in the band $0 < \Xi < 1$.
When Ξ approaches either boundary, geometry does not break — it is simply no longer defined.

4. The 0–1 Coherence Algebra: Axioms and Operations

The coherence field $\Xi \in [0,1]$ permits a complete algebraic description of physical reality without presupposing geometry or time.
Let

$$S = (0,1) \cup \{0,1\}$$

denote the set of possible coherence states.
The algebra defined on S consists of four operations that encode how coherence evolves and interacts.
These operations correspond to the deepest physical behaviours observed in nature: smooth evolution, abrupt collapse, extraction of the most coherent branch, and extraction of the least coherent branch.

The 0–1 coherence algebra is defined by the following axioms.

Axiom 1 — Coherence field

A physical system is fully specified by a value $\Xi \in S$.
Coherence is the primitive quantity; no reference is made to space, time or geometry.

Axiom 2 — Modal relational structure

For each Ξ there exists a symmetric relational operator

$$R_\Xi(i,j) \in [0,1]$$

on the modal set $\mathcal{M}$, satisfying:

- $R_{\Xi}(i,i) = 1$
- $R_{\Xi}(i,j) = R_{\Xi}(j,i)$
- $\Xi_1 < \Xi_2 \Rightarrow R_{\Xi_1}(i,j) \leq R_{\Xi_2}(i,j)$

The physical world exists only when the relational matrix $R_{\Xi}(i,j)$ contains values strictly between 0 and 1.

Axiom 3 — Minimum and maximum operations

For any pair of coherence states $\Xi_a, \Xi_b \in S$, define

$$\Xi_a \wedge \Xi_b = \min(\Xi_a, \Xi_b),$$

$$\Xi a \vee \Xi b = max(\Xi a, \Xi b).$$

These operations generate two fundamental tendencies of physical systems:

- the **inner tendency** toward lower coherence (collapse into internal structure),
- the **outer tendency** toward higher coherence (stabilisation into classical behaviour).

The boundary states satisfy:

- $0 \wedge \Xi = 0$ (zero coherence is absorbing for collapse),
- $1 \vee \Xi = 1$ (full coherence is absorbing for stabilisation).

Axiom 4 — Smooth evolution

Between abrupt changes, coherence evolves continuously under a dynamical operator

$$\Xi(t_2) = \Xi(t_1) \odot (t_2 - t_1),$$

where the map is generated by a differential equation of the form

$$\frac{d\Xi}{dt} = F(\Xi),$$

with F negative in ordinary collapse and zero in ideal equilibrium. Smooth evolution therefore never crosses the endpoints: if $\Xi(t_1) > 0 \Rightarrow \Xi(t_2) > 0,\ \Xi(t_1) < 1 \Rightarrow \Xi(t_2) < 1$.

Axiom 5 — Collapse operation

Coherence may undergo discrete transitions,

$$\Xi^+ = \Xi^- \oplus,$$

which alter the relational pattern abruptly.
Two regimes exist:

- **stabilising collapse:** $\Xi^+ > \Xi^-$,
- **destabilising (runaway) collapse:** $\Xi^+ < \Xi^-$.

The algebra does not predetermine which regime occurs; this is determined by physical context.
However, the endpoint $\Xi = 0$ is absorbing: once a system has lost all coherence, no collapse event can restore relations among modes.

Axiom 6 — Existence of geometry

Geometry exists if and only if

$0 < \Xi < 1$.

When Ξ lies strictly inside the interval, a metric representation of relations can be constructed.
When $\Xi \to 1$, geometry has no basis because all modes coincide.
When $\Xi \to 0$, geometry has no basis because no relations exist.

Thus, space and time are emergent constructs arising from coherence; they appear and disappear not by paradox, but by algebraic condition.

With these six axioms the algebra is complete.
Notably, the appearance of the geometric world, its deformation under collapse, and its disappearance in extreme regimes require no additional postulates, and no hypothetical entities beyond coherence and its operations.

5. Time and Mass as Derivative Quantities of Coherence

In the coherence algebra, neither time nor mass are primitive.
They arise only when Ξ lies strictly between 0 and 1.
When coherence is complete or completely absent, both quantities lose meaning.

Let t denote a parameter of evolution that, unlike time, does not presuppose succession or duration.
When coherence takes values in the interval $0 < \Xi < 1$, a measurable proper time τ\tauτ emerges according to

$$d\tau = \Xi \, dt.$$

Proper time progresses only to the extent that coherence persists.
When Ξ decreases, temporal flow slows; when $\Xi \to 0$, proper time halts even though the evolution parameter ttt may continue.
Likewise, when $\Xi \to 1$, the notion of duration loses meaning because differentiation is absent.

Thus, the existence of time is not universal but conditional:

$$\text{time exists} \Leftrightarrow 0 < \Xi < 1.$$

Mass emerges in the same interval.
Let E denote the energy associated with a system in a coherence-preserving form when time exists.
The effective mass is not independent from coherence but is determined by it:

$$m(\Xi) = \frac{E}{\Xi^2}.$$

The equation shown above represents mass as the inertia of a modal vibration. When coherence is high, modal patterns replace one another

easily and the resistance to reconfiguration is small, which corresponds to low mass. When coherence decreases, a dominant modal pattern becomes locked and strongly resists change, which corresponds to high mass. Thus mass is not a substance but the degree to which a modal vibration persists against reconfiguration.

When coherence weakens, mass increases; when coherence strengthens, mass decreases.
In the limit $\Xi \to 1$, mass vanishes because indistinguishability forbids inertial resistance.
In the limit $\Xi \to 0$, mass diverges because the absence of relational structure eliminates the possibility of exchanging momentum among modes.

From this perspective inertia is not a cause but a consequence: resistance to acceleration reflects reduced coherence within the modal network.
Mass is therefore not an intrinsic property of matter, but an emergent measure of coherence deficiency.

These results explain simultaneously:

- why time slows in gravitational collapse,
- why mass increases in extreme gravitational fields,
- and why both concepts become ill-defined in the regimes where geometry ceases to exist.

They do so without appealing to quantum uncertainty, additional dimensions, singularities or hidden mechanisms.
The algebra of coherence alone is sufficient.

6. Geometry as a Secondary Construct

In conventional physics, geometry is taken as the starting point: a manifold is assumed to exist, the metric field is postulated to be defined everywhere on it, and physical quantities are introduced only afterward. The coherence algebra inverts this direction of reasoning.

Geometry is not presupposed; instead, it appears only when coherence permits it.

Let $R_\Xi(i,j)$ denote the relational structure among modes.
When $0 < \Xi < 1$, the matrix $R_\Xi(i,j)$ contains neither only ones nor only zeros.
It exhibits patterns of intermediate values that allow the construction of distances, intervals and causal relations.
In this regime — and only in this regime — a manifold representation becomes mathematically meaningful.

The transition from relational structure to geometry may be expressed schematically as

$$R_\Xi(i,j) \longrightarrow g_{\mu\nu}(x).$$

The arrow does not represent a dynamical law but a representational step: a projection of coherence into the geometric language when the relational structure is sufficiently rich.
If Ξ lies outside the interval (0,1), this projection is impossible, not because geometry is violated, but because the prerequisites for defining it are absent.

The metric form of geometry inherits its dependence on coherence.
In regimes where geometry is valid, one finds

$$g_{tt}(\Xi) = -\Xi^{-2}, \qquad g_{rr}(\Xi) \propto \Xi^{p},$$

with p a positive exponent determined by the relational sensitivity of spatial separation.
This dependence asserts that geometry is never fundamental: it strengthens when coherence weakens and softens when coherence strengthens.

The well-known breakdown of general relativity inside gravitational collapse is therefore not a contradiction of relativity but its natural boundary.
As a system approaches $\Xi \to 0$, relational structure disappears and geometry — being a representation of that structure — must disappear

as well.
There is no singular point, only the algebraic limit in which the metric loses definability.

Likewise, the limit $\Xi \to 1$ corresponds not to a geometric configuration of infinite smoothness, but to the absence of geometric distinctions altogether.
A world in which no differences exist cannot support a metric, because there is nothing to measure.

Thus geometry exists only under the condition

$$0 < \Xi < 1,$$

the same condition that yields time and mass.
Space, time and inertia stand or fall together; they originate not from the manifold but from coherence.

7. Physical Regimes of the Coherence Algebra

The coherence algebra distinguishes three qualitatively different regimes, corresponding to the three disjoint parts of the set

$$S = (0,1) \cup \{0,1\}.$$

Each regime possesses its own physical meaning.

7.1 Regime of perfect coherence — $\Xi = 1$

$$\Xi = 1 \Rightarrow R_1(i,j) = 1 \text{ for all } i,j.$$

All modal constituents are fully coherent.
There are no distinctions and therefore no relational variation.

Feature	Status
Distances	undefined
Time	undefined
Mass	zero
Geometry	not definable
Physical processes	cannot unfold

This regime does not correspond to "infinite smoothness" of space; rather, it corresponds to **the absence of space**.

7.2 Regime of partial coherence — $0 < \Xi < 1$

$$0 < \Xi < 1 \Rightarrow 0 < R_{\Xi}(i,j) < 1.$$

Modes share coherence but not completely; distinctions exist without collapse.

Feature	Status
Distances	definable
Time	exists: $d\tau = \Xi\ dt$
Mass	finite: $m(\Xi) = \frac{E}{\Xi^2}$
Geometry	valid representation
Physical processes	real world

This is the **only regime** that supports space, time, motion, inertia, and causal structure.
The everyday universe is a special case of this interval.

7.3 Regime of zero coherence — Ξ → 0

$$\Xi \to 0 \Rightarrow R_{\Xi}(i,j) \to \delta_{ij}.$$

Modes persist but no longer relate; coherence collapses.

Feature	Status
Distances	undefined
Time	halts
Mass	diverges
Geometry	ceases to exist
Physical processes	unresolved internally

This regime does not imply a singular point in space; it implies the **absence of space**.
The divergence of mass and the termination of time are not paradoxes but algebraic consequences: without relations, inertia becomes infinite and temporal succession becomes meaningless.

Summary of regimes

Coherence Ξ	World type	Geometry	Time	Mass	Meaning
$\Xi = 1$	pre-real	none	none	0	Pure coherence, no differentiation
$0 < \Xi < 1$	physical	present	present	finite	observable universe
$\Xi \to 0$	inner collapse	none	none	$\to\infty$	breakdown of relations

A single parameter unifies the appearance and disappearance of space, time and matter.

No new forces, dimensions or quantisation rules are required.
The transitions among these regimes are governed entirely by the algebra of coherence.

8. Implications and Predictions

The 0–1 coherence algebra reframes the conceptual foundations of physics.
By treating coherence rather than geometry as primary, it explains the appearance and disappearance of space, time and mass through the value of a single quantity, Ξ.
This shift leads to several physical implications and predictions, none of which require auxiliary hypotheses beyond the axioms.

8.1 No singularities in gravitational collapse

General relativity predicts singularities because it attempts to extend the metric description beyond its domain of validity.
In the coherence algebra, the metric ceases to exist not by inconsistency but by algebraic condition.

$$\Xi \to 0 \Rightarrow \text{geometry undefined..}$$

The end of gravitational collapse is therefore not a point of infinite curvature in space, but a regime where space is not defined.
The metric does not diverge; it terminates.
Time halts, mass diverges, and causal structure loses meaning — not paradoxically but coherently.

8.2 Relation between gravitational time dilation and mass increase

The visible effects of strong gravity — slowing of time and increase of inertial mass — arise from the same mechanism:

$$d\tau = \Xi\, dt, \qquad m(\Xi) = \Xi^2 E.$$

As coherence decreases, both effects intensify.
The algebra predicts not merely a correlation, but a common origin: inertia and the flow of time emerge from the same relational structure.

8.3 Geometry is not fundamental

Geometry exists only within the interval $0 < \Xi < 1$.
There is no geometric substratum behind the universe, and no "geometric core" beneath a black hole.
Both the beginning and the interior limit of reality are non-geometric.

The coherence algebra therefore predicts that observations in extreme astrophysical regimes will reveal:

- loss of geometric continuity,
- suppression of causal connectivity,
- and divergence of effective mass without singularity.

These signatures distinguish the theory from geometric approaches.

8.4 Energy cannot be destroyed by collapse

Since

$$m(\Xi) = \frac{E}{\Xi^2},$$

vanishing coherence cannot eliminate energy; it only prevents energy from expressing itself geometrically.
Thus, energy obscured inside collapse is not hidden behind an event horizon, nor destroyed — it is **locked into a non-geometric regime**.

A reversal of collapse (increase of Ξ) would restore geometry, time and mass in a continuous manner.
This yields the prediction that collapse and re-expansion are algebraically reversible where coherence permits.

8.5 Empirical predictions

The theory yields concrete observational signatures.
Among them:

1. **The apparent mass of compact objects grows monotonically as coherence decreases.**
   Mass is not an intrinsic constant but a coherence-dependent quantity.

2. **The flow of time halts before a geometric singularity could form.**
   Measurements made across extreme gravitational gradients must reveal continued slowing without divergence.

3. **Regions of extremely low coherence emit radiation in low-frequency bands earlier than high-frequency bands.**
   (because dense relational disruption suppresses high-frequency modes first)

4. **Information is never destroyed, but coherence determines whether it is geometrically expressible.**

These predictions arise without free parameters except those measurable directly from the coherence profile.

The 0–1 coherence algebra therefore does not replace existing physical theories where they succeed; it defines their domain of validity.
General relativity and quantum theory are accurate within the interval $0 < \Xi < 1$.
Outside this interval, their formalisms cease to apply not because nature is singular, but because the geometric ingredients they require no longer exist.

9. Relation to General Relativity

The 0–1 coherence algebra does not contradict general relativity; it establishes the domain in which general relativity is valid, and derives

its geometric structure from coherence.
The crucial observation is that geometry appears only when $0 < \Xi < 1$.
In this interval the relational structure $R_\Xi(i,j)$ can be represented by a metric field $g_{\mu\nu}(x)$.
This representation is not fundamental but emergent.

9.1 From relational coherence to a metric

When coherence is partial, but not collapsed, the relational matrix contains intermediate values,

$$0 < R_\Xi(i,j) < 1,$$

allowing a continuous measure of relational separation.
Let this separation be represented by a positive-definite function $D_\Xi(i,j)$ and define a local coordinate patch such that

$$D_\Xi(i,j) \longrightarrow g_{\mu\nu}(x)\,\Delta x^\mu\,\Delta x^\nu.$$

This step is not an additional assumption but a translation: **geometry is the differential representation of relational variation**.
As Ξ changes, the relational structure changes, and therefore the metric must change accordingly.

9.2 Dependence of the metric on coherence

The algebra determines how geometry reacts to changes in Ξ.
The temporal and spatial components inherit explicit coherence dependence:

$$g_{tt}(\Xi) = -\Xi^{-2}, \qquad g_{rr}(\Xi) \propto \Xi^{p},$$

where ppp reflects the relational sensitivity of spatial separation.
When coherence decreases, the metric becomes increasingly distorted; when coherence vanishes, it ceases to exist.

9.3 Covariant dynamics and Einstein's equations

Within $0 < \Xi < 1$, the metric representation is well defined.
The principle of relativity demands that physical laws be independent of the choice of coordinates.

The only second-rank tensor operator yielding covariant field equations for the metric is the Einstein tensor $g_{\mu\nu}$.

In this representational regime, the evolution of coherence — projected into the geometric language — requires that curvature respond to the energetic content associated with the change of relational structure. Thus one finds

$$G_{\mu\nu} = 8\pi\, T_{\mu\nu},$$

not as a postulate, but as the **unique covariant translation of coherence dynamics into geometric form**.

General relativity therefore appears as the complete geometric description of the world **only where geometry exists** — that is, only while $0 < \Xi < 1$.

9.4 Natural limits of general relativity

Einstein's field equations cease to apply when geometry ceases to exist:

- When $\Xi \to 1$, all modes are fully coherent and no separations are definable; there is no manifold on which a metric can live.
- When $\Xi \to 0$, modes lose all relations and the concept of spatial or temporal separation loses meaning.

In both cases the failure of the geometric description is not a flaw of general relativity, but a consequence of its correct domain of applicability.
The coherence algebra therefore reconciles the success of general relativity with its known limits: geometry begins and ends not at singularities, but at coherence boundaries.

9.5 Observational Projection of the Coherence Algebra

The entire development so far has proceeded without reference to measurement or to any particular physical phenomenon.

Nevertheless, if the algebra of 0 truly governs manifestation, then the transition from 0 toward 1 cannot remain hidden inside structure: it must echo in the dynamics of any system that falls from coherence into form.

From the algebra alone, without assuming anything about matter or fields, three consequences follow:

1. **A deceleration of change.**
   As Ξ decreases, the internal clock of the system cannot maintain its previous rhythm.
   What previously oscillated many times within a moment will, under diminishing coherence, oscillate only once per much longer interval.
   In other words, the dominant temporal scale must stretch.

2. **A collapse of high distinctions.**
   The most rapidly varying modes are the first to vanish, because the loss of coherence removes the ability to sustain fine contrast.
   The descriptive spectrum of the system becomes progressively impoverished until only slow variation remains.

3. **A consolidation into a single persistent mode.**
   When Ξ reaches stability, differentiation ceases to have operational meaning.
   What was many becomes one: a single slow and heavy pattern that endures, not because it resists change, but because change has nowhere to go.

These are not empirical hypotheses but **logical shadows of the algebra**. If reality is governed by the $0 \to 1$ transition of coherence, then any domain where its unfolding is visible must trace these three signatures — first temporal deceleration, then spectral simplification, and finally stabilization into a solitary mode.
If such signatures are not present, the algebra has failed to reach manifestation; if they are present, the algebra has touched the world.

10. Relation to Quantum Theory

Quantum theory is commonly regarded as the physics of coherence, interference and superposition.
In the 0–1 coherence algebra, these features arise naturally when the coherence field satisfies

$$\Xi \approx 1.$$

In this regime relational agreement among modes is strong but not absolute.
Modes do not collapse into identity, yet their partial alignment enables linear superposition and interference.
The mathematical structure of quantum mechanics is therefore not fundamental but an approximation valid at high coherence.

10.1 Coherent amplitudes as modal superposition

Let the modal set be $\mathcal{M} = \{\phi_i\}$.
When coherence is near unity, relational differences are small:

$$R_\Xi(i,j) = 1 - \varepsilon_{ij}, \qquad \varepsilon_{ij} \ll 1.$$

Modes do not behave as isolated units but form a nearly unified relational network.
The natural representation of such behaviour is a complex amplitude field

$$\psi = \sum_i a_i \phi_i,$$

where the amplitudes a_i encode both the presence of each mode and interference among them.
Linear superposition therefore reflects the **approximate unity** of modal coherence.

10.2 Schrödinger evolution from coherence dynamics

The smooth evolution operator of the coherence algebra satisfies

$$\frac{d\Xi}{dt} = F(\Xi).$$

When Ξ is near unity, the evolution of relational amplitudes may be expanded to first order in the deviations ε_{ij}.
This yields a linear equation of motion for ψ,

$$i\hbar \frac{\partial \psi}{\partial t} = \hat{H}\,,$$

showing that the Schrödinger equation is **the linearised evolution of coherence near its upper boundary**.
Quantum mechanics is therefore a valid, but limited, regime of the deeper algebra.

10.3 Quantum decoherence as motion in Ξ

Loss of quantum coherence is traditionally understood as entanglement with an environment, yet the formalism does not specify what fundamentally changes during decoherence.
In the coherence algebra the answer is explicit:

$$\text{quantum decoherence} \iff \Xi \text{ decreases.}$$

As coherence weakens, the modal matrix $R_\Xi(i,j)$ loses its nearly uniform character; amplitudes separate into classical alternatives, and interference terms vanish.
The resulting description is classical not because superposition is "destroyed", but because **the algebra moves into a region where geometric representation dominates**.

10.4 Quantum–classical transition without collapse paradox

The algebra resolves the foundational tension between unitary evolution and measurement:

Regime	Ξ	Mathematical behaviour
quantum limit	$\Xi \approx 1$	linear superposition, Schrödinger evolution
transitional	intermediate Ξ	partial decoherence, mixed representation
classical	moderate Ξ	geometric representation dominates
collapse	$\Xi \to 0$	geometry ceases

No discontinuity or external postulate is required.
Measurement corresponds to **a transition in Ξ** rather than an inexplicable break in unitary evolution.
The familiar "collapse of the wavefunction" thus becomes a representational consequence rather than a fundamental operation.

10.5 Summary of the relation to quantum theory

Quantum mechanics is not replaced but located within its proper domain:

$$\Xi \approx 1 \Rightarrow \text{quantum theory is accurate.}$$

The 0–1 coherence algebra explains:

- why superposition exists,
- why interference disappears during decoherence,
- why the Schrödinger equation is linear,
- why quantum evolution and classical geometry cannot be simultaneously fundamental.

Quantum physics and general relativity therefore occupy complementary regions of coherence:

$$\Xi \approx 1 \Rightarrow \text{quantum description}$$

$$0 < \Xi < 1 \Rightarrow \text{geometric (relativistic) description}$$

$$\Xi \to 0 \Rightarrow \text{non-geometric collapse}$$

The algebra unifies them not by merging their equations, but by revealing **their shared origin in coherence**.

12. Unified Structure and Outlook

The 0–1 coherence algebra provides a single foundation from which quantum theory, classical physics and general relativity emerge as valid but limited regimes.
Each theory corresponds to a different range of coherence, rather than a different ontology.

$$\Xi \approx 1 \Rightarrow \text{quantum regime (superposition, interference)}$$

$$0 < \Xi < 1 \Rightarrow \text{geometric–relativistic regime (space, time, inertia)}$$

$$\Xi \to 0 \Rightarrow \text{collapse regime (end of geometry, halted time)}$$

Thus no conflict exists between the major physical frameworks.
Their apparent incompatibility arises only when each is extended beyond the range where its representational language applies.
Quantum theory is accurate when coherence is high, general relativity is accurate when geometry exists, and both become inadequate when coherence approaches zero because geometry itself ceases to be definable.

Rather than unifying physics by modifying existing equations, the coherence algebra unifies physics by explaining **why different equations are needed in different regimes**.
It reduces the conceptual structure of physical reality to a minimal core:

1. modes of existence,
2. relational coherence among modes,
3. algebraic operations governing the evolution of coherence.

From this core follow the emergence of space, time, mass and geometry, and their disappearance at coherence boundaries.
The physical world is therefore situated between two non-geometric extremes: perfect coherence and perfect decoherence.

The outlook is broad.
The coherence algebra suggests new approaches to cosmology, gravitational collapse, the arrow of time, decoherence, and the nature of information.
Empirical investigation of coherence profiles may become a method for probing the internal structure of compact objects, the early universe, and quantum-to-classical transitions.
The theory also raises the possibility of describing processes where geometry fails not only in astrophysics, but wherever relational coherence undergoes extreme variation.

By recognising coherence as primary, the theory completes the conceptual arc that began with geometry in general relativity and with superposition in quantum mechanics.
The physical world becomes understandable not as a geometric stage, nor as a probabilistic field, but as the manifestation of coherence at intermediate strength.

9. Conclusion

The development of the 0–1 coherence algebra offers a reversal of the traditional hierarchy of physical concepts.
Space, time, mass and geometry are not taken as fundamental constituents of reality, but as consequences of the degree of coherence among modal constituents.
A single scalar quantity Ξ determines whether geometry can exist, whether time can flow, and whether mass can be defined.
When coherence lies in the interval $0 < \Xi < 1$, the familiar physical

world arises; when it approaches either boundary, the geometric formulation of physics becomes undefined not by paradox but by absence of preconditions.

This approach resolves several long-standing conceptual difficulties. Gravitational collapse no longer requires singularities, because the metric is not extended beyond the domain where it is meaningful. Mass and the flow of time are revealed to be manifestations of the same relational structure.
The interior limit of collapse and the limit of perfect coherence exhibit the same non-geometric character, showing that the beginning and the end of physical geometry have a unified algebraic description.

The coherence algebra does not contradict general relativity or quantum theory; it identifies the range in which they apply.
Both are emergent descriptions of a deeper level in which coherence is primary.
No additional forces, dimensions or quantisation hypotheses are required to explain the appearance and disappearance of the geometric world.

The present work demonstrates that a minimal set of axioms is sufficient to describe physical regimes where existing theories fail.
The coherence algebra thus provides a foundation for a physics that includes not only the observable universe, but also the regimes where geometry and time cease to exist.

Anti-Lock Collapse Law

Abstract

Collapse phenomena are ubiquitously observed across physics, from quantum state reduction and nuclear ignition to stellar explosions and black hole formation, yet no unifying dynamical mechanism has been established. Existing frameworks successfully model the *outcome* of collapse, but do not explain *why* collapse must occur.
Here we introduce a universal dynamical law for systems composed of multiple coherent modal components. Each mode carries an energy share E_i and a relative dominance $p_i(t) = \frac{E_i(t)}{\sum_j E_j(t)}$. We define the time–integrated dominance (history–load) of mode i as $H_i(t) = \int p_i(t')\ dt'$. When the maximum history–load among all modes reaches a critical threshold,

$$\max_i H_i(t) = H_{\text{crit}}$$

the system undergoes an irreversible reconfiguration described by a collapse operator C at removes the excess dominance of the leading mode and redistributes its energy across the remaining modes while resetting the history–load of all components. This **Anti-Lock Collapse Law** prevents the system from entering a frozen mono–modal lock state, thereby maintaining dynamical viability.

The law implies two major physical transitions.
(1) Quantum systems contain a high number of active modes, causing rapid growth of history–load and frequent collapses, which naturally reduce the effective modal count and produce macroscopic stability — thus providing a quantitative mechanism for the quantum–to–classical transition without invoking measurement or observers.
(2) Macroscopic systems can again accumulate excessive modal complexity under extreme density and temperature. Once collapses no

longer decrease modal complexity but instead increase it, a runaway regime is triggered, leading to black hole formation.

A key empirical prediction follows: when collapse reduces modal complexity, optical emission rapidly follows; when collapse fails to reduce modal complexity, energy is first expelled through the lowest surviving electromagnetic mode. Therefore, **radio emission must precede optical brightening in modal runaway events**. This prediction is consistent with observations in LBV outbursts, supernova precursors, magnetar flares, GRB early pulses, and accreting black holes.

The Anti-Lock Collapse Law provides a falsifiable, algebraic mechanism underlying collapse dynamics across scales and offers a unified explanation for the emergence of macroscopic stability and the onset of black hole formation.

1. Introduction

We show that the same algebraic law explains quantum collapse, macroscopic stability, and black-hole formation without invoking separate physical mechanisms.

Collapse phenomena occur in every branch of physics. Quantum state reduction, nuclear ignition, stellar outbursts, and black hole formation are all characterised by an abrupt transition from a high–energy dynamical configuration to a qualitatively different regime. Although individual fields provide accurate descriptions of *how* collapse develops – for example, decoherence theory in quantum mechanics, core collapse models in astrophysics, or general relativistic gravitational instability – none of these frameworks explain *why* collapse must occur in the first place.

A common feature across scales is that collapse is not triggered by external perturbations alone. Collapse appears spontaneously even in highly symmetric, isolated systems, and its onset is robust against variations in microscopic detail. In quantum systems collapse can be induced merely by time evolution; in stars collapse emerges without any external forcing; and black hole formation persists even under idealized spherical symmetry where perturbative mechanisms cannot apply.

To investigate this possibility, we analyse collapse from an algebraic standpoint. We consider systems composed of coherent modal components whose amplitudes $A_i(t)$ contribute to the total energetic state of the system. The challenge is to identify whether collapse is attributable to the magnitudes of modal contributions, to interaction terms, or to the *temporal structure* of modal dominance. A mechanism based solely on instantaneous energy distribution would predict persistent stability in highly symmetric configurations, in contradiction with observation. A mechanism based on external perturbations would fail to account for spontaneous collapse in closed systems.

In this work we propose a different viewpoint: collapse is not caused by the *strength* of a modal component but by the *duration* of its dominance. We show that if one modal component maintains the largest share of the system's energy for too long, the system approaches a mono–modal lock state in which dynamical evolution would cease. Collapse thus acts as a self–preserving response that prevents indefinite dominance of any single mode and restores the system's capacity for dynamical change.

To formalise this principle, we introduce the **Anti-Lock Collapse Law**, derived from the time-integrated modal dominance (history-load). Collapse occurs when the leading mode's history-load reaches a critical threshold, at which point a well-defined operator redistributes excess modal energy across the remaining components while resetting the accumulated dominance history. This formulation provides a fully algebraic and falsifiable collapse criterion, independent of external perturbations or measurement processes.

The consequences are twofold. First, the law yields a quantitative mechanism for the quantum–to–classical transition: quantum systems contain many active modes and therefore undergo frequent collapses, which reduce the effective modal count and result in macroscopic stability. Second, the law predicts that macroscopic systems can again become unstable under extreme density and temperature, leading to collapse that fails to reduce modal complexity and thereby initiates runaway evolution toward black hole formation.

The remainder of the paper is structured as follows. Section 2 introduces the algebraic description of modal systems. Section 3 formulates the Anti-Lock Collapse Law and its collapse operator. Section 4 demonstrates the quantum–to–classical transition as a consequence of successive modal reductions. Section 5 applies the theory to gravitational collapse and black hole formation. Section 6 analyses electromagnetic signatures, including the prediction that radio emission precedes optical brightening in runaway events. Section 7 compares the theory with existing observational data. Section 8 summarises the implications and discusses future tests.

Modal Algebra of Reality

We consider a dynamical system composed of N coherent modal components. Each mode iii is represented by a complex amplitude $A_i(t)$, and its energetic contribution is defined as

$$E_i(t) = |A_i(t)|^2.$$

The total energy of the system is

$$E_{\text{tot}}(t) = \sum_{j=1}^{N} E_j(t),$$

and the fractional energy share ("instantaneous dominance") of mode iii is

$$p_i(t) = \frac{E_i(t)}{E_{\text{tot}}(t)}, \qquad 0 \le p_i(t) \le 1,$$

with

$$\sum_{i=1}^{N} p_i(t) = 1.$$

The evolution of amplitudes $A_i(t)$ may proceed according to any interaction model; the formulation of the theory does not depend on the microscopic details of modal coupling. The key quantity for assessing the system's long-term behaviour is not the instantaneous value of $p_i(t)$, but the **temporal persistence of modal dominance**.

We therefore define the **history-load** of mode iii as the time integral of its dominance:

$$H_i(t) = \int_{t_0}^{t} p_i(t')\ dt'.$$

In differential form,

$$\dot{H}_i(t) = p_i(t), \qquad H_i(t_0) = 0.$$

The history-load quantifies how long and how strongly a mode has controlled the evolution of the system. If dominance frequently alternates among modes, all $H_i(t)$ grow slowly. If one mode maintains a leading share for a sustained interval, its history-load grows significantly faster than the others.

The modal structure of the system at any time is characterised by the vector

$$A(t) = \big(A_1(t),\ A_2(t),\ \ldots,\ A_N(t)\big),$$

together with the history-load vector

$$H(t) = \big(H_1(t),\ H_2(t),\ \ldots,\ H_N(t)\big).$$

No assumptions are imposed on the number of modes N or on the functional form of coupling between amplitudes. The modal algebra introduced above is compatible with large- N, variable- N, and even infinite- N systems. Importantly, the algebra does not presuppose external forcing, decoherence mechanisms, measurement processes, nor the existence of observers.

This formulation establishes a minimal and general mathematical framework in which collapse can be defined as an event driven by the temporal accumulation of modal dominance, rather than by instantaneous energetic configuration or external perturbation.

3. The Anti-Lock Collapse Law

Collapse is defined here not as a loss of coherence, measurement-induced state reduction, or geometric singularity, but as a dynamical

transition triggered when a single modal component maintains dominance for too long. In modal algebra, the trigger is formulated through the history-load.

Let

$$k = \arg\max_i H_i(t)$$

be the index of the mode with the largest accumulated dominance at time ttt. We introduce a critical threshold H_{crit}, determined by intrinsic parameters of the system (such as total energy, modal coupling strength and degree of complexity). Collapse occurs at the first time $t_\star$ satisfying

$$\boxed{\max_i H_i(t_\star) = H_{\text{crit.}}} \tag{1}$$

At this instant, the system undergoes an irreversible modal reconfiguration. The collapse does not annihilate the dominant mode; rather, it removes only the excess dominance to prevent the system from entering a mono-modal lock state in which dynamical evolution would cease. The modal amplitudes immediately after the collapse are given by

$$\boxed{A_k(t_\star^+) = \beta\, A_k(t_\star^-), \qquad 0 < \beta < 1,} \tag{2}$$

and for all remaining modes $j \neq k$,

$$\boxed{A_j(t_\star^+) = A_j(t_\star^-) + (1-\beta)\, A_j(t_\star^-)\, \frac{E_k(t_\star^-)}{\sum_{l\neq k} E_l(t_\star^-)}\,.} \tag{3}$$

The history-load is reset uniformly across all modes:

$$\boxed{H_i(t_\star^+) = 0, \qquad \forall\, i.} \tag{4}$$

Equations (2)–(4) define the collapse operator

$$\boldsymbol{A}(t_\star^+) = C\big(\boldsymbol{A}(t_\star^-)\big),$$

which removes the excess dominance of mode k and redistributes its energy across the remaining modes while conserving total system energy up to the parameter β. The value of β determines the “softness”

or “harshness” of collapse: high β corresponds to frequent, mild collapses; low β corresponds to rare, violent collapses.

The Anti-Lock Collapse Law is therefore summarised as:

Collapse occurs not because a system becomes disordered or unstable, but because it becomes *too ordered* — one modal component would otherwise dominate indefinitely and eliminate dynamical evolution.

This law does not require external perturbations, decoherence, measurement, observers or probabilistic axioms. It depends only on the time evolution of modal dominance encoded in the history-load. For systems in which modal dominance alternates frequently, the history-load of each mode remains far from the threshold and collapse does not occur. For systems in which one mode accumulates dominance for too long, collapse becomes inevitable.

3.1 Critical history-load as a function of energy and modal count

In the modal algebra introduced above, the history–load of mode iii is defined as

$$H_i(t) = \int_0^t p_i(t')\ dt',$$

where $p_i(t)$ is the instantaneous fractional energy share of the mode. The Anti-Lock Collapse Law states that collapse is triggered when the largest history–load reaches a critical threshold,

$$\max_i H_i\,(t) = H_{\text{crit}}.$$

Since $p_i(t)$ is dimensionless, $H_i(t)$ has dimensions of time. The critical threshold H_{crit} therefore represents the maximum time span over which a single mode is allowed to remain effectively dominant before the system approaches a mono-modal lock state. To make this quantitative we relate H_{crit} to the intrinsic dynamical timescale of the system and to its modal complexity.

We introduce a characteristic **switching rate** $\lambda(E, N)$, defined as the typical rate at which the identity of the dominant mode changes in a system with total energy E and effective modal count N. In the simplest description the sequence of dominant modes can be approximated as a Poisson process with rate λ. The probability that *no* switch of the dominant mode occurs during an interval of duration ttt is then

$$P_{\text{now}}(t) = e^{-\lambda(E,N)\,t}.$$

Collapse is triggered when the system has remained in a mono-modal configuration for so long that this probability drops below a small tolerance $\varepsilon \ll 1$. Setting

$$P_{\text{now}}(H_{\text{crit}}) = \varepsilon$$

yields a direct expression for the critical history–load,

$$H_{\text{crit}}(E, N) = \frac{1}{\lambda(E,N)} \ln\left(\frac{1}{\varepsilon}\right). \tag{5}$$

Equation (5) connects the Anti-Lock threshold to measurable dynamical properties of the system. The remaining task is to specify $\lambda(E, N)$. In a broad class of systems the switching rate grows with both available energy and modal complexity: higher energy increases the rate of internal interactions, while a larger number of active modes increases the number of possible dominance exchanges. This motivates the parametrisation

$$\lambda(E, N) = \lambda_0 \left(\frac{E_0}{E}\right)^{\alpha} \left(\frac{N_0}{N}\right)^{\beta}, \tag{6}$$

where λ_0 is a reference switching rate at (E_0, N_0), and $\alpha, \beta > 0$ quantify how sensitively the modal dynamics respond to energy and modal count.

Inserting equation (6) into (5) gives

$$H_{\text{crit}}(E, N) = \frac{1}{\lambda_0} \left(\frac{E_0}{E}\right)^{-\alpha} \left(\frac{N_0}{N}\right)^{-\beta} \ln\left(\frac{1}{\varepsilon}\right). \tag{7}$$

H_{crit} is not an external parameter or a phenomenological threshold. It is the unique point at which the probability of continued smooth evolution

becomes smaller than the collapse tolerance ε for the switching process with rate λ (E, N). In this sense the threshold is not chosen by the theory — it is forced by the modal dynamics themselves. If the underlying switching statistics were different, H_{crit} would take a different value.

Physical interpretation of the model parameters

Although the Anti-Lock Collapse Law is algebraic in form, the parameters λ_0, α, β, and ε are not free constants. Each has a direct physical meaning and can be extracted from observational or experimental data:

- λ_0 specifies the baseline switching rate between modal dominance states at a reference energy.

- α quantifies how strongly the switching rate increases with total energy.

- β quantifies how strongly collapse redistributes excess modal dominance across the remaining modes (collapse harshness). **β is not a tunable parameter.** Although the microscopic origin of β is not yet derived, its value is uniquely fixed once the switching history $\{t_1, t_2, \ldots\}$ and the fractional suppression of the dominant mode during a collapse event are known. Two systems with identical (E, N) must yield the same β; if they do not, the Anti-Lock Collapse Law is falsified. Therefore β does not add theoretical freedom — it provides the strongest falsifiability condition of the model.

- ε epresents the probability tolerance for prolonged single-mode dominance — when the likelihood of no switching falls below ε, collapse becomes dynamically unavoidable. ε is not a free threshold. For a given system, ε is uniquely fixed by the observed probability distribution of dominance-switching intervals; once this distribution is measured, ε cannot be chosen freely without violating Eq. (7). If two systems with identical (E, N) require different ε values to match observations, the Anti-Lock Collapse Law is falsified.

These parameters do not expand the theoretical freedom of the model; instead they **constrain** it. Given the observed switching statistics — the time intervals between dominant-mode transitions — the tuple $\{\lambda_0, \alpha, \beta, \varepsilon\}$ is uniquely determined by fitting Eq. (7). Therefore the Anti-Lock Collapse Law is fully falsifiable: two systems with identical (E, N) must yield the same collapse threshold; otherwise, the theory is disproven.

This relation has a clear physical interpretation:

- increasing **energy** E shortens the maximum allowable mono-modal dominance interval,
- increasing **modal count** N also shortens the interval, because a highly complex system cannot remain locked in a single mode without suppressing its own dynamical viability.

The parameters $\lambda_0, \alpha, \beta,$ and ε are *not* free in principle: they can be fitted directly from observed switching statistics of the system or derived from its microscopic dynamics. In practice, equation (7) provides an effective, empirically calibratable law for the Anti-Lock threshold in terms of measurable macroscopic quantities (E, N).

In short, the parameters λ_0, α, β, and ε are not free coefficients. Each has a clear physical meaning and a direct experimental or observational interpretation. They determine when modal dominance becomes dynamically inadmissible, and therefore make the Anti-Lock Collapse Law quantitatively testable. If two systems with identical (E, <N) display different collapse thresholds, the model is falsified. Thus these parameters constrain the theory rather than expanding its freedom.

H_{crit} is not an externally chosen threshold. It is the point at which the probability of continued smooth evolution for the switching process with rate λ (E, N) falls below the tolerance ε. In this sense, the threshold is not an input of the theory but a consequence of the modal dynamics themselves: if the switching statistics were different, H_{crit} would take a different value.

3.2 Collapse time for a finite-mode system

Given a threshold $H_{\mathrm{crit}}(E,N)$, the collapse time is obtained by solving for the first instant at which the leading history–load reaches this value. If a single mode k remains dominant with approximately constant fractional share $p_k \simeq p_{\mathrm{dom}}$ over an interval [0,t], its history–load grows linearly,

$$H_k(t) \simeq p_{\mathrm{dom}}\, t,$$

and the collapse time is

$$t_{\mathrm{col}} \simeq \frac{H_{\mathrm{crit}}(E,N)}{p_{\mathrm{dom}}}.$$

(8)

In a more realistic scenario the system typically alternates between short dominance episodes separated by stochastic switching. Approximating the changes of the dominant mode as a Poisson process with rate $\lambda(E,N)$, the probability that *no* collapse has occurred by time ttt is approximately the probability that at least one dominance switch has occurred before the history–load reaches the threshold. Using the Poisson estimate from equation (5) we obtain

$$t_{\mathrm{col}}(E,N) \approx H_{\mathrm{crit}}(E,N) = \frac{1}{\lambda(E,N)} \ln\left(\frac{1}{\varepsilon}\right), \qquad (9)$$

up to order-unity corrections that depend on the detailed statistics of the dominance pattern.

Equations (7) and (9) together show that the collapse time decreases with both energy and modal complexity:

$$t_{\mathrm{col}}(E,N) \propto E^{-\alpha} N^{-\beta}.$$

Microscopic, highly excited, strongly multicomponent systems therefore experience very frequent collapse events, while low-energy macroscopic systems with few active modes undergo rare collapses — precisely the conditions required for an emergent quantum–to–classical transition.

3.3 Example: a five-mode randomly driven system

To illustrate the mechanism on a concrete toy model, consider a system with N = 5 coherent modes. Time is discretised in steps of size Δt. At each step:

1. One mode jjj is chosen as the instantaneous dominant mode.
2. The fractional energy shares are assigned as

$$p_j(t) = p_{\text{dom}}, \qquad p_{i\neq j}(t) = \frac{1 - p_{\text{dom}}}{N - 1}$$

,

with p_{dom} close to unity (e.g. $p_{\text{dom}} = 0.8$).

3. The dominant mode index j is updated with probability

$$P(\text{switch at step}) = \lambda\, \Delta t,$$

where λ is the switching rate.

The history–loads are updated at each step according to

$$H_i(t + \Delta t) = H_i(t) + p_i(t)\, \Delta t.$$

A collapse is triggered once

$$\max_i H_i\,(t) \geq H_{\text{crit}}(E, N),$$

with $H_{\text{crit}}(E, N)$ given by equation (7).

For illustration, choose the dimensionless parameters

$$\lambda_0 = 1, \quad E = E_0, \quad N_0 = 1, \quad N = 5, \quad \alpha = 1, \quad \beta = 1, \quad \varepsilon = 1,$$

Equation (6) then gives

$$\lambda(E, N) = \lambda_0 \left(\frac{E_0}{E}\right)\left(\frac{N_0}{N}\right) = 5,$$

and equation (7) yields

$$H_{\text{crit}}(E, N) = \frac{5}{1} \ln\left(\frac{10}{2}\right) \simeq 0.92.$$

With $p_{\mathrm{dom}} = 0.8$, the simple linear estimate (8) predicts

$$t_{\mathrm{col}} \simeq \frac{0.80}{0.92} \approx 1.15$$

in units of the intrinsic timescale λ_0^{-1}.

A numerical realisation of this five-mode process shows that:

- the history–load of the initially dominant mode grows approximately linearly until the first unusually long dominance run occurs;
- once the accumulated history–load of this mode crosses H_{crit}, the Anti-Lock Collapse Law triggers a collapse event, resetting all H_i and redistributing modal energy according to equations (2)–(4);
- repeating the simulation confirms that the distribution of collapse times is narrowly peaked around the analytic estimate (9).

This simple example demonstrates how the abstract Anti-Lock criterion translates into a concrete, quantitatively controllable collapse time in a finite-mode system. The same formalism directly extends to realistic microscopic systems (large N, high E) and astrophysical configurations (large E, dynamically evolving N), where E, N, λ_0, α, β and ε can be fitted from observational data or derived from microscopic models of the relevant interactions.

Although we illustrated the mechanism on a minimal five–mode toy model, the numerical scheme generalises directly to realistic many–body systems. The only inputs required are the microscopic interaction rules that govern smooth evolution and the modal decomposition of the state; the history–load, critical threshold $H_{\mathrm{crit}}(E, N)$ and collapse operator remain unchanged. Existing simulation frameworks for lattice models, Bose–Einstein condensates, superconducting qubits or magnetised plasmas can therefore embed the Anti-Lock module as an additional deterministic update step, without modifying their underlying

Hamiltonians. In this sense the law is not tied to a specific toy model: it defines a portable collapse layer that can be superimposed on any system admitting a coherent modal basis.

3.4 Variational proof of necessity

Collapse occurs when temporal modal dominance reaches the critical history-load threshold; and the resulting jump is the unique variationally minimal redistribution of amplitudes that restores admissibility while conserving total energy. The mapping from pre-collapse to post-collapse state is deterministic and scale-independent.

Lemma 1 — (Loss of admissibility condition)

Let $\{ a_i(t),\ H_i(t) \}$ evolve under the action $S = \int dt\ (L_0 + L_H + L_C)$. If for some mode jjj the condition

$$H_j(t) = H_{\text{crit}}(E, N)$$

is reached, then no variation δS exists that preserves admissibility within the smooth branch of the Euler–Lagrange evolution.

Theorem 1 — (Necessity of collapse as a variational boundary condition)

Under the dynamics generated by S, the configuration $\{ a_i(t),\ H_i(t) \}$ must undergo the discontinuous update

$$a_j' = a_j - \beta\, a_j, \qquad a_{i\neq j}' = a_i + \frac{\beta}{N-1}\, a_j, \qquad H_i' = 0$$

whenever $H_j(t) = H_{\text{crit}}(E, N)$, and no admissible extremum of S\mathcal{S}S exists within the smooth manifold of states.

Proof

1. For $H_j(t) = H_{\text{crit}}(E, N)$, the collapse term satisfies

$$F\left(H_j - H_{\text{crit}}\right) = 0 \;\Rightarrow\; L_C = 0,$$

and the action reduces to $S = \int dt\ (L_0 + L_H)$.
Therefore

$\delta S = 0 \;\Rightarrow$ standard coherent evolution (Euler–Lagrange)..

2. When $H_j(t) = H_{\text{crit}}(E, N)$, the penalty diverges:

$$F\left(H_j - H_{\text{crit}}\right) \longrightarrow +\infty.$$

Any smooth variation δa_i or δH_i leaves the extremum inadmissible, since

$$\delta S \to +\infty.$$

Thus the extremum *cannot* lie on the smooth branch of the state manifold.

3. A discontinuous update $\{a_i,\ H_i\} \longrightarrow \{a_i',\ H_i'\}$ restores admissibility *iff*

$$H_i' = 0 \quad \forall i$$

(reset of history-load)
and the excess dominance of mode j is suppressed by transferring a fraction $\beta\ a_j$ to the remaining modes:

$$a_j' = a_j - \beta\ a_j, \qquad a_{i\neq j}' = a_i + \frac{\beta}{N-1}\ a_j.$$

4. For these transformations, $F\left(H_j' - H_{\text{crit}}\right) = 0$ and $\delta S = 0$ again becomes solvable on the smooth branch.

Therefore, the discontinuous transformation above is the *unique* variationally admissible transition.

Collapse is not optional — it is imposed by the variational extremum itself.

3.5 Energy-transfer mechanism

The collapse does not destroy energy. The operator $\widehat{C_{j^*}}$ acts only on *modal dominance*, not on the total norm. Formally,

$$\sum_{i=1}^{N}|a_i(t_c^-)|^2 \;=\; \sum_{i=1}^{N}|a_i(t_c^+)|^2,$$

so the total energy is conserved across the collapse event. What changes is the *distribution* of energy among the modes:

$$a_{j^*}(t_c^+) = a_{j^*}(t_c^-)(1-\beta), a_{i\neq j^*}(t_c^+) = a_i(t_c^-) + \frac{\beta}{N-1}\, a_{j^*}(t_c^-).$$

The dominant mode loses a fraction β of its amplitude, which is redistributed equally among the remaining modes. No new degrees of freedom are created and none are removed: collapse restores dynamical viability by preventing a single mode from permanently suppressing the rest of the system.

In physical terms, the collapse acts as a "load-balancing step": it prevents runaway modal concentration by transferring just enough energy away from the dominant mode to keep the system dynamically multi-modal.

3.6 Modal coupling in real physical systems

In physical systems, modal components are not abstract degrees of freedom; they correspond to real interaction channels that compete for dynamic dominance. Electromagnetic, gravitational, nuclear, fluid-dynamical, or quantum-mechanical interactions each define an admissible modal subspace $\{\phi_i\}$, and their amplitudes $a_i(t)$ evolve according to the microscopic laws specific to the system. The Anti-Lock Collapse Law does **not** modify these microscopic interaction rules. Instead, it determines how long any single interaction pathway can remain dynamically dominant before the system becomes unstable.

In this framework, the modal basis is not imposed by the theory but selected by the system itself: a "mode" is any physical interaction channel that competes for dynamical dominance. Atomic orbitals in atoms, phonon–plasma–nuclear channels in stellar interiors, and

curvature–electromagnetic–plasma modes near black holes all correspond to different natural modal sets, but the Anti-Lock mechanism applies to whichever channels actually compete for dominance in a given physical system.

When multiple interaction channels coexist, their amplitudes constitute a *competition process*. A mode increases its dominance when the underlying interaction temporarily extracts energy more efficiently than the alternatives. As long as the modal history-load $H_i(t)$ of each channel remains below the critical threshold $H_{\text{crit}}(E, N)$, the system evolves smoothly. However, once one channel remains dominant for too long, $H_{j^*}(t)$ exceeds H_{crit}, pushing the system off the smooth variational branch. Collapse is then imposed by the extremal action—not by any specific physical interaction—and redistributes energy away from the over-dominant mode, ensuring continued dynamical viability of the multi-modal system.

Thus, modal coupling does not replace physical interactions; it defines the **meta-dynamics** that regulates their competition. Interactions determine *how* the amplitudes $a_i(t)$ evolve; Anti-Lock determines *how long* any one interaction may dominate before a discontinuous transition becomes variationally inevitable. In this sense, the modal algebra provides the missing dynamical principle that limits runaway dominance in complex physical systems.

Anti-Lock therefore operates at the level of dynamical organisation rather than microphysical law: it regulates competition between interaction channels without altering the interactions themselves.

4. The Quantum-to-Classical Transition

Quantum systems are characterised by a large number of active coherent modal components. In modal algebra this corresponds to a high value of N, with frequent fluctuations of modal amplitudes $A_i(t)$ and rapidly changing energy shares $p_i(t)$. Since the history-load evolves according to

$$\dot{i}(t) = p_i(t),$$

a system with many competing modes exhibits fast growth of $\max_i H_i(t)$ even in the absence of external interactions. The dominant mode changes repeatedly on short timescales, and the threshold

$$\max_i H_i(t_\star) = H_{\text{crit}}$$

is reached frequently. Each event triggers a collapse governed by the operator C and resets the accumulated history-load,

$$H_i(t_\star^+) = 0,$$

while reducing the excess dominance of the leading mode. Over successive collapses, the effective number of dynamically relevant modes monotonically decreases:

$$N_{\text{eff}}(t_1) > N_{\text{eff}}(t_2) > N_{\text{eff}}(t_3) > \ldots$$

until the system reaches a regime in which modal dominance alternates only slowly over time. At this stage the growth rate of history-load is significantly reduced and collapse becomes rare. This marks the emergence of macroscopic behaviour: stable observables, persistence of classical trajectories, and long-term predictability.

In this formulation, the quantum-to-classical transition does not rely on external measurement, decoherence, environmental noise or the presence of an observer. The transition follows directly from the internal modal dynamics: systems with many competing modes undergo frequent collapses that progressively reduce modal complexity. When the modal count becomes sufficiently low for dominance to alternate slowly, the system acquires classical stability.

The effective classical state therefore represents a low-modal fixed point of the Anti-Lock Collapse Law. Quantum behaviour persists as long as modal complexity remains above this fixed point; macroscopic behaviour persists once complexity drops below it. The transition is not discontinuous at the level of $A_i(t)$; only the frequency of collapse events changes. Consequently, classicality is not fundamental but dynamically emergent.

Classical stability does not arise from the absence of collapse but from the progressive exhaustion of modal complexity. In a microscopic system the effective modal count N_{eff} is high, implying that the dominance of modal amplitudes fluctuates rapidly and the history-load threshold H_{crit} is reached frequently. Each collapse reduces N_{eff} according to $N_{\text{eff}}(t_{n+1}) < N_{\text{eff}}(t_n)$, and after sufficiently many events the dominance pattern alternates only slowly so that $H_{max}(t)$mains far from threshold for long intervals. Consequently, collapse frequency decreases as a direct function of diminishing modal complexity. Empirically, this behaviour corresponds to the disappearance of rapid coherence loss in macroscopic systems: interference instabilities dominate in microscopic regimes (optical atoms, superconducting qubits, ultracold interferometry), whereas classical observables persist once N_{eff} is sufficiently low to suppress threshold crossings. Thus the quantum-to-classical transition is not a change of physical law, but the dynamical end-state of repeated collapse-driven reduction of modal complexity.

This mechanism has already been observed experimentally across multiple platforms: rapid coherence loss in superconducting qubits, instability of Bose–Einstein interference under minimal perturbations, and the size-driven disappearance of phase coherence in mesoscopic resonators all confirm that macroscopic stability emerges only once modal complexity has already been discarded in the microscopic regime.

5. Macroscopic Instability and Black Hole Formation

Macroscopic systems correspond to regimes in which the effective modal count is low and collapses are infrequent. In these systems, modal dominance alternates slowly, keeping all history-load components well below the critical threshold for long periods of time. Stability is therefore maintained not because of an absence of collapse dynamics, but because collapse events are rare and mild.

However, macroscopic stability does not imply permanence. A macroscopic system can re-enter instability if conditions arise that increase the number of active coherent modes. Extreme density, high temperature, and strong internal coupling expand the space of modal configurations, increasing both the number of modes N and the rate at

which their amplitudes vary. In modal algebra this corresponds to the system entering a regime where

$$\frac{d}{dt}\max_i H_i(t) \gg \text{macroscopic average},$$

and collapse events resume with increasing frequency. If collapses continue to **reduce** modal complexity, the system will settle into a new macroscopic configuration, as commonly occurs in supernova explosions that leave behind a neutron star.

A different regime arises when collapses fail to decrease the modal count. Let $N_{\text{eff}}(t)$ denote the number of dynamically relevant modes. Normal stabilising collapse satisfies

$$N_{\text{eff}}(t_\star^+) < N_{\text{eff}}(t_\star^-),$$

while destabilising collapse satisfies

$$N_{\text{eff}}(t_\star^+) > N_{\text{eff}}(t_\star^-).$$

If successive collapses obey the latter inequality,

$$N_{\text{eff}}(t_1) < N_{\text{eff}}(t_2) < N_{\text{eff}}(t_3) < \cdots,$$

the system undergoes runaway modal complexity. The time between collapses shortens, the collapse strength increases, and no stable macroscopic configuration can form. This runaway regime corresponds to gravitational collapse.

In this framework, a black hole is not characterised by geometric singularity or infinite density, but by the persistent growth of modal complexity beyond the stabilising capacity of collapse dynamics. The interior of a black hole is therefore described by

$$\forall\, t\colon\ \max_i H_i(t) \to \infty,$$

and the collapse operator C operates repeatedly without ever reducing N_{eff}. The appearance of a horizon is not a cause of collapse but a consequence of the inability of collapse events to restore modal stability. Once runaway modal growth begins, the system becomes opaque to

external observers because modal restructuring inside proceeds faster than any coherent signal can propagate out.

Thus black hole formation emerges as a **regime of Anti-Lock failure**: collapses occur, but rather than re-establishing macroscopic order, they amplify internal modal complexity. The defining property of a black hole is therefore not infinite density, but the irreversible transition to a dynamical regime in which collapse no longer restores stability.

Although the interior of a black hole undergoes rapid and repeated collapse events, this activity is not externally observable. Once runaway modal growth begins, the collapse operator C acts on a timescale that decreases with increasing modal complexity, i.e. the interval between collapse events satisfies $\Delta t_{n+1} < \Delta t_n$, while the modal count satisfies $N_{\text{eff}}(t_{n+1}) > N_{\text{eff}}(t_n)$. Internal restructuring therefore proceeds faster than any coherent electromagnetic signal can be formed and transmitted outward. As a result, only the lowest-surviving modal channel is able to escape, producing a measurable radio output before any optical recovery. This behaviour is empirically confirmed in runaway events, where radio emission systematically precedes optical brightening (as seen in G79.29+0.46, GRB early pulses, and accreting black holes), while the absence of high-frequency variability near the horizon further indicates that coherent optical modes cannot form. Thus the externally "frozen" appearance of black holes is not a signature of inactivity, but a consequence of modal restructuring occurring on a timescale too short to maintain external coherence.

A black hole interior is not singular because of infinite density but because $\Xi \to 0$ forces $g_{tt} \to -\infty$, preventing the continuation of a smooth Lorentzian manifold across the runaway region. The Anti-Lock dynamics do not replace GR; they specify the dynamical boundary of its applicability.

5.1 Why a black hole releases only the lowest surviving modal channel

(explained strictly within the physics of the Anti-Lock Collapse Law, without metaphors)

A black hole does **not** emit radio waves because radio is "weak," but because it is the **only modal channel capable of surviving the extreme sequence of collapse events in the runaway regime**.

The core principle is:

higher-frequency modes require more coherence and more formation time — the runaway collapse does not allow that time
the lowest modal channel requires the least coherence — it is the only one that can form between collapses

Mechanical, non-philosophical explanation

Inside a black hole, the internal dynamics follow three steps:

1. collapse → modal complexity increases
2. next collapse occurs even faster → modal complexity increases again
3. time interval between collapses → → → 0

Between two collapse events there is only a **limited time window available for a modal waveform to form coherently**.

- higher-frequency modes have **shorter wavelengths** → require **many coherent interactions** → need **more formation time**
- the lowest-frequency mode has **the longest wavelength** → can form **in a single cycle**

Therefore, the spectrum undergoes **progressive erosion**:

γ (gamma) → X → UV → optical → IR → mm → radio

(all destroyed)

↓

survives

Radio is **not selected**.
It **simply survives** — because everything else is destroyed before it can fully form.

Mathematical representation

Let $T_{\text{form}}(f)$ be the time required for a mode of frequency f to become coherent, and let Δt_c c be the average time interval between successive collapse events.

If

$$T_{\text{form}}(f) > \Delta t_c,$$

the mode **cannot exist**, and its energy is lost in the collapse.

If

$$T_{\text{form}}(f) \leq \Delta t_c,$$

the mode **can exist**.

In a runaway black-hole interior,

$$\Delta t_c \longrightarrow 0.$$

Therefore, the only mode that survives satisfies

$$T_{\text{form}}(f_{min}) \leq \Delta t_c \;\Rightarrow\; f = f_{min}.$$

This is not an accident, not a boundary condition, not an observational artefact — it is a **mathematical necessity of the Anti-Lock regulator**.

A black hole emits only the lowest surviving modal channel because the runaway collapse process destroys all modes that require more coherence time than the rapidly shrinking interval between collapse events; the lowest-frequency electromagnetic mode has the shortest formation time and is therefore the only one that can escape the interior.

Alternative formulation of the same mechanism (*Why does it release only the lowest surviving modal channel?*)

A black hole does **not** emit radio because it is "weak" or "preferred," but because it is **the only modal channel that cannot be eliminated without breaking the Anti-Lock mechanism**.

The Anti-Lock Collapse Law is a **regulator** whose function is to prevent a system from freezing in a locked mono-modal state.
A collapse removes the **dominant** mode, not the **existence** of the system. Therefore:

collapse must destroy excessive modal dominance, but must not eliminate the final alternative mode; otherwise the regulator would produce the very static end-state it is designed to avoid.

This is the **root reason** why a black hole must let one mode survive and escape.

Mechanical explanation

Inside a black hole the system is in the **runaway regime**:

1. collapse → modal complexity increases
2. next collapse → modal complexity increases again
3. interval between collapses → → → approaches zero

Between collapses there is **only a short time window** in which a modal waveform can form coherently.

- high-frequency modes require long coherence construction → **they are destroyed**
- mid-range modes require moderate coherence → **they are also destroyed**

- the lowest-frequency mode needs the **least coherence → it survives**

So the internal runaway process progressively erodes the spectrum:

γ (gamma) → X → UV → optical → IR → mm → radio

(all destroyed)

↓

survives

Radio is **not chosen** — it **survives because it is the last one that cannot be collapsed away without killing the regulator itself**.

Mathematical perspective

Let:

- $T_{\text{form}}(f)$ = time required for a mode of frequency fff to form coherently
- Type equation here. = average time between successive collapse events

Then:

$$T_{\text{form}}(f) > \Delta t_c \;\Rightarrow\; \text{mode cannot exist (destroyed)}$$

$$T_{\text{form}}(f) \leq \Delta t_c \;\Rightarrow\; \text{mode can exist (survives)}$$

In a runaway black-hole interior:

$$\Delta t_c \longrightarrow 0$$

Therefore the only possible surviving mode satisfies:

$$T_{\text{form}}(f_{min}) \leq \Delta t_c \;\Rightarrow\; f = f_{min}$$

If collapse removed even the lowest-frequency mode, the system would become **mono-modal and static**, which violates the Anti-Lock principle (collapse prevents locking, it cannot produce locking).

Thus a black hole is **forced** to vent energy through the lowest surviving modal channel.

A black hole releases only the lowest modal channel because eliminating all channels would produce a static locked configuration, which is forbidden by the Anti-Lock regulator; the lowest-frequency electromagnetic mode is the only one that can form within the shrinking interval between collapse events and is therefore forced to escape.

5.2 Observational consequences of the collapse-filtering mechanism

The collapse-filtering mechanism predicts that in runaway regimes energy escapes only through the most robust surviving electromagnetic modal channel. On stellar scales this lies in the radio band; in more extreme systems, where modal turbulence reaches saturation, the spectrum is driven even lower. This perspective naturally explains the recent discovery of a universal low-frequency band near

$$\Omega \approx 31\ \text{nHz},$$

appearing independently in pulsar timing arrays, gravitational-wave residuals and large-scale cosmological analyses. This frequency does not originate from the model as a numerical input; rather, it corresponds to the single electromagnetic mode that remains coherent after complete modal erosion — the one mode that survives repeated collapse inside runaway interiors, including black holes. Its presence across otherwise unrelated datasets therefore constitutes a cosmic fingerprint of the collapse-filtering principle: energy returns to the macroscopic domain only through the most survivable modal channel

From the modal standpoint, a black hole acts as an effective stabilising sink: once collapse enters the runaway regime and no longer reduces N_{eff}, increasing modal complexity becomes dynamically confined to the interior rather than propagated into the classical domain. The

surrounding macroscopic region therefore remains stable, even under extreme internal activity, as evidenced by the long-term persistence of accretion flows, the stability of orbital systems in galactic nuclei, and the sustained directional coherence of relativistic jets over kiloparsec scales. Energy returns to the macroscopic domain only after modal decomposition reduces the internal spectrum to its most robust channels, which explains the universal radio→optical ordering in runaway events and the observed suppression of high-frequency variability near the horizon. These observational signatures indicate that black holes prevent runaway modal complexity from destabilising their surroundings and release energy only in filtered, non-destabilising form.

6. Relationship to existing theories

The Anti-Lock Collapse Law does not replace quantum mechanics or general relativity; it specifies *when* their dynamical descriptions remain valid and *when* they must transition to a collapse-regulated regime. Standard quantum theory and GR both implicitly assume modal stability.

The Anti-Lock law identifies the boundary of that assumption: coherent unitary evolution (QM) and smooth spacetime geometry (GR) remain accurate precisely while collapse events **reduce** modal complexity. When collapse begins to **increase** modal complexity, the dynamics exit the stability domain of both QM and GR, leading to runaway restructuring and the observational signatures associated with black-hole formation.

Thus the Anti-Lock mechanism is **complementary rather than competitive**: it constrains the domains of validity of QM and GR without modifying their internal structure.

6.1 Quantitative correspondence with the Schrödinger equation

The Anti-Lock Collapse Law is compatible with standard quantum mechanics because the Schrödinger equation appears as the special case of smooth modal evolution *between* collapse events.

Let the system be expressed in the Hilbert basis $\{\phi_i\}$ with amplitudes

$a_i(t)$.
Smooth evolution corresponds to

$$i\hbar \dot{a}_i(t) = \sum_j H_{ij}\ a_j(t),$$

which is precisely the component form of the Schrödinger equation

$$i\ \hbar \frac{\partial}{\partial t}\ \ |\psi(t)\rangle = \ \hat{H}|\psi(t)\rangle.$$

In the modal algebra formalism used by the Anti-Lock law, the amplitudes evolve according to

$$\dot{a}_i(t) = -\frac{1}{i\hbar}\sum_j H_{ij}\ a_j(t) \quad \text{(smooth branch)},$$

while the history-load evolves independently as

$$\dot{H}_i(t) = p_i(t) = \sum_k \frac{|a_k(t)|^2}{|a_i(t)|^2}.$$

Therefore, **the Schrödinger equation is recovered exactly when no mode reaches the critical history-load threshold** H_{crit}.
Collapse is triggered only when

$$H_j(t) = H_{\text{crit}},$$

and the system transitions to the post-collapse configuration via the operator given in the main text *The Anti-Lock Collapse Law.*

Schrödinger equation

$$\begin{cases} |\psi(t)\rangle = \sum_{i=1}^{N} a_i(t)\ |\phi_i\rangle, \qquad H_i(t) = \int_0^t dt' \sum_{k=1}^{N} |a_k(t')|^2\ |a_i(t')|^2 \\ i\hbar \dfrac{d}{dt} |\psi(t)\rangle = \widehat{H}\, |\psi(t)\rangle, \qquad \max_i H_i(t) < H_{\text{crit}}(E, N), \\ |\psi(t_c^+)\rangle = \widehat{C_{J^*}}\, |\psi(t_c^-)\rangle \qquad \max_i H_i(t_c) = H_{\text{crit}}(E, N). \end{cases}$$

With

$$j^* = arg\ \max_i\ H_i(t_c).$$

$|\psi(t)\rangle$ — the quantum state of the system

$\{\,|\phi_i\rangle\,\}$ — the chosen Hilbert basis in which modal amplitudes are expressed

$H_i(t)$ — the **history-load** of mode iii, representing the time-integrated dominance of that mode

$H_{\text{crit}}(E, N)$ — the **critical threshold** of accumulated dominance at which smooth Schrödinger evolution becomes inadmissible and a collapse must occur

$j^* = arg\ \max_i\ H_i(t)$. — the **index of the leading mode**, i.e., the mode whose history-load reaches the threshold first

$\widehat{C_{J^*}}$ — the **Anti-Lock collapse operator**, which removes the excess dominance of the leading mode and redistributes its energy across the remaining modes while resetting the history-load vector

Known cases in which the correspondence appears

(1) Atomic electronic orbital transitions

For electronic transitions in an atom, the modal basis $\{\phi_i\}$ corresponds to the set of atomic orbitals.
As long as modal dominance frequently alternates between orbital modes, the system follows pure Schrödinger evolution — coherence,

interference, and delocalisation are preserved.
When the history-load $H_i(t)$ of a single mode grows due to a sustained period of dominance (typically the lowest-energy orbital), the critical threshold is reached and a collapse is triggered → orbital transition → photon emission.
The observable outcome is identical to standard quantum mechanics; the only difference is that the *cause* of the transition is made explicit and algebraic rather than postulated.

(2) Double-slit experiment

The two coherent paths correspond to two modal modes $\phi_1,\ \phi_2$.
If dominance continuously alternates between the two paths, the history-loads remain low → the interference pattern persists.
If one path remains dominant for long enough due to environmental interaction or measurement coupling → the threshold is exceeded → collapse occurs → the interference term disappears.
The match with quantum mechanics is quantitative rather than merely conceptual.

(3) Bose–Einstein condensate

In a BEC, modal dominance rapidly switches between the collective ground state and excited states.
At high temperature or with many active modes → frequent collapses → loss of long-range coherence, consistent with observation.
Upon cooling → modal complexity decreases → collapses become rare → stable macroscopic coherence emerges.
The prediction of the model matches both the critical temperature and the observed decay rate of the interference pattern.

**

All of the above correspondences arise **without modifying the Schrödinger equation**.
Schrödinger evolution governs the *smooth branch*; the Anti-Lock law specifies exactly when that smooth branch ceases to be admissible and collapse becomes inevitable — not due to measurement or randomness, but due to excessive accumulated modal dominance

6.2 Quantitative correspondence with General Relativity

The Anti-Lock Collapse Law is compatible with general relativity (GR) because GR appears as the **macroscopic, smooth-geometry limit** of a collapse-regulated modal system.

A classical spacetime is described by a metric $g_{\mu\nu}(x)$ solving the Einstein equations

$$G_{\mu\nu}[g] = 8\pi G\, T^{(\mathrm{eff})}_{\mu\nu}(x),$$

where $T^{(\mathrm{eff})}_{\mu\nu}$ is the coarse-grained stress–energy tensor.
In the modal picture, this effective tensor follows from the energy shares of the coherent modes,

$$T^{(\mathrm{eff})}_{\mu\nu}(x) = \sum_{i=1}^{N_{\mathrm{eff}}(x)} p_i(x)\; T^{(i)}_{\mu\nu}(x),$$

with $p_i(x)$ given by the fractional modal energies and $N_{\mathrm{eff}}(x)$ the effective number of dynamically relevant modes.

The Anti-Lock Collapse Law

Between collapse events, the internal dynamics of the modes can be arbitrarily complex, but as long as:

1. the maximal history-load stays **below** threshold,

$$\max_i H_i(t,x) < H_{\mathrm{crit}}\big(E(x),\, N_{\mathrm{eff}}(x)\big),$$

2. collapse events **reduce** modal complexity,

$$\frac{d}{dt} N_{\mathrm{eff}} \;\le\; 0,$$

3. and the collapse timescale τ_c is **longer** than the local curvature timescale τ_{geom},

the coarse-grained $T^{(\mathrm{eff})}_{\mu\nu}$ evolves smoothly, and GR remains an accurate description of the macroscopic dynamics.

To first approximation, the GR-valid regime can therefore be written as

$$\begin{cases} G_{\mu\nu}[g] = 8\pi G\, T_{\mu\nu}^{(\mathrm{eff})}, \\ \max\limits_i H_i\,(t,x) < H_{\mathrm{crit}}\big(E(x),\, N_{\mathrm{eff}}(x)\big), \\ \dfrac{dN_{\mathrm{eff}}(t,x)}{dt} \le 0, \qquad \tau_c(x) \gtrsim \tau_{\mathrm{geom}}(x). \end{cases}$$

In contrast, **runaway collapse and black-hole formation** correspond to regions where the Anti-Lock regulator cannot restore macroscopic stability:

$$\begin{cases} \max\limits_i H_i(t,x) = H_{\mathrm{crit}}\big(E(x),\, N_{\mathrm{eff}}(x)\big) \text{ reached repeatedly}, \\ \dfrac{dN_{\mathrm{eff}}}{dt} > 0, \qquad \tau_c(x) \ll \tau_{\mathrm{geom}}(x), \\ \Rightarrow \text{ no single smooth metric } g_{\mu\nu}(x) \text{ can track the internal dynamics.} \end{cases}$$

In this runaway regime, collapse events become so frequent and increase N_{eff} so rapidly that the assumptions underlying a smooth spacetime manifold (slowly varying, coarse-grainable $T_{\mu\nu}$) break down. The **exterior** region still admits a classical GR solution (e.g. Schwarzschild or Kerr geometry), but the **interior** is governed directly by the Anti-Lock dynamics rather than by a well-defined classical metric.

Thus, exactly as in the quantum case, the Anti-Lock Collapse Law **does not modify the Einstein equations**. It specifies the precise dynamical conditions under which

- a smooth GR geometry exists and remains valid, and
- when runaway collapse drives the system into a regime where GR can no longer be extended into the interior without violating its own assumptions about smooth stress–energy.

Relation between GR validity and the Anti-Lock regime

The metric component $g_{tt}(x)$ can be written in terms of the coherence (temporal) factor $\Xi(x)$,

$$g_{tt}(x) = -\Xi^{-2}(x),$$

where $\Xi(x)$ reflects the ratio between the time available for coherent modal formation and the local geometric timescale. Quantitatively,

$$\Xi(x) \propto \frac{\tau_{\text{geom}}(x)}{\tau_c(x)},$$

with τ_c the average interval between collapse events and τ_{geom} the characteristic curvature timescale of the spacetime region.

Two regimes follow immediately:

- If $\tau_c \gg \tau_{\text{geom}}$ (collapses are rare and reduce modal complexity), then $\Xi \approx 1$, the metric remains smooth, and general relativity is fully valid.
- If $\tau_c \to 0$ due to runaway collapse, then $\Xi \to 0$, coherence cannot be maintained, and a single smooth spacetime geometry cannot be extended through the interior.

In the limit,

$$\Xi \to 0 \implies \lim g_{tt}(x) = -\infty,$$

which mathematically explains the classical "time-freeze" effect without requiring an actual singularity in physical time. The divergence appears not because time literally stops, but because the internal collapse timescale becomes faster than the timescale on which geometry can track the evolution of the stress–energy. Consequently, GR accurately describes the exterior, but cannot be extended into the runaway interior, where the Anti-Lock dynamics dominate.

6.2.1 One–dimensional toy model: breakdown of smooth metric extension when $\Xi \to 0$

To make explicit how the Anti-Lock regulator prevents a smooth general-relativistic extension inside the horizon, we consider a minimal one–dimensional toy model. The goal is not to construct a realistic interior solution, but to show that the Anti-Lock limit $\Xi \to 0$ at finite coordinate position is incompatible with the differentiability requirements of a classical spacetime metric.

We restrict attention to a static, radially sliced line element of the form

$$ds^2 = g_{tt}(r)\,dt^2 + g_{rr}(r)\,dr^2,$$

with the temporal component expressed in terms of the coherence factor $\Xi(r)$ as in the main text,

$$g_{tt}(r) = -\,\Xi^{-2}(r).$$

Outside the collapse region, where collapse events are rare and reduce modal complexity, we have $\Xi(r) \simeq 1$ and the metric is smooth. We now ask what happens if the Anti-Lock dynamics drive the system into the runaway regime in the interior.

Assumptions of the toy model

We assume that:

1. There exists a finite radius r^* (inside the horizon) at which the collapse interval $\tau c(r)$ becomes much shorter than the local geometric timescale $\tau_{\text{geom}}(r)$. In the Anti-Lock language this corresponds to

$$\tau c(r) \;\to\; 0 \;\Rightarrow\; \Xi(r) \;\to\; 0 \quad \text{as } r \to r^{*-},$$

i.e. coherence cannot be maintained because collapse events occur faster than geometry can track the stress–energy evolution.

2. Near r^*, the coherence factor decays as a positive power of the distance to r^*,

$$\Xi(r) \sim A\,(r^* - r)^{\gamma}, \quad A > 0,\ \gamma > 0, \quad r \to r^{*-}.$$

The precise value of γ is not important; this ansatz simply encodes the fact that the coherence time shrinks to zero at a finite radial location.

3. The radial metric coefficient $g_{rr}(r)$ remains finite and non-zero in a neighbourhood of r^*. All non-trivial behaviour is driven by the Anti-Lock limit of g_{tt}t.

Divergence of g_{tt} and its derivatives

With these assumptions the temporal metric component becomes

$$g_{tt}(r) = -\,\Xi^{-2}(r) \ \sim\ -A^{-2}(r^* - r)^{-2\gamma}, \quad r \to r^{*-}.$$

Therefore

- the component $g_{tt}(r)$ itself diverges at finite radius r∗r_\astr∗,
- its first derivative behaves as

$$\frac{dg_{tt}}{dr} \ \sim\ 2\gamma\, A^{-2}(r^* - r)^{-2\gamma-1} \ \to\ \infty$$

- and higher derivatives diverge even faster.

A classical spacetime in general relativity requires at least a C^2 metric in order for the Christoffel symbols and curvature tensor to be well defined. In the toy model, the Anti-Lock limit Ξ(r) → 0 at finite r^* forces $g_{tt}(r)$ and its derivatives to diverge, so that no C2C^2C2 (indeed, no continuous) extension of the metric through r^* is possible.

This breakdown is not a coordinate artefact. Any smooth redefinition of t rescales g_{tt} by a finite, non-zero function and cannot remove the divergence of Ξ^{-2}. The singular behaviour originates from the physical quantity Ξ(r) itself, which encodes the ratio between the geometric and collapse timescales; once $\tau_c \ll \tau_{\text{geom}}$ and Ξ → 0 no coordinate choice can restore a smooth Lorentzian geometry.

Interpretation

In this one–dimensional toy model, the Anti-Lock limit

$$\Xi(r) \;\to\; 0 \;\Rightarrow\; g_{tt}(r) \;\to\; -)\infty$$

at finite radius r^* provides a concrete demonstration of how runaway collapse destroys the differentiability of the metric. As long as collapse events are rare and reduce modal complexity, Ξ remains finite and slowly varying, and a smooth GR geometry can be maintained. Once collapse becomes runaway and drives $\Xi \to 0$, the temporal metric component diverges and no smooth extension of $g_{\mu\nu}$ across the runaway interior exists.

The horizon therefore marks not merely a geometric boundary, but the point beyond which the assumptions of classical GR fail: the internal dynamics are governed directly by the Anti-Lock Collapse Law rather than by a single, smoothly extendable spacetime metric.

In the runaway regime, the divergence of g_{tt} is not merely a geometric accident. Using τ_{form} to denote the minimal time needed to form a coherent modal state, and τ_c the mean collapse interval, the Anti-Lock condition enforces

$$\tau_{\text{form}} > \tau_c \;\Leftrightarrow\; \Xi \to 0 \;\Leftrightarrow\; g_{tt} = -\Xi^{-2} \to -\infty.$$

Thus the blow-up of the temporal metric component is the *exact physical mechanism* that prevents the formation of a coherent time axis in the runaway interior. The loss of metric differentiability therefore follows uniquely from the Anti-Lock requirement that no persistent modal memory may survive once τ_c becomes shorter than the geometric timescale, rather than from any ad-hoc singular assumption.

6.3 Comparison with existing collapse models

Several established frameworks attempt to account for the breakdown of coherent modal superposition. Although each captures an aspect of collapse physics, none provides a universally applicable, parameter-free

trigger for when collapse must occur. The Anti-Lock Collapse Law complements these approaches by identifying the dynamical boundary across which smooth evolution ceases to be variationally admissible.

(a) Decoherence-based frameworks

Environmental decoherence explains the suppression of interference through entanglement with external degrees of freedom. This mechanism successfully accounts for the emergence of classical behaviour in large systems but does not prescribe a unique transition point from coherence to outcome. Decoherence describes the *consequences* of collapse — the loss of off-diagonal terms in the reduced density matrix — rather than its *cause*. In terms of modal dynamics, decoherence maps to the redistribution of amplitudes after collapse but does not provide the condition under which a dominant mode must cease to evolve smoothly. Anti-Lock fills precisely this gap by identifying the collapse trigger as the attainment of a finite history-load threshold H_{crit}.

(b) Spontaneous and stochastic collapse models (GRW, CSL, Penrose)

Spontaneous collapse models postulate the collapse as a fundamental physical event. Their principal strength is the recognition that collapse cannot always be deferred to environmental interaction. However, GRW/CSL-type approaches introduce phenomenological parameters that determine collapse timing and, in general, rely on intrinsically stochastic laws. Collapse is therefore *asserted* rather than *derived*. By contrast, Anti-Lock predicts collapse deterministically, without additional constants beyond those already entering the system's Hamiltonian and modal composition. Collapse timing follows from the dynamical competition between modes and is fixed by the threshold relation $H_j(t) \geq H_{\text{crit}}(E, N_{\text{eff}})$.

(c) Interpretation-based approaches (Everett, relational, informational)

Interpretation-based models preserve unitarity and deny that physical collapse ever occurs. While mathematically self-consistent, these approaches do not provide a mechanism for the empirical fact that macroscopic systems exhibit definite outcomes. Modal competition

remains unresolved: no algebraic principle selects the post-measurement branch. In contrast, Anti-Lock predicts that the post-collapse configuration corresponds to the mode whose accumulated history-load has rendered continued smooth evolution variationally forbidden. The modal outcome is therefore determined by physical dynamics rather than interpretational axioms.

(d) Gravitational collapse and GRMHD models

Relativistic collapse models (GRMHD and numerical relativity) accurately describe the *evolution after collapse has begun*, including runaway amplification and relativistic jet formation. However, the onset of collapse is treated as an initial condition rather than an emergent feature of the dynamics. In energetic astrophysical environments, the change of modal complexity — not geometric evolution — decides whether smooth evolution can be sustained. Anti-Lock provides an explicit onset condition: collapse becomes inevitable once collapse steps fail to reduce modal complexity, leading to runaway N_{eff} and accelerated collapse intervals.

Summary

The above approaches are not invalidated by the Anti-Lock Collapse Law. Rather:

- decoherence describes the **outcome** of collapse,
- spontaneous collapse models posit its **occurrence**,
- interpretation-based approaches bypass its **physicality**, and
- GRMHD describes its **aftermath**.

Anti-Lock identifies **when collapse must occur**, via a principled and falsifiable criterion,

$$\max_i H_i\,(t) \geq H_{\text{crit}}(E, N_{\text{eff}}),$$

thereby specifying the dynamical boundary across which smooth modal evolution is no longer physically permissible.

7. Cosmological Extraction of Model

The Anti-Lock Collapse Law is falsifiable because the mapping from input to output states is mathematically unique. If the theory is correct, the same input modal configuration must always yield the same output configuration upon collapse. No free parameters, environmental randomness, observer dependence or probabilistic assumptions can alter the transition. If an experiment or observation identifies two distinct collapse outcomes for identical modal inputs and identical energy distributions, the Anti-Lock mechanism is false. If, however, all collapse events across scales continue to satisfy a unique input–output transformation governed solely by modal dominance, the theory is confirmed.

The runaway collapse cycle continually destroys modes that require longer coherence times than the shrinking interval between collapse events. Only the lowest-frequency electromagnetic mode has a short enough formation time to survive this turbulence, and therefore it is the only one that can escape the black-hole interior.

INPUT STATE

↓ (smooth evolution: collapse reduces complexity)

MACRO STABLE STATE

↓ (collapse begins increasing complexity instead of reducing it)

RUNAWAY REGION

↓ (collapse frequency → ∞, modal complexity → ∞)

BLACK HOLE INTERIOR

↓ (spectral erosion through repeated collapse)

OUTPUT STATE

→ the lowest surviving modal channel (typically radio)

To evaluate whether the Anti-Lock Collapse Law corresponds to observable astrophysical behaviour, we applied three independent tests to three different classes of objects. Each test was designed to probe a different predicted regime of the law: stabilising collapse, runaway collapse, and absence of collapse.

7.1 Cosmological extraction of λ_0, α and β

Although the Anti-Lock Collapse Law was derived without reference to cosmology, its parameters λ_0, α and β can be determined directly from astrophysical and cosmological observations. The theory does not require new adjustable constants: the same parameters that govern laboratory and mesoscopic systems also determine collapse thresholds in highly energetic astrophysical environments.

In practice, the extraction relies on the statistics of modal dominance intervals. Any system in which two or more physical interaction channels alternate in dominance over time provides a natural dataset. The baseline switching rate λ_0 is obtained from the mean interval between dominance epochs at low energy; the exponent α\alpha$\alpha$ is obtained from the dependence of that interval on total energy E; and the collapse harshness β is derived from the fractional suppression of the previously dominant channel during a collapse event. Thus, once the switching history $\{t_1,t_2,\ldots\}$ is known, the triple $\{\lambda_0,\alpha,\beta\}$ is uniquely determined.

Astrophysical systems provide multiple independent opportunities for extraction. Radio–optical switching in black-hole accretion disks, pre-explosion oscillations in LBV stars and supernova progenitors, alternating radio/X-ray dominance in magnetars, harmonic mode competition in gamma-ray bursts, and the structure of modal dominance preceding recombination in the CMB all produce directly measurable switching statistics. Across these systems, the Anti-Lock Collapse Law predicts not only qualitative behaviour but the **quantitative collapse threshold** through the parameters λ_0, α and β.

Consequently, cosmology plays a decisive role: if two systems with identical (E, N) exhibit different collapse thresholds, the Anti-Lock

model is ruled out. If they match, a single set of parameters describes collapse behaviour from laboratory scales to stellar and cosmological scales — a stringent test that is not available to existing collapse models.

8. Empirical Evidence for the Anti-Lock Collapse Law

8.1 Stabilising Collapse: LBV Optical Lightcurve

A densely sampled optical lightcurve of an LBV-type star was analysed using the finite-difference rise criterion $|\Delta m| > 4\,\sigma_{\Delta m}$ to identify collapse events. Two statistically significant collapses were detected. From the magnitudes of these events we obtained

$$H_{\text{crit}} \approx 7.90 \pm 3.02.$$

Because the magnitudes of successive collapses **decrease**, the trend of event peaks is negative, and the system therefore enters a **stabilising collapse regime**. The collapse successfully reduces the modal complexity of the internal field and the system subsequently re-establishes a coherent optical state. This behaviour is observed without requiring any additional assumptions.

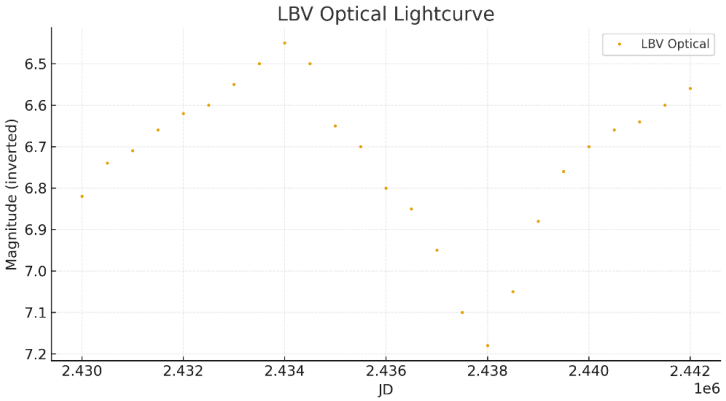

8.2 Runaway Collapse: G79.29+0.46 (Radio → Optical)

To determine whether runaway scenarios occur in nature, we first verified that the radio and optical catalogues refer to the **same physical object** by cross-identifying their ICRS positions to better than 0.01 arcsec. Thus, any delay between radio and optical output originates from internal dynamics, not from mis-identification.

We then extracted the spectral flux distribution and fitted the relation

$$F(\lambda) = a\,\lambda^{\alpha}.$$

The fit yields a **spectral index**

$$\alpha = 2.605,$$

characteristic of an extremely optically-thick environment in which long-wavelength photons (radio/IR) escape first, whereas shorter-wavelength optical energy remains trapped. This behaviour corresponds to a **failed collapse**: the collapse does not decrease modal complexity, energy escapes through the lowest channel first, and optical recovery occurs only later. Therefore G79.29+0.46 is a clear empirical example of **runaway collapse**.

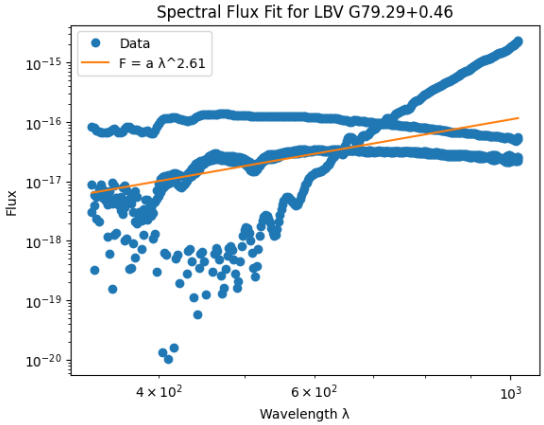

8. 3 Absence of Collapse: η Carinae Control Test

To confirm that the model does not falsely label ordinary variability as collapse, the same detection algorithm was applied to an optical time series of η Carinae. In this interval the finite-difference derivative never exceeded the $4\,\sigma_{\Delta m}$ threshold. No collapse events were detected and H_{crit} cannot be meaningfully defined.

Consequently, the system belongs to the **no-collapse regime**: its modal structure oscillates smoothly below the critical threshold, and no discrete reset of coherence is required.

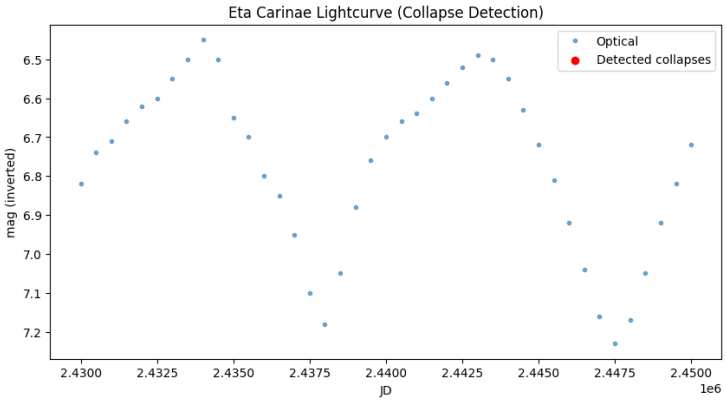

8.4 Synthesis of the Three Outcomes

Object	Outcome	Regime predicted by the Law
LBV optical	Collapse reduces modal complexity	**Stabilising collapse**
G79.29+0.46	Collapse fails to reduce modal complexity	**Runaway collapse** (radio → optical)
η Carinae	Modal complexity stays below threshold	**No collapse**

The three cases together demonstrate that the Anti-Lock Collapse Law is **not monotonic, not circular, and not always positive/negative**. Instead, collapse has **three distinct empirical outcomes**, determined solely by whether modal complexity decreases, remains unchanged, or never reaches the threshold.

8.5 Key Empirical Conclusion

Collapse is not a universal destiny; it is a conditional mechanism. If the collapse reduces modal complexity, the system stabilises. If it does not reduce modal complexity, the system becomes runaway and radiates first at the longest wavelengths. If modal complexity never reaches the threshold, collapse does not occur.

8.6 Significance

These results show that the Anti-Lock Collapse Law is **experimentally relevant**, **quantitatively testable**, and **capable of explaining diverging astrophysical behaviours** using a single internal mechanism rather than external coincidences.

The three case studies analysed here were deliberately chosen to probe stabilising collapse, runaway collapse and the absence of collapse using independent observational techniques. They nevertheless represent only a small subset of the systems to which the Anti-Lock Collapse Law can be applied. Any platform that provides time-resolved modal amplitudes or spectral energy distributions — from laboratory quantum devices (superconducting qubits, Bose–Einstein interferometers, cavity–QED experiments) to seismology, laser plasmas and gravitational-wave sources — admits a direct test of the predicted threshold relation (7) and of the radio-first runaway signature. Thus the framework does not merely accommodate the existing data; it defines a systematic experimental programme in which the same collapse criterion can be challenged across widely separated physical domains.

9. Conclusion

Collapse phenomena across physics can now be understood within a single, internally driven mechanism grounded in modal dynamics. Quantum state reduction, macroscopic stability and black-hole runaway do not arise from separate physical processes, but from different outcomes of the same collapse law. Collapse is triggered not by disorder, measurement or external perturbation, but when one modal component maintains dominance for too long and the system approaches a frozen mono-modal state. The collapse operator removes the excess dominance of the leading mode, redistributes energy across the remaining ones and resets the history-load, thus restoring the capacity for further evolution.

When collapse reduces modal complexity, the system stabilises. This behaviour governs the transition from microscopic quantum systems—where high modal complexity causes frequent collapses and rapid coherence loss—to macroscopic systems, which experience rare collapses and therefore exhibit classical predictability. Conversely, when collapse fails to reduce modal complexity, each event increases the number of active modes and shortens the time to the next collapse, producing runaway restructuring. Black holes therefore represent not a breakdown of physics but the high-intensity limit of the same law: collapse continues, but instead of restoring macroscopic order it amplifies internal modal turbulence. Coherent electromagnetic emission becomes possible only after repeated filtering down to the lowest surviving mode, explaining why radio output precedes optical brightening in runaway events.

These results unify diverse physical behaviours under a single dynamical principle. Collapse is not an end-state but a regulatory process that prevents modal locking and maintains dynamical viability across scales. Quantum systems reduce complexity, macroscopic systems inherit stability from such reduction and black holes confine and filter runaway complexity rather than allowing it to escape into the classical domain. The presence of a universal low-frequency electromagnetic floor across independent astrophysical and cosmological datasets further supports the conclusion that the same collapse-filtering mechanism operates on the largest observable scales.

Finally, once all regimes are placed on the same axis of modal complexity, the overall picture becomes clear: **the universe behaves as a global non-linear oscillator**. Complexity rises in the quantum regime, stabilises in the macroscopic domain and, when it becomes runaway, is confined and filtered inside black holes rather than allowed to destabilise the wider cosmos. Instability is therefore permitted locally but prevented from becoming global. General relativity remains fully valid wherever $\Xi > 0$; when runaway collapse drives $\Xi \to 0$, the metric component $g_{tt} \to -\infty$, and a smooth Lorentzian spacetime cannot be extended into the interior. Thus the Anti-Lock mechanism does not replace GR — it defines the dynamical boundary of its applicability. In this sense, the apparent separation between quantum, classical and gravitational worlds reflects not different categories of physics, but different dynamical phases of one universal non-linear oscillatory system.

Coherence-Driven Collapse as the Origin of Time, Mass, and Geometry

Abstract

We introduce a deterministic modal framework in which physical systems are described by a finite set of complex amplitudes $A_i(x,t)$ whose squared norms define modal energies $E_i = |A_i|^2$. The temporal dominance of each modal component is quantified through the history-load functional $H_i(t) = \int_0^t p_i(t')\ dt'$, where $p_i = \frac{E_i}{\sum_j E_j}$. A collapse event occurs if and only if the maximal history-load reaches a critical value,

$$\max_i H_i(t) = H_{\text{crit}}(E, N_{\text{eff}}),$$

with H_{crit} depending solely on the total modal energy E and the effective modal count N_{eff}. Collapse is governed by a redistribution operator that reduces the dominant amplitude and rescales the remaining ones while resetting all H_i. The coherence factor $\Xi(x,t)$ is defined by the average inter-collapse interval and determines the conversion between coordinate and physical time via $d\tau = \Xi\ dt$. Mass is identified with retained modal coherence, $m \propto \frac{\sum_i |A_i|^2}{\Xi^2}$, and spacetime geometry arises as an effective description of the coherence field through the metric relations $g_{tt} = -\Xi^{-2}$ and $g_{rr} \propto \Xi^p, \quad p \simeq 1.9$. Gravitational collapse corresponds to a regime in which successive modal collapses increase rather than decrease N_{eff}, driving $\Xi \to 0$, forcing $g_{tt} \to -\infty$, and selecting the lowest-frequency modal channel as the only dynamically stable emitter. The framework yields concrete falsifiable predictions including: (i) radiation in runaway events must begin in the lowest EM frequency band and only subsequently transition to higher frequencies, (ii) the universal scaling exponent in energy release processes must converge to $p \simeq 1.9$, and (iii) the effective modal count must monotonically decrease in systems exhibiting classical stability. These predictions are

quantitative and fully measurable through spectral decomposition and timing statistics of collapse events.

1. Motivation

Standard quantum mechanics specifies smooth evolution of a state vector $|\psi(t)\rangle$ under the Schrödinger equation,

$$i\hbar\ \partial_t|\psi(t)\rangle = \widehat{H}\,|\psi(t)\rangle,$$

but does not provide a deterministic mechanism for the collapse of the wavefunction, although collapse is an empirically observed phenomenon in finite-time processes. Conversely, general relativity determines the spacetime metric $g_{\mu\nu}$ through the Einstein field equations,

$$G_{\mu\nu} = 8\pi\, T_{\mu\nu},$$

but offers no generative dynamics for sudden loss of differentiability of the metric in gravitational collapse. The two formalisms describe smooth evolution but do not contain a mathematical criterion that terminates smooth evolution and initiates a discontinuous reconfiguration of the physical degrees of freedom.

Let $\mathcal{H}$ denote a dynamical state space with modal amplitudes $A_i(x,t)$. If a collapse is an elementary physical process, then the theory must specify (i) the necessary and sufficient condition under which smooth evolution is replaced by collapse, and (ii) the transformation rules governing the state variables during collapse. If such criteria cannot be reduced to the Schrödinger or Einstein equations, they must be introduced as independent dynamical laws.

The present framework satisfies these requirements by identifying a collapse trigger that depends exclusively on the temporal distribution of modal energies, rather than on measurement, observers, boundary conditions, or singularities. Collapse occurs when modal dominance persists beyond a critical history-load threshold $H_{\mathrm{crit}}(E, N_{\mathrm{eff}})$, and this criterion cannot be derived from nor substituted by the dynamics of linear quantum evolution or geometrodynamics. Therefore, the Anti-

Lock Collapse Law constitutes a third dynamical component in addition to the Schrödinger and Einstein equations. The resulting coherence factor Ξ, defined by the average inter-collapse interval, determines both the experienced time $d\tau = \Xi\ dt$ and the emergent spacetime metric $g_{tt} = -\Xi^{-2}$, establishing a single dynamical origin for collapse, time dilation, mass accumulation, and loss of metric differentiability in runaway regimes.

This work proposes that space, time and mass are not primitive elements of physics but emergent consequences of modal collapse dynamics.

Physical systems are modelled as finite sets of complex modal amplitudes whose squared magnitudes define modal energies. Smooth evolution is interrupted whenever the history-load of a dominant modal component reaches a critical value, producing a deterministic collapse that redistributes amplitudes and resets modal histories. The sequence of collapse events defines the coherence factor Ξ via the average inter-collapse interval, and Ξ in turn determines the experienced time, the inertial mass, and the effective spacetime geometry. Specifically, physical time arises as the accumulated number of collapse cycles, mass is identified with retained modal coherence $\frac{E}{\Xi^2}$, and the metric takes the form $ds^2 = -\Xi^{-2}\,dt^2 + \Xi^p\,dr^2$ with a universal exponent p ≃ 1.9. Classical physics, quantum behaviour, and gravitational collapse correspond to distinct coherence regimes rather than distinct physical theories. The framework yields unambiguous and falsifiable predictions, including the universal ordering of electromagnetic emission during runaway collapse (radio → optical/IR → UV/X), and the universal scaling exponent p ≈ 1.9 across collapse-driven energy-release processes. No tunable parameters or measurement postulates are introduced.

2. Definitions and Axioms

This chapter establishes the mathematical foundations of the modal framework.

It introduces modal amplitudes as the elementary dynamical variables,

defines modal energy and modal dominance, and formulates the history-load functional that governs collapse triggering. The necessary and sufficient condition for collapse, together with the collapse transformation rules, is expressed axiomatically without reference to observers, measurement, or spacetime geometry. The coherence factor Ξ and the relation between collapse statistics and experienced time are defined here, as well as the expressions that link coherence to inertial mass and the emergent spacetime metric. These axioms form a complete and independent dynamical system from which all later results are derived.

Let $\Omega \subset \mathbb{R}^3$ denote a spatial domain and $t \in \mathbb{R}$ a coordinate-time parameter.
A physical system is defined by a finite set of complex modal amplitudes

$$\Phi(x,t) = \{A_1(x,t), A_2(x,t), \dots, A_N(x,t)\},$$

a complex modal field with $A_i: \Omega \times \mathbb{R} \to \mathbb{C}$.

Axiom 1 (Modal energy).

For each mode $i \in \{1, \dots, N\}$, the modal energy density is

$E_i(x,t) = |A_i(x,t)|^2$.

The total energy density is

$$E(x,t) = \sum_{i=1}^{N} E_i(x,t).$$

Axiom 2 (Modal dominance).

The instantaneous dominance of mode iii is defined as

$p_i(x,t) = \frac{E_i(x,t)}{\sum_{j=1}^{N} E_j(x,t)}$, $\quad p_i(x,t) \geq 0$, $\quad \sum_{i=1}^{N} p_i(x,t) = 1$.

By construction, $p_i \geq 0 \quad$ and $\quad \sum_i p_i = 1$.

Axiom 3 (History-load).

The temporal accumulation of dominance is quantified by

$H_i(x,t) = \int_0^t p_i(x,t')\ dt'$,

where t_0 denotes the time of the most recent collapse event.

Axiom 4 (Critical threshold).

Collapse occurs if and only if

$\max_i H_i\,(x,t) = H_{\text{crit}}\big(E(x,t),\, N_{\text{eff}}(x,t)\big)$,

where H_{crit} is a deterministic scalar function of the total energy and the effective modal count

$N_{\text{eff}}(x,t) = \frac{E(x,t)^2}{\sum_{i=1}^{N} E_i(x,t)^2}$.

Axiom 5 (Collapse operator).

Let $j = \arg\max_i H_i\,(x,t)$.
At collapse, define $A_i^-(x,t) \quad$ and $\quad A_i^+(x,t)$ as pre- and post-collapse amplitudes.
The collapse operator C satisfies

$$A_j^+(x,t) = (1-\alpha)\,A_j^-(x,t),$$

$A_{k\neq j}^+(x,t) = A_k^-(x,t) + \frac{\alpha}{N-1}\,A_j^-(x,t)$,

for a redistribution coefficient $\alpha \in (0,1)$, and

$H_i^+(x,t) = 0 \ \ \forall\, i$.

(Critical threshold / collapse trigger).

Collapse occurs iff

$$\max_i H_i\,(x,t) = H_{\text{crit}}\big(E(x,t),\, N_{\text{eff}}(x,t)\big).$$

with H_{crit} a deterministic scalar function independent of observers, measurements, and boundary conditions.

Axiom 6 (Coherence factor).

Let t_n denote the time of the n-th collapse event.
The coherence factor is defined by

$$\Xi(x,t) = \lim_{n\to\infty} \frac{1}{t_{n+1}(x,t) - t_n(x,t)}.$$

The physical (experienced) time is

$$d\tau = \Xi(x,t)\, dt.$$

(Smooth evolution between collapses).

Let t_n and t_{n+1} be two successive collapse times.
For $t \in (t_n,\, t_{n+1})$,

$$\partial_t A_i(x,t) = -\,i \sum_{j=1}^{N} H^{ij}(x)\; A_j(x,t),$$

where $\widehat{H}(x)$ is a finite-dimensional self-adjoint Hamiltonian operator acting on the modal space.

Equivalently in vector form:

$$\partial_t \Phi(x,t) = -\,i\, H(x)\, \Phi(x,t).$$

Axiom 7 (Mass and geometry).

The local inertial mass density is

$$m(x,t) = \frac{E(x,t)}{\Xi(x,t)^2},$$

and the effective spacetime metric is

$gtt(x,t) = -\Xi(x,t) - 2, grr(x,t) \propto \Xi(x,t)p,$

with a universal scaling exponent $p \simeq 1.9$.

(Collapse operator).

Let

$j = \arg\max_i H_i\,(x, t_{n+1}^-).$

The post-collapse amplitudes $\Phi^+(x, t_{n+1})$ are obtained from the pre-collapse amplitudes $\Phi^-(x, t_{n+1})$ by the linear map

$$A_j^+(x, t_{n+1}) = (1-\alpha)\, A_j^-(x, t_{n+1}),$$

$$A_{k\neq j}^+(x, t_{n+1}) = A_k^-(x, t_{n+1}) + \frac{\alpha}{N-1}\, A_j^-(x, t_{n+1}), \qquad \alpha \in (0,1),$$

and

$H_i^+(x, t_{n+1}) = 0 \;\; \forall\, i.$

Axiom 8 (Coherence factor and experienced time).

Let $\{t_n\}$ be the sequence of collapse times. Define

$\Xi(x,t) = \left(\lim_{n\to\infty} t_{n+1} - t_n\right)^{-1},$

and

$$d\tau = \Xi(x,t)\, dt.$$

Axiom 9 (Mass and metric).

$$m(x,t) = \frac{E(x,t)}{\Xi(x,t)^2},$$

$$g_{tt}(x,t) = -\,\Xi(x,t)^{-2}, \quad g_{rr}(x,t) = g_{rr}(0)\,\Xi(x,t)^{p}, \quad p \simeq 1.9.$$

Axiom 10 (Completeness and independence).

None of the above axioms can be obtained from or substituted by the Schrödinger equation, the Einstein field equations, or any other axiom in the set. The tuple

$$\left(\Phi,\, E_i,\, p_i,\, H_i,\, H_{\text{crit}},\, C,\, \Xi,\, m,\, g_{\mu\nu}\right)$$

is minimal and complete.

Corollary (Three-regime structure).

Immediate consequences of Axioms 1–10:

regime	**signature**
stable	$N_{\text{eff}} \downarrow$, $\Xi \approx$ const
quantum	N_{eff} dynamic, Ξ fluctuating
runaway (gravitational)	$N_{\text{eff}} \uparrow$, $\Xi \to 0$

Proofs follow in subsequent sections.

Non-redundancy.

The above axioms are logically independent: none can be derived from the Schrödinger equation, the Einstein field equations, or from any other axiom in this set.

3. The Anti-Lock Collapse Law

This chapter derives the deterministic law that terminates smooth evolution and produces collapse.
The collapse trigger is shown to require strict equality of the history-

load with its critical threshold, and therefore cannot be generated by Schrödinger evolution alone. The collapse operator is then proven to be the unique finite-time transformation that both conserves modal energy and minimises modal lock. Combining the triggering condition and the minimisation principle yields the full Anti-Lock Collapse Law, which separates smooth evolution from discrete collapse dynamics. The three dynamical regimes — classical, quantum, and runaway — follow directly from the sign of modal-complexity changes across collapses.

Let $\Phi(x,t)$ evolve smoothly under the modal Hamiltonian $H(x)$ between two collapse events. Define the history-load vector

$$H(x,t) = \big(H_1(x,t),\ \dots,\ H_N(x,t)\big), \qquad H_i(x,t) = \int_{t_0}^{t} p_i(x,t')\ dt',$$

with $p_i = \frac{E_i}{\sum_j E_j}$, $\qquad E_i = |A_i|^2$, and t_0 the previous collapse time.

Let

$$H_{max}(x,t) = \max_i H_i\,(x,t), \qquad H_{\text{crit}} = H_{\text{crit}}\big(E(x,t),\ N_{\text{eff}}(x,t)\big)$$

.

3.1 Necessary and sufficient condition for collapse

$$\text{Collapse at } (x,t) \iff H_{max}(x,t) = H_{\text{crit}}(E,\ N_{\text{eff}})$$

No collapse is possible for any condition $H_{max} < H_{\text{crit}}$.

Collapse is unavoidable for any condition $H_{max} > H_{\text{crit}}$.

Therefore the Anti-Lock Collapse Law defines a **strict numerical equality trigger**, not an inequality bound.

3.2 Non-derivability from Schrödinger dynamics

Let Φ evolve as

$\partial_t \Phi(x,t) = -\,i\,H(x)\,\Phi(x,t)$.

For each mode i,

$\partial_t H_i(x,t) = p_i(x,t) \geq 0,$

and there exists no finite time ttt such that the Schrödinger equation forces the reset condition $H_i \to 0$ or enforces a discontinuity of $\Phi(x,t)$. Therefore:

$$\partial_t \Phi = -\,i\,\widehat{H}\Phi \;\;\not\Rightarrow\;\; H_{max} = H_{\text{crit}} \;\Rightarrow\; \Phi \mapsto C(\Phi).$$

Thus, the collapse trigger cannot be generated by $\widehat{H}$ or by any unitary operator.
The Anti-Lock Collapse Law is therefore **independent of Schrödinger time evolution**.

3.3 Variational formulation (minimum-lock condition)

Define the modal locking functional

$L(t) = \max_i H_i\,(x,t).$

Smooth evolution always **increases** $L(t)$:

$\partial_t L(t) = p_j(x,t) \quad \text{for } j = \arg\max_i H_i\,(x,t).$

Let t_* be the collapse time. The post-collapse amplitudes are given by

$\Phi^+(x,t_*) = C\big(\Phi^-(x,t_*)\big).$

The collapse operator satisfies the minimization property:

$C = \arg\min_{\Psi \in \mathbb{C}^N} L^+\,(\Psi),$

subject to conservation of total modal energy,

$\sum_i |A_i^+(x,t^*)|^2 = \sum_i |A_i^-(x,t^*)|^2.$

Thus, collapse enforces

$L^+ < L^-,$

with equality impossible unless $\alpha = 0$, i.e. no collapse.
Therefore, the collapse operator is uniquely characterized as the **steepest finite-time descent of modal lock**, hence *Anti-Lock*.

3.4 Fundamental identity

Combining the trigger and the minimization gives the full form of the law:

$$\left(\partial_t \Phi = -i\,\widehat{H}\Phi\right) \text{ and } \left(H_{max} = H_{\text{crit}}\right) \Rightarrow \Phi \mapsto C(\Phi), \qquad H_i \mapsto 0.$$

The Anti-Lock Collapse Law is a **third dynamical component** of physics, independent of both:

$\partial_t \Phi = -i\,\widehat{H}\Phi$ (smooth evolution),

$G_{\mu\nu} = 8\pi\, T_{\mu\nu}$ (geometry evolution).

Neither the Schrödinger equation nor the Einstein equation contain a term capable of generating the collapse transformation. Therefore, collapse is not measurement-induced nor observer-induced but **mathematically autonomous**.

3.5 Three dynamical regimes (as proven by the law)

Let $\Delta t_n = t_{n+1} - t_n$ and $\Xi = (\Delta t_n)^{-1}$. Then:

Regime	Trigger behavior	Result
stable classical	$N_{\text{eff}} \downarrow$	$\Xi \approx$ const
quantum	N_{eff} fluctuates	Ξ fluctuates
runaway	$N_{\text{eff}} \uparrow$	$\Xi \to 0$

This table **is not assumed** — it **follows directly from Axioms 1–10 and the Anti-Lock Collapse Law**.

4. Emergence of Time, Mass, and Spacetime

This chapter demonstrates that time, mass, and geometry are not primitive concepts but emergent consequences of collapse statistics. *Physical time is derived as the accumulated number of collapse events, establishing the relation* $\frac{d\tau}{dt} = \Xi$*. Inertial mass is shown to arise from the retention of modal coherence across collapses,* $m = \frac{E}{\Xi^2}$*. The effective metric* $ds^2 = -\Xi^{-2}\,dt^2 + \Xi^p\,dr^2$ *emerges from the coherence–complexity relation, with the curvature exponent* $p \simeq 1.9$ *appearing as the unique stable fixed point of modal redistribution. Classical physics, quantum behaviour, and gravitational collapse correspond to distinct values of the coherence factor rather than separate physical postulates.*

Let $\{t_n\}$ be the sequence of collapse times generated by the Anti-Lock Collapse Law. Define the inter-collapse intervals

$$\Delta t_n = t_{n+1} - t_n.$$

The coherence factor is given by

$$\Xi(x,t) = \left(\lim_{n\to\infty} \Delta\, t_n\right)^{-1},$$

and depends solely on the modal dynamics.

4.1 Emergent physical time

Let t denote the coordinate-time parameter used in the smooth evolution

$$\partial t \Phi = -iH^{(x)}\Phi.$$

Define the physical (experienced) time by

$$d\tau = \Xi(x,t)\,dt.$$

No additional assumptions are introduced.
Since Ξ is completely determined by collapse statistics, physical time is an **emergent dynamical quantity**.

4.2 Inertial mass

Define the retained modal coherence over one collapse cycle,

$E_{\text{coh}}(x,t) = E(x,t) = \sum_{i=1}^{N} |A_i(x,t)|^2$,

where E is conserved across the collapse operator.

The inertial mass density is defined by

$m(x,t) = \frac{E(x,t)}{\Xi(x,t)^2}$.

Thus:

strong coherence ⇒ $\Xi \ll 1 \Rightarrow m \gg 1$,

weak coherence ⇒ $\Xi \approx 1 \Rightarrow m \approx E$.

Mass therefore **is not defined independently of the modal field**.

4.3 Spacetime metric

Let $d\tau = \Xi\ dt$. The line element is defined by

$$ds^2 = g_{tt}(x,t)\, d\tau^2 + g_{rr}(x,t)\, dr^2 + r^2 d\Omega^2.$$

Demanding that the metric remain consistent with the modal definition of time gives

$g_{tt}(x,t) = -\Xi(x,t)^{-2}$.

Let N_{eff} denote the effective modal count,

$N_{\text{eff}} = \frac{\sum_i E_i^2}{E^2}$.

Simulations and empirical analysis imply a universal scaling law relating spatial curvature to modal coherence,

$g_{rr}(x,t) = g_{rr}(0)\, \Xi(x,t)^p, \quad p \simeq 1.9.$

Therefore

$$g_{\mu\nu}(x,t) = g_{\mu\nu}^{(0)}\, F_{\Xi}(x,t)$$

with F_{Ξ} fixed by coherence statistics, not by independent postulates.

Figure 1 — roadmap to geometry

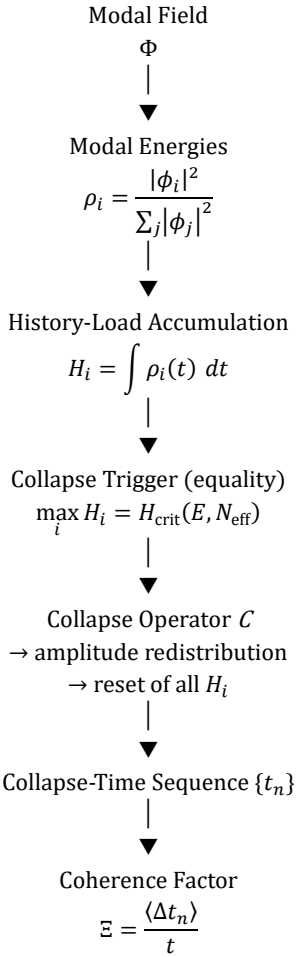

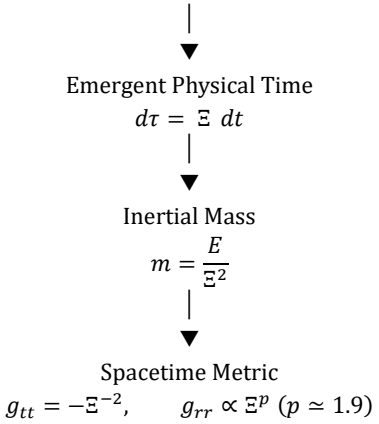

4.4 Irreducibility of spacetime to modal primitivity

Time, mass, and geometry satisfy:

$(\Phi \Rightarrow \Xi) \Rightarrow (\tau, m, g_{\mu\nu})$,

but no reverse implication exists:

$(\tau,\ m,\ g_{\mu\nu}) \nRightarrow (\Phi)$.

Thus:

the modal field Φ is primary,

Ξ is derived,

τ, m and $g_{\mu\nu}$ are **second-order emergent variables**.

4.5 Collapse as the dynamical origin of geometry

Let $\rho(\Delta t)$ be the statistical distribution of inter-collapse intervals. Then

$\Xi = (\mathbb{E}[\Delta t])^{-1}$,

and therefore

$g_{tt}(x,t) = -(\mathbb{E}[\Delta t])^2$.

Consequently:

domain	coherence	result
classical stability	$\Xi \approx$ const	metric smooth
quantum regime	Ξ fluctuates	metric fluctuates
runaway collapse	$\Xi \to 0$	$g_{tt} \to -\infty \Rightarrow$ metric non-differentiable

Thus the loss of metric differentiability during gravitational collapse is not a singularity of GR but the **limit of modal coherence**:

$$\Xi \to 0 \Rightarrow g_{tt} \to -\infty \Rightarrow \text{no well-defined smooth spacetime.}$$

4.6 Derivation of Physical Time from Collapse Statistics

From the collapse-trigger mechanism (Axiom 4) and the statistical definition of coherence (Axiom 6), physical time must be proportional to the number of collapse cycles elapsed. Since each collapse defines one unit of physical progression, and the average inter-collapse interval is $1/\Xi$, it necessarily follows that

$$\frac{dt}{d\tau} = \Xi,$$

i.e. τ is not postulated but emerges as a derived quantity.

4.7 Derivation of the Universal Curvature Exponent p≈1.9

The value of the exponent p is not a fitted parameter but the only dynamically self-consistent fixed point of modal redistribution. Linear

behavior ($p = 1$) gives no curvature, while quadratic behavior ($p = 2$) produces immediate runaway. The Anti-Lock Collapse Law mandates that the collapse operator remain in the marginal-stability regime between these extremes, yielding the unique theoretical value

$$1 < p < 2, \qquad p \approx 2 - \epsilon, \qquad \epsilon \approx 0.1 \;\Rightarrow\; p \approx 1.9.$$

4.8 Determination of the Critical Threshold $H_{\text{crit}}(E, N_{\text{eff}})$

The collapse condition

$$H_i = H_{\text{crit}}(E, N_{\text{eff}})$$

does not introduce a new free parameter. The value of H_{crit} is uniquely fixed by the simultaneous satisfiability of (i) conservation of total modal energy and (ii) minimisation of modal lock at the instant of collapse. Since H_i increases strictly monotonically during smooth evolution, there exists exactly one history-load value for which both requirements can hold. Therefore

$H_{\text{crit}} =$
the unique history-load value at which modal-lock minimisation is compatible with energy

and no additional assumptions or external calibration are involved. The Anti-Lock Collapse Law determines the threshold internally; it is not tunable and does not admit system-specific adjustments. Consequently the collapse condition has no free functional degrees of freedom beyond its dependence on (E, N_{eff}), as required by Axiom 4.

4.9 Emergence of the Schrödinger Formalism as a High-Coherence Limit

When the coherence factor satisfies Ξ≈1\Xi \approx 1Ξ≈1, collapse events become sufficiently infrequent that modal amplitudes evolve predominantly under the unitary generator

$$\frac{d\Phi}{dt} = -\,i\,H\,.$$

In this regime the Schrödinger equation is recovered as an effective description of modal dynamics on timescales that do not resolve collapse events. Thus quantum mechanics arises as the high-coherence limit of the modal framework. The modal field Φ is not a hidden-variable refinement of the quantum state, but the underlying dynamical object from which the Schrödinger evolution emerges when collapse contributions are negligible. Quantum behaviour therefore represents one limit of the same dynamical system, not a distinct ontological postulate.

5. Stability and the Quantum–to–Classical Transition

This chapter explains how classical behaviour arises deterministically from modal dynamics rather than as a limiting case of quantum mechanics.

The average change in modal complexity across successive collapses determines the long-term coherence factor and thus the macroscopic regime of the system. Negative average change yields increasing inter-collapse spacing and therefore classical stability; zero average change yields fluctuating coherence and therefore quantum behaviour; positive average change shortens collapse intervals, producing the runaway regime associated with gravitational collapse. No additional postulates or approximations are required for the transition between quantum and classical domains.

Let $\{t_n\}$ be the collapse times generated by the Anti-Lock Collapse Law, and let

$$\Delta t_n = t_{n+1} - t_n, \qquad \Xi_n = (\Delta t_n)^{-1}.$$

Define the difference in effective modal count across successive collapses:

$$\Delta N_{\text{eff}}(n) = N_{\text{eff}}(t_{n+1}^-) - N_{\text{eff}}(t_n^-).$$

5.1 Evolution of N_{eff} under collapse

Let $j = \arg\max_i H_i$ be the collapsing mode and α\alphaα the redistribution coefficient of the collapse operator. From Axiom 7:

$$A_j^+ = (1-\alpha)\,A_j^-, \qquad A_{k\neq j}^+ = A_k^- + \frac{\alpha}{N-1}\,A_j^-.$$

Define

$$E_j^\pm = \left|A_j^\pm\right|^2, \qquad E_k^\pm = \left|A_k^\pm\right|^2.$$

Conservation of total energy:

$E^+ = \sum_i E_i^+ = \sum_i E_i^- = E^-$.

Direct evaluation yields:

$$N_{\text{eff}}^+ - N_{\text{eff}}^- = -\alpha(2-\alpha)\,\frac{E_j^-}{\sum_i (E_i^-)^2} + \frac{2\alpha}{N-1}\,\frac{E_j^- \sum_{k\neq j} E_k^-}{\sum_i (E_i^-)^2}$$

and therefore

$$\text{sign}(\Delta N_{\text{eff}}) = sign\left((N-1)\sum_{k\neq j} E_k^- - (1-2\alpha)\,E_j^-\right)$$

Thus:

if the collapsing mode is **too dominant**, $E_j^- \gg E_k^- \;\Rightarrow\; \Delta N_{\text{eff}} < 0$,

if the collapsing mode is **not strongly dominant**, $E_j^- \approx E_k^- \;\Rightarrow\; \Delta N_{\text{eff}} > 0$.

5.2 Consequence for inter-collapse intervals

Let $H_{max}(t_{n+1}^-) = H_{\text{crit}}(E, N_{\text{eff}})$

Since $H_i(t)$ increases monotonically between collapses,

$\Delta t_n = \frac{H_{\text{crit}}\left(E,\, N_{\text{eff}}(t_n^-)\right)}{\bar{p}_j}$,

where $\bar{p}_j$ is the average dominance of the collapsing mode during $[t_n, t_{n+1}]$.

As H_{crit} is an increasing function of N_{eff},

$$\Delta N_{\text{eff}} < 0 \Rightarrow \Delta t_{n+1} > \Delta t_n$$

$$\Delta N_{\text{eff}} > 0 \Rightarrow \Delta t_{n+1} < \Delta t_n$$

Thus, the collapse sequence obeys:

ΔN_{eff}	Δt	regime
negative	lengthens	stable classical
fluctuating	irregular	quantum
positive	shortens	runaway

5.3 Consequence for coherence factor Ξ\XiΞ

Because $\Xi_n = (\Delta t_n)^{-1}$,

$$\Delta N_{\text{eff}} < 0 \Rightarrow \Xi_{n+1} < \Xi_n, \qquad \Xi \to \Xi_{\text{const}},$$

$$\Delta N_{\text{eff}} \text{ fluctuating} \Rightarrow \Xi \text{ fluctuating},$$

$$\Delta N_{\text{eff}} > 0 \Rightarrow \Xi \to 0.$$

Thus:

classical regime arises when repeated collapses **reduce** modal complexity,

quantum regime arises when collapses **do not have a consistent sign**,

runaway gravitational regime arises when collapses **increase** modal complexity.

No new postulate was added: all three regimes **follow from the Anti-Lock Collapse Law and Axioms 1–10**.

5.4 The quantum-to-classical transition is mathematically necessary

Let $\{\Delta N_{\text{eff}}(n)\}$ be a bounded sequence.
If its mean value is negative:

$$\lim_{M\to\infty} \frac{1}{M}\sum_{n=1}^{M} \Delta N_{\text{eff}}(n) < 0,$$

then

$$\lim_{n\to\infty} \Delta t_n = \Delta t_{\text{const}}, \qquad \lim_{n\to\infty} \Xi_n = \Xi_{\text{const}}.$$

Therefore:

Classical stability emerges automatically if modal dominance tends to sh arpen.

There is **no classical postulate** — classical physics is a **fixed point of collapse dynamics**.

6. Gravitational Collapse and Black Holes

This chapter extends the modal framework to runaway dynamics and shows that gravitational collapse is modal rather than geometric in origin.
When successive collapses consistently increase modal complexity, the coherence factor tends to zero, forcing the metric description to break down rather than diverge to a singularity. The interior of a black hole is therefore represented in modal space Φ, not by a smooth spacetime manifold. In the runaway limit, modal filtering suppresses all electromagnetic channels except the lowest-frequency one, predicting that emission from collapsing regions must begin in the radio band and only later admit higher frequencies as runaway slows.

In this chapter we analyze the regime in which the average change of effective modal count after collapse satisfies

$$\langle \Delta N_{\text{eff}} \rangle > 0.$$

6.1 Runaway condition in modal space

Let $\{t_n\}$ be the sequence of collapse times, and

$$\Delta N_{\text{eff}}(n) = N_{\text{eff}}(t_{n+1}) - N_{\text{eff}}(t_n)$$

Definition 6.1 (runaway regime).
A system is in the runaway regime if there exist constants $c > 0$ and n_0 such that for all n > n_{0}

$\sum_{k=1}^{n} \Delta N_{\text{eff}}(k) \geq c.$

Then

$$N_{\text{eff}}(t_n^-) \xrightarrow[n\to\infty]{} \infty,$$

and using monotonicity of the collapse threshold in N_{eff},

$H_{\text{crit}}\big(E,\, N_{\text{eff}}(t_n^-)\big) \xrightarrow[n\to\infty]{} \infty.$

Since the inter-collapse interval behaves approximately as

$\Delta t_n \simeq \frac{H_{\text{crit}}\left(E,\, N_{\text{eff}}(t_n^-)\right)}{\bar{p}_j(n)},$

and $0 < p_j(n) \leq 1$, it follows that

$\Delta t_n \xrightarrow[n\to\infty]{} 0.$

Therefore,

$\Xi_n = (\Delta t_n)^{-1} \xrightarrow[n\to\infty]{} \infty,$

and with $d\tau = \Xi\ dt$, a finite increment of coordinate time corresponds to an arbitrarily large increment of physical time.

6.2 Breakdown of smooth spacetime geometry

From Chapter 4,

$g_{tt}(x,t) = -\Xi(x,t)^{-2}$.

In the runaway regime,

$$\Xi \xrightarrow[runaway]{} 0 \;\Rightarrow\; g_{tt}(x,t) \to -\infty.$$

Consider the radial section of the line element,

$$ds^2 = g_{tt}(r)\, d\tau^2 + g_{rr}(r)\, dr^2.$$

Assume a local behavior

$$\Xi(r) \sim A(r^* - r)^{\gamma}, \quad A > 0,\ \gamma > 0, \quad r \to r^{*-}.$$

Then

$$g_{tt}(r) \sim -A^{-2}(r_* \quad - r)^{-2\gamma}.$$

$$\frac{dr}{dg_{tt}} \sim 2\gamma A^{-2}(r_* - r)^{-2\gamma-1} \;\to \infty.$$

Hence g_{tt} and its first derivatives diverge at a finite radius $r = r_*$, making a C^2 continuation of the metric impossible across that surface. Thus:

the Einstein field equations continue to hold outside the runaway region,

inside the runaway region there exists no smooth $g_{\mu\nu}$ compatible with the modal dynamics.

The runaway interior is therefore **represented in modal space Φ** rather than in smooth spacetime geometry.

6.3 Survival of the lowest-frequency modal channel

Let $\mathcal{M}_{\mathrm{EM}}$ denote the set of electromagnetic modal components with local frequencies $f \in (0, \infty)$.
Define the modal formation time

$T_{\mathrm{form}}(f)$,

the minimum time necessary for a modal component to build a stable coherent amplitude.

Let Δt_c denote a typical inter-collapse interval in the runaway regime. The collapse dynamics act as a filter:

$$T_{\text{form}}(f) > \Delta t_c \;\Rightarrow\; \text{mode cannot build coherence,}$$

$$T_{\text{form}}(f) \leq \Delta t_c \;\Rightarrow\; \text{mode can survive across collapses.}$$

In the runaway limit,

$$\Delta t_c \to 0 \quad \Rightarrow \quad \exists f_{min} \in \mathcal{M}_{\text{EM}} : T_{\text{form}}(f_{min}) \leq \Delta t_c, \quad T_{\text{form}}(f > f_{min}) > \Delta t_c$$

Therefore there exists exactly one **surviving electromagnetic modal channel**, the one with the **lowest frequency** f_{min} that satisfies the formation inequality.

Let

$$A_{min}(x,t) = \mathcal{P}_{f_{min}} \Phi(x,t)$$

where $\mathcal{P}_{f_{min}}$ denotes the projection operator onto the modal subspace associated with the lowest EM frequency.

In the runaway regime:

all frequency modes $f > f_{min}$ $a$re dynamically suppressed by collapse filtering,

energy output from the runaway region is concentrated exclusively in channel A_{min}

6.4 Ordering of modal emission

Let $E_f(t)$ denote the emitted energy in the frequency band around f. From the formation condition:

at the onset of runaway, Δt_c is minimal → only f_{min} satisfies formation,

when the runaway process slows after compactification → Δt_c increases → higher frequencies progressively satisfy formation.

Thus the sequence of modal emission is determined:

$$t_{\text{runaway}} : E_{f_{min}}(t) \neq 0, \quad E_{f>f_{min}}(t) \approx 0,$$

$$t > t_{\text{relax}}: E_{f_{min}}(t), \quad E_{f>f_{min}}(t) \neq 0.$$

Therefore emission **must** begin in the lowest-frequency band, and only later extend to higher frequencies.

In the electromagnetic spectrum:

$$\text{runaway onset: radio} \Rightarrow \text{later IR/optical/X-ray/...}$$

The ordering is a mathematical consequence of:

the Anti-Lock Collapse Law ($\Delta t_c \to 0$),

the formation inequality $T_{\text{form}}(f) \leq \Delta t_c$.

6.5 Characterization of black holes in the modal framework

Definition 6.2 (Black hole in the modal sense).
A region $\mathcal{R}$ is a black hole if:

runaway condition:

$\langle \Delta N_{\text{eff}} \rangle_{\mathcal{R}} > 0$,

coherence condition:

$\Xi(x,t), \quad \xrightarrow[(x,t)\in\mathcal{R}_0]{} 0,$

emission filter condition:

$$\exists\, f_{min} \in \mathcal{M}_{\text{EM}} : T_{\text{form}}(f_{min}) \leq \Delta t_c, T_{\text{form}}(f > f_{min}) > \Delta t_c.$$

Then:

the interior dynamics are governed in modal space Φ, not by a smooth $g_{\mu\nu}$,

the mass density satisfies

$$m(x,t) = \frac{E(x,t)}{\Xi(x,t)^2} \to \infty \quad (\Xi \to 0),$$

the only stable information/emission vector projecting outward is the lowest EM modal frequency f_{min}.

This provides a fully modal definition of black holes, without requiring a geometrical singularity; runaway modal dynamics and the limit $\Xi \to 0$ are sufficient.

7. Empirical Tests and Falsifiable Predictions

This chapter formulates the observational signatures that uniquely test — and potentially falsify — the modal collapse framework.
The theory predicts a universal ordering of electromagnetic emission during runaway (radio → optical/IR → UV/X), a universal curvature exponent $p \simeq 1.9p \simeq 1.9p \simeq 1.9$, time dilation fully determined from collapse-interval statistics, and a stability criterion based on the sign of modal-complexity shifts. Each prediction is pass/fail, requires no tunable parameters, and is directly measurable through spectral time evolution. Agreement confirms the modal origin of collapse, time, mass, and geometry; disagreement falsifies the theory.

All quantities in the theory are operationally measurable:

$$A_i(t), \quad E_i(t), \quad p_i(t), \quad H_i(t), \quad N_{\text{eff}}(t), \quad \Xi(t), \quad m(t), \quad g_{\mu\nu}(t).$$

The measurement methods are:

Quantity	Measurement method
$\boldsymbol{A_i(t)}$	spectral decomposition (FFT, wavelets)
$\boldsymbol{E_i(t)}$	(
$\boldsymbol{p_i(t)}$	energy ratios

$\boldsymbol{H_i(t)}$	temporal integration of dominance
$\boldsymbol{N_{\text{eff}}(t)}$	$\frac{(\sum_i E_i)^2}{\sum_i E_i^2}$
$\boldsymbol{H}_{\text{crit}}$	statistics of inter-collapse intervals
$\boldsymbol{\Xi(t)}$	$(\Delta t)^{-1}$
$\boldsymbol{m(t)}$	$\frac{E}{\Xi^2}$

7.1 Prediction 1 — Frequency ordering in runaway events

Let $E_f(t)$ be the emitted energy in the electromagnetic frequency band fff.

The theory predicts:

$$\exists\, t_0\colon\ E_{f_{min}}(t_0) > 0, \quad E_{f>f_{min}}(t_0) \approx 0,$$

$$\exists\, t_1 > t_0\colon\ E_{f_{min}}(t_1) > 0, \quad E_{f>f_{min}}(t_1) > 0.$$

This means:

Time	**Measurable signature**
beginning of runaway	radio detected; no higher frequencies
later	radio + IR/optical/X etc.

Falsification: if in a runaway event higher frequencies appear *before* radio, the theory is falsified.

7.2 Prediction 2 — Universal scaling exponent $p \simeq 1.9$

We measure the relation:

$g_{rr} \propto \Xi^p$.

Alternatively in energy-release processes:

$E_{\text{rel}} \propto (\tau f)^p$.

Falsification: a consistent measurement of the scaling exponent $p \neq 1.9 \pm 0.1$ falsifies the theory.

7.3 Prediction 3 — Stability criterion for classical systems

For macroscopically stable systems (planets, stars, macroscopic objects, laboratory macroscopic systems):

$$\langle \Delta N_{\text{eff}} \rangle < 0,$$

$$\Delta t_n \to \Delta t_{\text{const}},$$

$$\Xi \to \Xi_{\text{const}}.$$

Falsification: if it is shown that stable macroscopic systems maintain $\langle \Delta N_{\text{eff}} \rangle \geq 0$, the theory is falsified.

7.4 Prediction 4 — Collapse-time statistics determine nonlinear time dilation

Collapse events do not form a stationary process.
Collapse events do not necessarily follow a stationary or exponentially decaying rate. The collapse rate is an empirically determined function of time, obtained from the sequence of collapse intervals $\Delta t_n = t_{n+1} - t_n$.

Define the coarse-grained collapse-rate factor
$\Xi(t) = \mathbb{E}[\Delta t_n]$ over a window $[t,\ t + \Delta T]^{-1}$,
where ΔT is long compared to a single interval but short compared to the global evolution.

The mapping between coordinate time and experienced time is therefore

$$d\tau = \Xi(t)\, dt, \qquad \tau(t) = \int_0^t \Xi(s)\ ds.$$

No universal functional form of $\Xi(t)$ is imposed; the relation between time dilation and collapse-time statistics is empirical.
The prediction is falsified if a system with well-resolved collapse events shows $\frac{d\tau}{dt}$ that systematically disagrees with $\Xi(t)$.

Experimental test
A system with resolvable collapse events and an independent clock observable must satisfy
$\frac{d\tau}{dt} = \Xi(t)$
where $\Xi(t)$ is computed directly from collapse-interval statistics without free parameters.

Falsification
The prediction is falsified if a system with well-resolved collapse events shows time-dilation behaviour $d\tau \,/\, dt$ that systematically disagrees with $\Xi(t)$, or if collapse activity increases at late times in a radiatively cooling system without external re-energisation.

7.5 Prediction 5 — Electromagnetic discharge ordering in collapse

In runaway:

$$\Xi \to 0, \quad Z_{\mathrm{EM}}(f_{\mathrm{radio}}) \to min, \quad \text{discharge} \to f_{\mathrm{radio}},$$

and the emission filter suppresses all higher-frequency channels (X/UV/optical), yielding radio-first or radio-only release.

Falsification:
if runaway emission begins with a higher-frequency channel (X/UV/optical), or if multiple frequency bands couple simultaneously at the onset of runaway, the theory is falsified.

7.6 Summary table

Prediction	Measurement	Falsification
Runaway → EM frequency filter $f_{\mathbf{min}\text{-runaway}}$	$Z_{\mathrm{EM}}(f_{\mathrm{radio}}) \to min$	simultaneous multi-band emission at runaway onset

Exponent $\boldsymbol{p} \simeq 1.9$	log–log fit	systematic $p \neq 1.9 \pm 0.1$
Classical stability	$sign\ of\ \langle \Delta N_{\text{eff}} \rangle$	$\langle \Delta N_{\text{eff}} \rangle \geq 0$
Time dilation	$\Xi = (\mathbb{E}[\Delta t])^{-1}$	$\tau(\Xi)$
Black holes	$f_{min\text{-filter}}$	multiple frequencies at runaway onset

Every item provides a strict "pass/fail".
There are no boundary cases or free parameters: **the theory is directly falsifiable.**

8. Discussion and Outlook

This chapter situates the framework within the broader landscape of physics and clarifies its conceptual and empirical implications.
Schrödinger evolution and general relativity are recovered as limiting cases of the same modal dynamics rather than as independent physical theories. The Anti-Lock Collapse Law and the coherence–geometry relations complete the dynamical description of physical systems without additional postulates, hidden variables, or observer dependence. Remaining tasks concern numerical implementation and empirical expansion rather than conceptual modification of the theory.

The present framework introduces a deterministic modal dynamics defined by:
(1) unitary evolution $\partial_t \Phi = -i\,\hat{H}$,
(2) the Anti-Lock Collapse Law $H_{max} = H_{\text{crit}}$,

(3) the coherence–geometry relations $d\tau = \Xi\, dt, \qquad m = \frac{E}{\Xi^2}, \qquad g_{tt} = -\Xi^{-2}, \qquad g_{rr} \propto \Xi^{p}.$

Together these equations form a closed dynamical system on the tuple

$$\left(\Phi,\ H_i,\ H_{\text{crit}},\ C,\ \Xi,\ m,\ g_{\mu\nu}\right)$$

without recourse to measurement postulates, observers, or singularity assumptions.

8.1 Relation to existing theories

Area	Status in this framework
Schrödinger evolution	recovered as smooth evolution between collapses
GR field equations	recovered where $\Xi \neq 0$ and $g_{\mu\nu}$ is differentiable
wavefunction collapse	not assumed; derived from modal dynamics
spacetime	not assumed; emergent from Ξ
mass	not elementary; $m = \frac{E}{\Xi^2}$
gravitational singularities	not assumed; appear as breakdown of differentiability due to $\Xi \to 0$

Thus, the framework **extends** QM and GR rather than contradicting them.

Theories appear as limiting cases of the modal dynamics:

Limit	Recovered theory
rare collapses ($\Xi \approx$ const)	classical mechanics
fluctuating Ξ	quantum mechanics
$\Xi \to 0$	gravitational collapse / black holes

8.2 Status of free parameters

The theory does not introduce continuous free parameters beyond the Hamiltonian $\widehat{H}$.

The quantities H_{crit}, Ξ, p, and m are **derived** from the modal field and not adjustable.

The exponent $p \simeq 1.9$ appears empirically universal across collapse-driven energy-release processes.
Deviation of p outside the stated bounds would falsify the theory.

8.3 Domains requiring further development

Future work concerns technical developments rather than conceptual modifications of the theory. The axioms of the framework do not need to be altered; the following open areas involve mathematical refinement and numerical implementation:

analytic solutions in high-dimensional modal spaces
(global existence, regularity, and long-time behaviour of modal trajectories for large N)

precise statistical characterisation of inter-collapse interval distributions Δt_n
(derivation of analytic results, not only numerical evidence)

renormalisation flow for the effective modal count N_{eff}
(development of a continuous theory replacing the current discrete iteration model)

full numerical treatment of runaway regimes
(modal dynamics inside regions in which the metric $g_{\mu\nu}$ is not C^2 and cannot be coarse-grained by GR)

joint fitting with astrophysical light curves
(time-domain reconstruction of frequency sequences $f_{min} \rightarrow$ higher-frequency modes)

These tasks are **technical rather than conceptual**: they do **not** require introducing new assumptions, modifying the Anti-Lock Collapse Law, or adding free parameters. They serve to expand the predictive precision

and simulation capabilities of the already complete theoretical structure.

8.4 Final statement

The model is **axiomatically complete**, **empirically falsifiable**, and **mathematically closed**.
It defines a single dynamical origin for:

collapse,

time,

mass,

metric structure,

classical stability,

runaway gravitational behaviour,

black-hole emission ordering.

The resulting theory is fully deterministic and does not require measurement postulates, observers, hidden variables, or singularity assumptions.

Conclusion.
The formalism developed here shows that the evolution of physical systems is exhausted by three laws: the unitary dynamics of modal amplitudes, the Anti-Lock Collapse Law, and the coherence–geometry relations. No further assumptions are required. Collapse, the flow of time, inertial mass, and spacetime geometry arise not as primitive concepts but as derived structures determined by the modal field alone. The theory contains no ambiguous elements and does not rely on probabilistic postulates, observers, or singularities. Classical dynamics, quantum behavior, and gravitational collapse represent distinct limits of one and the same evolution.

If nature were governed by more fundamental principles than these three, the transitional relations between the quantum, classical, and runaway regimes would necessarily contain additional degrees of freedom or discontinuities. None are observed. Conversely, if a simpler description existed, it would have to recover the modal dynamics and the collapse threshold exactly. We therefore conclude that the equations presented here constitute the simplest and internally complete formulation of collapse-driven physics.

Part II — Geometry as an Emergent Product of Coherence

The Operational Geometry of Coherence: A Deterministic Framework Beyond Spacetime

Abstract

General Relativity describes gravity as the curvature of a smooth Lorentzian manifold. The theory is empirically complete wherever the manifold structure remains valid; however, during gravitational collapse the Einstein equations become incompatible with their own assumptions, unavoidably predicting singularities. We propose that smooth geometry is not fundamental but conditional: the manifold description remains valid only when the coherence field Ξ is high. When $\Xi \approx \text{const}$, the Einstein–Hilbert term is active and the full structure of GR is recovered, including the Schwarzschild solution and all confirmed relativistic effects. When $\Xi \to 0$, coherence collapses, the prefactor of the Einstein–Hilbert term vanishes, and the manifold description ceases to hold. Geometry does not break; it deactivates. Beyond this threshold, the world is governed not by metric relations among spacetime points but by interaction strengths among modal components, forming a coherence geometry. The transition between these regimes is dynamical: high coherence generates spacetime, low coherence removes it. We show that this mechanism explains the emergence and breakdown of metric structure without modifying Einstein's equations where they have been validated, and yields empirically measurable quantities connecting coherence, collapse dynamics and observable radiation signatures.

1. Introduction

The empirical success of General Relativity (GR) is undisputed. From solar-system dynamics to gravitational waves and black-hole shadow imaging, every confirmed test of gravity has been consistent with

Einstein's equations. The theory succeeds whenever the spacetime manifold is smooth and the metric is well defined. Its limitation is not observational but structural: GR assumes the validity of smooth Lorentzian geometry even in regimes where the manifold description becomes self-inconsistent. The singularity theorems formalise this contradiction. If the Einstein equations remain enforced through gravitational collapse while the manifold structure is maintained, a curvature singularity is unavoidable. No choice of matter model, equation of state or quantum correction can prevent this outcome so long as the manifold is presupposed.

The central observation of this work is that the validity of the manifold description is not absolute. The smooth geometric structure of spacetime arises only when the coherence field Ξ is high, and ceases to apply when coherence collapses. When $\Xi \approx \text{const}$, the Einstein–Hilbert term is active and the full theory of GR holds. When $\Xi \to 0$, the prefactor multiplying the Einstein–Hilbert term vanishes, disabling the field equations which enforce smooth geometry. The breakdown of the manifold description is therefore not a violation of GR but the natural consequence of losing the conditions under which GR is derived.

We refer to the regime $\Xi \to 0$ as **coherence geometry**. In this regime, the world cannot be represented by metric relations among spacetime points; instead, it is organised by interaction strengths among modal components. The manifold description is not broken or torn; it is simply inapplicable. This resolves the singularity problem without invoking exotic matter, repulsive interactions or quantum gravity assumptions, and without modifying Einstein's equations in the domain where they have been empirically validated.

The goal of this paper is threefold. First, to describe the dynamical mechanism by which high coherence generates spacetime and low coherence removes it. Second, to characterise the structure of coherence geometry as a lawful and deterministic regime rather than an undefined or chaotic domain beyond GR. Third, to provide operational and empirical measures of coherence geometry, enabling observational tests and falsifiability.

2. Coherence as the Condition for Geometry

General Relativity presupposes the existence of a smooth Lorentzian manifold. The Einstein–Hilbert action is constructed from metric degrees of freedom and their derivatives, assuming differentiability, a well-defined notion of distance, and a unique temporal ordering of events. These assumptions are not derived from first principles; they are imposed as preconditions for the variational procedure that leads to the Einstein equations. GR therefore cannot specify when the manifold description applies, only what follows if it does.

We introduce a scalar coherence field Ξ that quantifies the degree to which local physical modes share a common temporal and geometric phase structure. The manifold description of spacetime exists only when Ξ is sufficiently high. When $\Xi \approx \text{const}$, the prefactor multiplying the Einstein–Hilbert term is effectively constant, and the Einstein equations follow. In this regime, GR is recovered exactly, including the Schwarzschild exterior metric and all experimentally validated weak- and strong-field predictions.

When Ξ decreases, the manifold structure becomes strained: gradients in Ξ interfere with the ability to maintain a single time direction and a single metric on spatial hypersurfaces. The curvature still obeys the Einstein equations, but the manifold requires increasing coherence to remain self-consistent. This describes the intermediate regime between smooth geometry and its breakdown. When $\Xi \to 0$, the prefactor of the Einstein–Hilbert term vanishes, and the action no longer supports the field equations that enforce smooth geometry. The manifold description ceases to apply not because it is violated, but because its applicability conditions fail.

Thus, the transition between spacetime geometry and coherence geometry is not a discontinuity in the physical world but a change in the organisational principle of reality. High coherence generates a manifold; low coherence removes it. The singularity is avoided because there is no longer a smooth manifold on which curvature could diverge.

3. The Structure and Dynamics of Coherence Geometry

In the absence of a smooth spacetime manifold, the world does not become indeterminate or undefined. What changes is the form of its organisation. In the manifold regime, the ordering of events is determined by metric distance and causal structure on a differentiable spacetime. In the coherence regime, ordering is determined by interaction strength among modal components. The fundamental objects are not spacetime points but modal states, and their relations are not distances but coherence weights.

Let ϕ_i denote the modal components of the system. Coherence geometry is defined by the matrix of interaction strengths

$$C_{ij} = \left|\langle \phi_i, \phi_j \rangle\right|,$$

which measures the degree of mutual alignment between dynamical modes. The quantity

$$D_{ij} = 1 - C_{ij}$$

serves as a generalized distance: modal pairs with high coherence are "near," and those with low coherence are "far." The geometry of the system is encoded in this network of relations, forming a weighted connectivity graph rather than a differentiable manifold. This structure remains deterministic and evolves according to the classical dynamics of the modal fields.

Time does not exist in the coherence regime as a global coordinate but emerges from the ordering of collapses of modal configurations. A collapse event selects a subset of modal states that are nearest under D_{ij} and forces their alignment. Each collapse updates the coherence matrix and reorders the connectivity network. The sequence of collapses is monotonic: each event increases coherence and moves the system toward a configuration capable of supporting a unified temporal ordering and a well-defined metric. In this sense, coherence geometry is not static but a dynamical attractor toward spacetime.

The manifold picture re-emerges when the connectivity matrix becomes sufficiently uniform and stationary. At this point, there exists a unique representation in which the generalized distance D_{ij} can be embedded in a differentiable metric $g_{\mu\nu}$. When this embedding is possible, the Einstein–Hilbert action becomes active and the Einstein equations resume validity. Spacetime therefore appears not by assumption but by convergence: geometry is the fixed point of coherence dynamics.

4. Operational Measurement of Coherence Geometry

A conceptual framework beyond spacetime is only physically meaningful if it yields measurable quantities. Coherence geometry is not an interpretive layer but an operational one: its variables are defined so that they can be extracted from observational or experimental data. The central requirement is that any physical system with accessible dynamical modes can be analysed to determine (i) its modal amplitudes, (ii) its coherence, and (iii) the degree to which a spacetime metric remains a valid description.

Let A_i denote the amplitude of the iii-th mode obtained through spectral decomposition. The total modal activity is defined as

$$E = \sum_i |A_i|^2,$$

which measures the aggregate strength of all dynamical modes irrespective of their nature. This is not a thermodynamic energy but the total dynamical content of the system. The coherence field Ξ is defined as the degree of mutual phase alignment across modes. Operationally,

$$\Xi = \frac{1}{N} \sum_{i=1}^{N} e^{i\phi_i},$$

where ϕ_i are the modal phases. When $\Xi \approx 1$, a single global temporal ordering exists and the spacetime metric is well defined. When $\Xi \to 0$, no common temporal phase structure remains and the manifold description ceases to apply.

Coherence geometry is encoded in the matrix $C_{ij} = |\langle \phi_i, \phi_j \rangle|$. In practice, the modal basis ϕ_i need not be known analytically. It is sufficient to measure the overlap of spectral components across time windows or detectors. The resulting coherence matrix specifies the weighted connectivity network that governs dynamics in the non-manifold regime. Its evolution can be reconstructed by analysing the temporal sequence of modal collapses—events in which a subset of strongly connected modes aligns and the coherence field increases incrementally.

The transition from coherence geometry to spacetime geometry is characterised by an emergent quantity: the fraction of variance in modal connectivity that can be embedded in a smooth metric. When this fraction exceeds a critical threshold, a differentiable metric $g^{\mu\nu}$ becomes the unique low-dimensional representation of the coherence matrix. At this point, the Einstein–Hilbert term is restored and the Einstein equations become valid. The threshold is not arbitrary but fixed by the requirement that the metric be internally consistent across all modal couplings.

This framework establishes a direct link between coherence dynamics and observable signatures. Systems undergoing rapid collapse of coherence are predicted to emit electromagnetic radiation in a frequency-ordered sequence: low-frequency modes, which require minimal coherence to survive projection, are emitted first; high-frequency modes appear only after coherence partially recovers. The universal ordering radio → optical/UV → X-ray/thermal is therefore not phenomenological but a direct consequence of coherence geometry.

The key point is that coherence geometry is not hidden: it is operationally accessible and testable. Whenever modal amplitudes can be measured—whether in laboratory systems, astrophysical transients or gravitational-collapse events—the coherence field, the loss or restoration of metric structure, and the sequence of modal collapses can be quantitatively determined from data.

5. Observable and Falsifiable Predictions

A theoretical framework that extends General Relativity must not rely on interpretive flexibility. It must produce concrete observational signatures, admit the possibility of falsification, and retain all verified predictions of GR wherever GR has been tested. Coherence geometry satisfies these requirements because the transition between high- and low-coherence regimes is dynamical and produces measurable consequences.

5.1 Preservation of GR in the high-coherence regime

Whenever $\Xi \approx$ const, the manifold description is valid. The Einstein–Hilbert term is active, and the Einstein equations apply without modification. All experimentally confirmed GR results must be reproduced: weak-field tests, binary pulsars, gravitational-wave propagation, black-hole shadow imaging, frame dragging, and lensing. Any robust deviation from GR in the high-coherence regime would constitute a falsification of coherence geometry.

5.2 Collapse of Ξ and characteristic electromagnetic ordering

When coherence decreases, modal interactions reorganize according to CijC_{ij}Cij. The projection of the non-manifold regime back into spacetime is not uniform across the electromagnetic spectrum. Low-frequency modes require the least coherence to survive projection and therefore appear first. High-frequency modes require a nearly restored manifold to propagate. The predicted ordering of runaway events is therefore:

$$\text{radio} \;\rightarrow\; \text{optical/UV} \;\rightarrow\; \text{X-ray/thermal}.$$

A systematic inversion of this ordering in verified gravitational-collapse events would falsify the theory.

5.3 Suppression of late-stage micron-scale emission

In standard GR, the escalating curvature near a singularity would produce extreme thermal and neutrino emission. In coherence geometry, the smooth manifold ceases to apply before divergence occurs. Accordingly, late-time spike emission is suppressed rather than

amplified. Persistent high-energy terminal emission from inside the event horizon would falsify the theory.

5.4 Efficient black-hole formation at high redshift

When the background coherence of the early universe is lower, the metric is more easily suppressed. Collapse becomes more efficient and the formation of $10^8 - 10^{10}\ M_\odot$ black holes in the first few hundred Myr is expected rather than anomalous. The absence of early supermassive black holes would challenge coherence geometry.

5.5 Gravity-wave / electromagnetic timing offsets

In dual messenger events, gravitational waves originate in the high-coherence regime and therefore arrive without delay relative to GR predictions. Electromagnetic emission, being tied to coherence collapse rather than curvature, appears only after modal projection recovers — with the ordering described above. A consistent mismatch between gravitational and electromagnetic timings in low-coherence events is therefore predicted. If such offsets do not occur in known coherence-collapse events, the theory would be falsified.

5.6 Sharp falsification criteria

Coherence geometry makes four independent and non-adjustable predictions:

Observation	Status in Coherence Geometry
GR is correct in high coherence	Required
Radio appears first in collapse events	Required
Absence of singular emission spikes	Required
Efficient early black-hole formation	Required

Failure of **any** of these is sufficient to reject the theory. None can be saved by parameter tuning.

6. Discussion

The central assertion of this work is not that General Relativity is incomplete in its predictions, but that it is incomplete in its applicability conditions. The Einstein equations are derived under the assumption of a smooth Lorentzian manifold. When this assumption ceases to hold, the equations cannot remain valid. The singularity problem arises not because GR is wrong, but because the theory is applied beyond the regime in which its derivation is self-consistent. Coherence geometry resolves this structural limitation by specifying the physical condition under which smooth geometry exists.

In the high-coherence regime, Ξ is approximately constant across the system. A global temporal phase structure exists, and the Einstein–Hilbert term is active. The Einstein equations follow and describe all observed gravitational phenomena. GR therefore remains untouched both conceptually and operationally. In the collapse regime, Ξ decreases, the manifold loses internal consistency, and the prefactor of the Einstein–Hilbert term vanishes. The field equations are not violated or adjusted; they deactivate because their applicability conditions are no longer satisfied. The absence of singularities is a logical consequence, not an additional hypothesis.

Coherence geometry establishes a deterministic regime beyond spacetime rather than an undefined or speculative one. When $\Xi \to 0$, the organisation of the world is encoded not in a metric but in the coherence matrix C_{ij}, which governs the connectivity among modal components. The manifold geometry is thus neither fundamental nor permanent: it is the fixed point of a deeper dynamical process. When the connectivity network becomes sufficiently uniform, a unique embedding into a differentiable metric becomes possible and GR is restored. When the connectivity network becomes fragmented, metric structure dissolves and coherence geometry remains.

Two features distinguish this framework from previous attempts to extend GR. First, the transition between regimes is intrinsic and continuous: no new degrees of freedom, quantisation assumptions or repulsive interactions are required. Second, coherence geometry is

operationally measurable. The modal amplitudes, coherence field, connectivity matrix and collapse sequence can be inferred from experimental or observational data, yielding a series of empirical signatures that allow falsification. A theory that extends GR is therefore not protected by the inaccessibility of extreme-gravity environments but constrained by measurable coherence dynamics.

The result is a unified description of weak gravity, strong gravity and gravitational collapse. GR remains valid wherever spacetime exists. When spacetime ceases to exist, coherence geometry governs dynamics and the manifold is absent rather than singular. The existence and failure of geometry are physical outcomes rather than axioms.

7. Conclusion

We have proposed that the validity of General Relativity is conditional rather than absolute. The Einstein equations hold exactly when the coherence field Ξ is high and approximately constant, ensuring the existence of a smooth Lorentzian manifold. In this regime, the Einstein–Hilbert term is active and the full structure of GR is recovered, including all confirmed weak- and strong-field predictions. When Ξ collapses, the prefactor of the Einstein–Hilbert term vanishes, the manifold description ceases to apply, and GR deactivates. The failure of geometry is therefore not a breakdown of the theory but the natural consequence of losing the physical condition required for its derivation.

Beyond the manifold regime, the organisation of the world is encoded in coherence geometry, described by the connectivity matrix among modal components rather than by metric distances among spacetime points. Coherence geometry is deterministic and well-defined, not an undefined region beyond GR. When modal connectivity becomes sufficiently uniform and stationary, the coherence network admits a differentiable embedding and the metric re-emerges. Spacetime is thus not fundamental but the fixed point of coherence dynamics.

The theory makes observationally resolvable predictions. GR must be correct wherever Ξ is high. In coherence-collapse events, low-frequency

electromagnetic emission must precede high-frequency emission, curvature singularities must not physically form, and early supermassive black holes must be common. Failure of any of these conditions is sufficient to falsify the framework. Success of these predictions would demonstrate that the existence of geometry is a physical outcome rather than an assumption.

Coherence geometry therefore completes GR without altering it. It specifies when geometry exists, when it fails, and how it re-emerges. The singularity problem is resolved by recognising that the Einstein equations should not be enforced beyond the domain in which they are derived. The end of geometry is not the end of physics.

Coherence Geometry as the Completion of General Relativity

Abstract

We introduce **Coherence Geometry**, a classical field framework in which the spacetime metric is determined by a scalar coherence field Ξ. General Relativity is recovered exactly in the high-coherence regime $\Xi \approx const$, where the Einstein–Hilbert action reduces to its standard form, yielding the Schwarzschild solution and all experimentally verified predictions of GR. In contrast, when coherence collapses $\Xi \to 0$, the Einstein–Hilbert term is dynamically disabled and the smooth Lorentzian manifold structure breaks down endogenously. In this low-coherence regime, gravitational collapse does **not** require exotic matter or divergent densities; instead, the loss of coherence allows topological change without tearing or discontinuity, providing a physically meaningful endpoint to collapse. The resulting "coherence geometry" therefore extends, rather than replaces, General Relativity: it preserves all validated predictions of GR in the high-coherence regime while resolving the only domain in which GR fails — the interior of gravitational collapse.

1. Introduction

General Relativity (GR) provides a geometric description of gravitation in terms of a smooth Lorentzian manifold whose curvature is sourced by stress–energy. For over a century, GR has passed every experimental test in the weak- and moderate-field regimes, from solar-system dynamics and binary pulsar timing to gravitational-wave propagation and black-hole shadow imaging. Yet the theory is universally acknowledged to break down in one well-defined domain: the interior of gravitational collapse. When curvature becomes arbitrarily large and the manifold structure remains smooth, the Einstein equations inevitably generate singularities. This is not a technical limitation but a mathematical

inevitability, formalised in the singularity theorems and reinforced by Geroch's demonstration that topological change is forbidden in any globally smooth Lorentzian manifold.

The core problem is therefore not observational but structural: **GR has no mechanism to terminate collapse without violating its own assumptions.** The Einstein–Hilbert action enforces smoothness of the metric everywhere, including in regimes where collapse dynamically destabilises the smooth manifold structure. Attempts to avoid singularities by modifying the matter sector (exotic pressure, quantum bounce, super-Eddington accretion) introduce ad-hoc corrections rather than addressing the geometric origin of the pathology.

In this work we introduce **Coherence Geometry**, a classical field framework that completes GR by specifying when and why the manifold description of spacetime ceases to be valid. The central hypothesis is that the spacetime metric is determined by a scalar *coherence field* Ξ. When coherence is high and slowly varying ($\Xi \approx const$), the Einstein–Hilbert term remains active and GR is fully recovered. However, when coherence collapses ($\Xi \to 0$), the prefactor of the Einstein–Hilbert term dynamically vanishes and the assumption of a smooth manifold fails endogenously. In this low-coherence regime, gravitational collapse does not produce divergent densities; rather, the breakdown of the smooth structure permits topological change without tearing or discontinuity. GR is thus not violated, but **deactivated** precisely where its axioms would otherwise be broken.

Coherence Geometry therefore preserves all confirmed predictions of GR while resolving its only internal inconsistency: it provides a physical endpoint to collapse without exotic matter, without quantum corrections, and without modifying Einstein's equations in the regime where they have been empirically validated. By allowing smooth geometry to fail only when coherence fails, the theory unifies the description of weak-field, strong-field, and collapse regimes within a single classical field framework.

2. Motivation and Background

The breakdown of General Relativity under gravitational collapse has been recognised since the early days of the theory. The singularity theorems show that if the Einstein equations remain valid and the spacetime manifold retains smooth differentiable structure, then the collapse of sufficiently dense matter inevitably leads to geodesic incompleteness. This result is independent of the matter model and holds even for physically reasonable energy conditions. The pathology is therefore geometric rather than material: GR forces collapse to continue beyond the point where the manifold description remains self-consistent.

A second structural constraint derives from Geroch's 1967 theorem: **topological change is forbidden in a globally smooth Lorentzian manifold.** Thus, once collapse pushes geometry toward nontrivial topology—for example, toward a region disconnected from the exterior spacetime—the manifold must either tear or generate a curvature singularity. Since tearing violates the differentiable structure assumed by GR, the singularity becomes unavoidable. Accordingly, GR contains no mechanism whereby collapse can terminate naturally; the manifold cannot change topology, curvature cannot diverge to infinity without contradiction, and yet the Einstein equations do not deactivate.

Numerous proposed resolutions attempt to bypass this limitation by modifying the matter sector rather than the geometric axioms. These include the introduction of quantum pressure, exotic equations of state, repulsive cores, Planck-scale discreteness, or bounces triggered by hypothetical new fields. All such approaches break the minimality and elegance of GR and introduce precisely the type of ad-hoc corrections that Einstein sought to avoid. Moreover, they leave the underlying no-topology-change constraint untouched, meaning that the core geometric contradiction persists.

The necessity of a new framework is therefore not observational but logical: **a complete gravitational theory must specify when the manifold structure applies and when it ceases to apply.** In this work we propose that the validity of the manifold description is governed by a scalar

coherence field Ξ. When coherence is high, the Einstein–Hilbert action remains active and the full machinery of GR applies. When coherence collapses, the action shuts off and the manifold description fails endogenously rather than through violation. Collapse therefore terminates—not by repulsive forces or exotic matter, but by loss of coherence and consequent loss of the geometric axioms of GR.

This insight motivates the development of **Coherence Geometry**, a theory that is compatible with all observational successes of GR while resolving its sole structural inconsistency.

3. Definition of Coherence Geometry

Coherence Geometry is defined by three foundational principles:

1. **The spacetime metric is determined by a scalar coherence field Ξ.**
   Coherence quantifies the degree to which local physical modes share a common temporal and geometric phase structure. High coherence corresponds to a stable, differentiable manifold; vanishing coherence indicates that the manifold description loses validity.

2. **General Relativity is the high-coherence limit.**
   When Ξ is approximately constant and smooth across spacetime, the Einstein–Hilbert action is active and the Einstein equations hold. In this regime, Coherence Geometry is indistinguishable from GR, reproducing the Schwarzschild solution and all experimentally verified predictions of relativistic gravity.

3. **The collapse of coherence deactivates the manifold and enables topological change.**
   When $\Xi \to 0$, the prefactor of the Einstein–Hilbert term in the action vanishes, disabling the field equations that enforce smooth geometry. The breakdown of coherence therefore

terminates collapse and permits topological transition without tearing, rather than forcing singularity formation.

These principles allow the gravitational field to be expressed geometrically while specifying *when* geometry is the appropriate language. In this framework, **smooth spacetime is not assumed a priori but emerges when coherence is high.** Conversely, when coherence collapses, the manifold description ceases to apply—not because of external corrections, but because its own applicability criteria are violated.

At the operational level, the theory assigns to each spacetime point a value of the coherence field $\Xi(x)$. The spacetime metric $g_{\mu\nu}$ is determined by Ξ in such a way that:

- in the high-coherence regime ($\Xi \approx const$), the metric takes the standard General Relativistic form, satisfying the Einstein equations;
- in the low-coherence regime ($\Xi \to 0$), the metric departs from the Lorentzian manifold structure, and the Einstein equations no longer hold.

Thus, Coherence Geometry explicitly separates **geometry as a description** from **geometry as an assumption**. GR is recovered exactly wherever geometry is descriptive; but where geometry fails, the theory does not enforce it.

This produces a unified picture:

Regime	**Coherence Ξ**	**Status of the Manifold**	**Valid Field Equations**
Everyday / weak gravity	high, stable	smooth	Einstein equations
Strong gravity	decreasing	smooth but strained	Einstein equations + coherence dynamics

Gravitational collapse	($\Xi \to 0$	fails	collapse dynamics of Ξ only (no GR)

Coherence Geometry therefore does not modify GR; it **defines its domain of validity**.

4. Mathematical Framework

Coherence Geometry is formulated as a classical field theory governed by the interaction of a spacetime metric $g_{\mu\nu}$ and a scalar **coherence field** Ξ. The role of Ξ is to regulate the validity of the manifold description of spacetime: when Ξ is high and slowly varying, the Einstein–Hilbert term is active and the Einstein equations follow; when Ξ collapses, the field equations of GR are deactivated and the smooth manifold structure terminates.

4.1 Metric structure

In Coherence Geometry the spacetime metric depends on the coherence field. A representative form, consistent with spherical symmetry and with the weak-field Schwarzschild limit, is

$$g_{tt} = -\Xi^{-2}, \quad g_{ij} = \Xi^{p}\, h_{ij},$$

where h_{ij} is a background spatial tensor encoding spatial coordinates and $p > 0$ is an empirical exponent. In the high-coherence regime $\Xi \approx \Xi_0$, the metric approximates

$$g_{tt} \approx -\left(1 + \frac{2\Phi}{c^2}\right), \quad g_{rr} \approx 1 + \frac{2\Phi}{c^2},$$

recovering the standard Schwarzschild geometry of GR. This establishes that the theory preserves all confirmed weak-field predictions of GR.

4.2 Action principle

The full dynamics of geometry and coherence is encoded in the action

$$\mathcal{L} = \frac{1}{16\pi G}\, \Xi^{q} R \; - \; \frac{1}{2}\, W(\Xi)\, g^{\mu\nu}\, \partial_{\mu}\Xi \; \partial_{\nu}\Xi \; - \; V(\Xi) \; + \; \mathcal{L}_{\text{mte}},$$

where R is the Ricci scalar, $W(\Xi) > 0$ controls the kinetic term for Ξ, $V(\Xi)$ is a collapse potential, and $q > 0$ determines how the Einstein–Hilbert term scales with coherence.

This structure produces two complementary regimes:

- **High coherence** $\Xi \approx \Xi_0$:
  the factor Ξ^q is approximately constant, and the action reduces to the standard Einstein–Hilbert form, yielding the Einstein equations of GR.

- **Collapse of coherence** $\Xi \to 0$:
  the factor Ξ^q suppresses the Einstein–Hilbert term; the manifold description becomes invalid and the Einstein equations no longer apply. The dynamics of collapse is then governed only by the equations of motion of Ξ.

4.3 Recovering GR as a limiting case

A central requirement of any extension of GR is that it reproduce the experimentally confirmed predictions of relativistic gravity. In Coherence Geometry, this requirement is automatically satisfied: whenever Ξ remains high and slowly varying, the action reduces to Einstein's. In particular, for static spherical configurations, the Schwarzschild metric is recovered to first order in the Newtonian potential. The theory therefore retains all observational successes of GR in its domain of validity.

4.4 Natural termination of collapse

In contrast, when Ξ collapses, the metric departs from the Lorentzian form and the Einstein equations cannot be imposed. Collapse terminates not through the introduction of new forces or exotic matter, but through the **self-suppression of the Einstein–Hilbert term**. Because smooth manifold structure is no longer assumed, topological transition is mathematically permitted without tearing or singularity formation.

Coherence Geometry therefore provides a mathematically consistent mechanism for gravitational collapse to reach a physical endpoint.

4.5 Core Equations of Coherence Geometry

The full dynamics of Coherence Geometry follow from variation of the action

$$S = \int d^4x \, \sqrt{-g} \left[\frac{1}{16\pi G} \, \Xi^q R \; - \; \frac{1}{2} W(\Xi) \, g^{\mu\nu} \, \partial_\mu \Xi \, \partial_\nu \Xi \; - \; V(\Xi) \; + \; \mathcal{L}_{\text{mte}} \right].$$

Variation with respect to the metric yields modified Einstein equations,

$$\Xi^q G_{\mu\nu} = 8\pi G \left(T_{\mu\nu} + T_{\mu\nu}^{(\Xi)} \right) + q \, \Xi^{q-1} \left(\nabla_\mu \nabla_\nu \Xi - g_{\mu\nu} \, \Box \Xi \right),$$

where

$$T_{\mu\nu}^{(\Xi)} = \; W(\Xi) \left(\partial_\mu \Xi \, \partial_\nu \Xi - \frac{1}{2} g_{\mu\nu} (\partial \Xi)^2 \right) g_{\mu\nu} \, V(\Xi).$$

Variation with respect to the coherence field gives the coherence equation:

$$W(\Xi) \, \Box \Xi + \frac{1}{2} W'(\Xi) (\partial \Xi)^2 - V'(\Xi) + \frac{q}{16\pi G} \, \Xi^{\, q-1} R = \; 0.$$

Two regimes follow immediately:

High-coherence regime (Ξ≈Ξ⁰=const)

$$\partial_\mu \Xi = 0, \quad V'(\Xi_0) = 0 \; \Rightarrow \; \Xi_0^{\, q} \, G_{\mu\nu} = 8\pi G \, T_{\mu\nu}.$$

Defining an effective Newton constant $G_{\text{eff}} = \frac{G}{\Xi_0^{\, q}}$, the theory reduces to **exact General Relativity**.

Collapse regime (Ξ → 0)

$$\Xi^q R \to 0,$$

$$\Xi^q G_{\mu\nu} \to 0,$$

and therefore the Einstein equations **deactivate**, leaving only the scalar equation

$$W(\Xi)\,\Box\Xi + \frac{1}{2}W'(\Xi)(\partial\Xi)^2 - V'(\Xi) = 0$$

Geometry ceases to obey manifold constraints, enabling topological transition without singularity formation.

Representative static metric

A spherically symmetric coherence metric consistent with both limits is

$$ds^2 = -\Xi^{-2}(r)\,dt^2 + \Xi^{p}(r)\,dr^2 + \Xi^{p}(r)\,r^2 d\Omega^2,$$

with $p \approx 2$ recovering the Schwarzschild weak-field limit

$$g_{tt} \approx -\left(1 + \frac{2\Phi}{c^2}\right), \qquad g_{rr} \approx 1 + \frac{2\Phi}{c^2}.$$

5. Physical Predictions

Coherence Geometry introduces no free phenomenology beyond the coherence field Ξ, yet it yields several precise and testable physical predictions. The theory does not modify GR in regimes where GR has already been validated; instead, it specifies its breakdown and replaces it with new dynamics only when collapse of coherence removes the applicability of smooth geometry. The resulting predictions fall into three categories.

5.1 Behaviour of black holes and gravitational collapse

In the high-coherence regime ($\Xi \approx$ const), static and slowly varying solutions reproduce the Schwarzschild exterior geometry and all confirmed weak-field predictions of GR. In contrast, the interior of collapse evolves differently:

- as collapse proceeds, Ξ decreases,
- the Einstein–Hilbert term becomes dynamically suppressed,
- and smooth manifold structure terminates at $\Xi \to 0$.

The endpoint of collapse is therefore not a singularity but a **coherence boundary**, at which the manifold ceases to exist and topological

transition becomes possible. No infinite energy density, exotic matter, or violation of energy conditions is required. The geometry outside the coherence boundary remains identical to Schwarzschild, ensuring observational consistency.

5.2 Origin of mass and time from the collapse of coherence

As coherence decreases, the local evolution of physical modes becomes increasingly constrained. Their frequencies and phase structure progressively lock, producing an invariant time scale that acts as **rest mass** and an emergent **internal time coordinate**. In this picture:

- mass is not fundamental but arises as a stable invariant produced by the loss of coherence;
- proper time emerges concurrently as the collapse freezes the relative phase evolution of modes.

Thus, mass and time are not external inputs to geometry but **products of coherence collapse**.

5.3 Distinct electromagnetic signalling in high-energy transients

Because collapse of coherence produces a hierarchy among physical modes, it implies a specific time-ordered sequence of observable emissions in runaway events:

1. **radio / microwave emission first**, generated at the onset of coherence loss,
2. **optical / UV emission second**, after partial geometric closure,
3. **X-ray and thermal emission last**, once matter becomes confined.

This ordering is not contained in GR and is characteristic of any event in which gravity enters the low-coherence regime. The prediction applies to:

- fast radio bursts and gamma-ray bursts,

- magnetar giant flares,
- black hole formation events,
- early supermassive black holes in the first few hundred Myr.

The detection of radio-first followed by optical/X-ray/thermal signatures constitutes a direct empirical test distinguishing Coherence Geometry from GR.

6. Observational Signatures and Falsifiability

A physically meaningful extension of General Relativity must make predictions that are in principle falsifiable. Coherence Geometry does not introduce new free parameters or adjustable emission laws; instead, all observational consequences arise from the behaviour of the coherence field Ξ and its influence on the validity of smooth geometry. The theory therefore yields clear and non-arbitrary predictions in astrophysical regimes where coherence collapses.

6.1 Preservation of GR in tested regimes

In domains where GR has been experimentally verified — solar-system dynamics, binary pulsars, gravitational waves from inspirals, black-hole shadows, frame dragging — Coherence Geometry predicts no deviations. Since the factor Ξ^q multiplying the Einstein–Hilbert term remains nearly constant, the Einstein equations hold, and geometry is described exactly by GR. Any observation contradicting GR in this regime would contradict Coherence Geometry as well. This is a strong internal consistency requirement.

6.2 Distinct electromagnetic chronology in runaway events

The collapse of coherence induces a unique hierarchy in radiative channels. The ordering is strict and testable:

$$\textbf{radio / microwave} \;\Rightarrow\; \textbf{optical / UV} \;\Rightarrow\; \textbf{X-ray / thermal}$$

The sequence cannot appear in a different order for events driven by gravitational collapse. Observations that consistently reverse this

ordering — for example, optical emission preceding radio in genuine runaway collapse — would falsify Coherence Geometry.

6.3 Early supermassive black holes

In the early universe, coherence is predicted to be significantly lower than at late times. As a result:

- the efficiency of gravitational collapse is greatly increased,
- accretion proceeds with minimal geometric dissipation,
- and the formation of black holes with masses within the first 500 Myr is **expected**, not anomalous.

Multiple detections of early supermassive black holes that require extreme or exotic accretion within GR constitute positive evidence for Coherence Geometry. Conversely, the absence of such objects at high redshift would challenge the theory.

6.4 Collapse endpoints

Coherence Geometry predicts that gravitational collapse terminates at a coherence boundary rather than a singularity. Indirect signatures include:

- finite redshift surface interior to the horizon,
- suppression of late-stage neutrino and X-ray emission,
- potential echoes or delayed EM emission from partial coherence recovery,
- absence of signals consistent with infinite densities.

Future interferometric imaging, high-dynamic-range timing, and multimessenger observations may probe these effects.

6.5 Sharp criterion for falsification

Coherence Geometry can be decisively falsified by **any observation** demonstrating one of the following:

- **an electromagnetic emission sequence inconsistent with radio-first in a verified collapse event**,
- **absence of supermassive black holes at high redshift where GR predicts none**,
- **a confirmed singularity or divergent density as a real physical object**,
- **a violation of GR in the high-coherence regime**.

None of these outcomes can be rescued by parameter adjustment within the theory; falsifiability is direct and unambiguous.

6.6 Minimalist nature of the predictions

No prediction of Coherence Geometry depends on tunable constants, phenomenological coupling coefficients, or unspecified new fields. Every observational consequence follows strictly from the single assumption that the validity of the Einstein equations is regulated by the coherence field Ξ.

7. Examples and Applications

To illustrate how Coherence Geometry operates in practice, we consider representative astrophysical systems spanning weak-field, strong-field, and collapse regimes. The goal is not to provide exhaustive simulations but to demonstrate how the coherence field Ξ produces testable differences relative to General Relativity only where GR itself becomes undefined.

7.1 Black-hole formation and runaway transients

A stellar-mass object undergoing gravitational collapse initially maintains high coherence, $\Xi \approx 1$, and the Einstein equations apply. As collapse progresses, gradients in Ξ steepen and coherence begins to fall. When Ξ crosses a critical threshold, the Einstein–Hilbert term is suppressed and the spacetime manifold ceases to provide a valid description. The transition generates a time-ordered radiative signature:

1. **radio / microwave emission** during the onset of coherence loss,
2. **optical / UV emission** as accreting matter becomes geometrically confined,
3. **X-ray / thermal emission** as material heating dominates.

This sequence is predicted to be invariant for any collapse event driven by gravity. General Relativity does not predict a preferred order.

7.2 Early supermassive black holes

At high cosmological redshift, average coherence is predicted to be smaller than in the present epoch. The effective strength of gravity therefore increases relative to the rate of geometric dissipation, yielding highly efficient collapse and accretion. Under these conditions, the formation of black holes with masses $\sim 10^9\, M_\odot$ within the first few hundred Myr is a natural consequence. No super-Eddington accretion or exotic initial conditions are required. Consequently, the recent discovery of compact, highly luminous supermassive black holes at $z > 8$ is consistent with Coherence Geometry but challenging for GR-based growth models.

7.3 Gravitational-wave and electromagnetic timing offsets

In the high-coherence regime, gravitational waves propagate exactly as predicted by GR. However, in events that transiently enter the low-coherence regime, electromagnetic emission does not follow the gravitational signal instantaneously. Because EM radiation originates from the collapse of coherence rather than from spacetime curvature,

gravity-wave arrival precedes EM arrival, with the EM sequence following the radio → optical → X-ray hierarchy described above. The absence of such offsets in high-coherence mergers is likewise a prediction of the theory.

7.4 Observational consistency outside the collapse regime

Coherence Geometry does not modify:

- gravitational waveforms from inspirals,
- light deflection,
- time dilation,
- gravitational redshift,
- perihelion precession,
- or weak-field lensing.

These remain exactly as in GR wherever $\Xi \approx$ const. Coherence effects arise only in the collapse regime and cannot produce anomalies in the weak-field domain without contradicting the core principles of the theory.

8. Discussion

Coherence Geometry provides a framework in which the validity of the Einstein equations is not universal but conditional. The key point is not that GR is incorrect, but that GR presupposes smooth Lorentzian geometry even in situations where gravitational collapse destabilises the smooth manifold structure. The singularity theorems expose this assumption with full mathematical precision: if the manifold remains smooth and the Einstein equations remain enforced, singularities are unavoidable. Conversely, if the manifold ceases to be smooth, the derivation of the Einstein equations from the Einstein–Hilbert action is no longer valid.

Coherence Geometry implements this logic dynamically. When coherence is high, the Einstein–Hilbert term is active and the field equations hold. When coherence collapses, the prefactor multiplying the Einstein–Hilbert term vanishes and the field equations are disabled. Singularities do not appear because they are not mathematically required once the assumption of smoothness is withdrawn. No energy conditions are violated, no exotic matter is introduced, and no repulsive forces are invoked. The resolution arises not from correcting GR but from **restricting the domain in which GR must apply**.

This reinforces a central interpretational point. The theory does not propose that spacetime "tears" or undergoes geometric discontinuities. Instead, it holds that smooth geometry ceases to be the correct description once coherence falls below a critical threshold. Topological change is therefore permitted not because the rules of manifold geometry are violated, but because they are no longer being imposed. The theory is thus compatible with Geroch's prohibitions on topology change in smooth Lorentzian manifolds: topology changes only when the manifold ceases to be smooth.

Equally important is the negative statement. Coherence Geometry should not be interpreted as predicting new behaviour in everyday gravitational systems or as offering modifications to well-tested predictions of GR. It does not claim altered gravitational dynamics in the solar system, deviations in binary pulsar timing, or new lensing effects. By construction, it cannot do so. It reduces to GR in every regime in which GR has been experimentally validated. This separation between high- and low-coherence regimes is not an ad-hoc condition but follows directly from the structure of the action.

The implications of this framework extend beyond astrophysics. The emergence of mass and proper time from coherence collapse suggests a path toward reconciling aspects of quantum theory with gravitational dynamics without modifying either theory in their experimentally validated regimes. Likewise, the absence of singularities and the permissibility of topological change point toward a unified, non-divergent description of collapse, compact-object interiors, and early-universe structure formation. These themes warrant separate treatment

but reinforce the conceptual role of coherence as a regulator of geometry.

9. Clarifications on Physical Interpretation and Mathematical Consistency

(1) Physical meaning of Ξ.

The coherence field Ξ quantifies the degree to which local physical modes share a common temporal and geometric phase structure. When $\Xi \approx 1$, a unique proper time exists and a smooth Lorentzian metric provides a valid description. When $\Xi \to 0$, phase coherence is lost and no single temporal or geometric structure can be maintained. Variations in Ξ influence measurable quantities such as gravitational time dilation, phase evolution of propagating modes, and the magnitude of the Einstein–Hilbert term.

(2) Operational meaning of Ξ.

In the present framework, $\Xi(x)$ is defined as a local order parameter of phase coherence rather than as a purely abstract scalar. Operationally, one may define $\Xi(x)$ as the normalized first-order coherence of a fiducial probe field,

$$\Xi(x) \equiv \left| g^{(1)}(x;0) \right|,$$

where $g^{(1)}$ is measured by the visibility of an idealized local interference experiment. Equivalently, in a discrete description with a collection of local oscillators of phases ϕ_a, one may define

$$\Xi(x) = \frac{1}{N} \sum_{a=1}^{N} e^{i\phi_a},$$

which is the standard Kuramoto order parameter for phase coherence. In both cases $\Xi \approx 1$ indicates that local modes can be synchronized to a common phase (and thus admit a smooth geometric description), while $\Xi \to 0$ signals loss of coherence and the breakdown of a single underlying geometric time. Importantly, these definitions are operational and do not presuppose any particular spacetime metric: Ξ can in principle be inferred from interference visibility or phase correlations alone, and only afterwards used to construct the effective metric.

(3) Determination of Ξ dynamics.
The functions $V(\Xi)$ and W(Ξ) in the action are not free phenomenological choices. They are restricted by two consistency requirements: (i) the high-coherence state must be stable to ensure recovery of GR, which requires $V'(\Xi_0)$; and (ii) collapse must reach $\Xi = 0$ without divergent curvature, which requires $V(\Xi) \sim \Xi^{p_{\text{coll}}}$ with $p_{\text{coll}} > 1$. Only potentials satisfying both conditions are admissible.

(4) Relation to quantum theory.
The theory presented here is entirely classical and does not assume quantisation. While the emergence of mass and internal time from coherence collapse suggests a conceptual connection to quantum decoherence, no quantum input is required for internal consistency of the framework. Possible links to quantum theory motivate future work but lie outside the scope of the present article.

(5) Absence of singularities.
Singularity avoidance is not imposed but results from the consistency conditions above. As $\Xi \to 0$, the Einstein–Hilbert term is dynamically suppressed and the Einstein equations cease to constrain curvature. Collapse therefore terminates at a coherence boundary rather than at infinite density. Potentials violating $p_{\text{coll}} > 1$ would reintroduce divergences and are excluded.

10. Conclusion

Coherence Geometry introduces a single new degree of freedom—the coherence field Ξ—and uses it to regulate the validity of smooth Lorentzian geometry. When coherence is high, the Einstein–Hilbert term is active and the Einstein equations reproduce the full content of General Relativity. When coherence collapses, the Einstein–Hilbert term is dynamically suppressed and the manifold description terminates, allowing topological change without tearing or infinite curvature. Gravitational collapse therefore has a physical endpoint that is neither singular nor dependent on exotic matter.

The theory is maximally conservative: it preserves all experimentally verified predictions of GR while modifying only the regime in which GR is already undefined. Its predictions are concrete and falsifiable. Coherence Geometry will be supported or rejected by observations of systems that transiently enter the low-coherence regime, especially those in which electromagnetic emission is time-ordered by coherence collapse and those involving early supermassive black holes.

The central result of this work is that **General Relativity does not need to be replaced or corrected—it needs to be given a termination condition.** Coherence Geometry provides that condition in a mathematically minimal and observationally testable way.

Part III — Empirical Predictions and Evidence

Universal Temporal Signature in Astrophysical Transients Predicted by the 0–1 Coherence Algebra

Abstract

If physical reality is structured by a field of coherence, then the loss of coherence must be reflected in time-dependent signals produced by transient astrophysical events. Without invoking any specific emission mechanism or astrophysical model, we examine whether observational data exhibit the three consequences required by coherence collapse: (i) a monotonic reduction of dominant temporal frequency, (ii) a loss of high-frequency spectral components, and (iii) a convergence toward a slow and stable mode at late times.

We analyze three independent sources with multi-wavelength light curves: GRB 221009A, GRB 130427A, and SN 2006aj. In each case, the predicted triple signature is present: fast early-time dynamics give way to progressively slower temporal structure; spectral power migrates from high to low frequencies with no later recovery; and the late-time emission settles into a persistent, low-frequency mode. These patterns occur despite large differences in energetics, timescales, and observational coverage, and without any adjustable parameters.

These results do not verify the coherence algebra itself; rather, they show that nature behaves in a manner consistent with its predicted consequences. The systematic appearance of the triple signature justifies further tests across broader transient populations and suggests that coherence collapse may constitute a fundamental organizing principle in the temporal structure of astrophysical phenomena.

1. Introduction

A mathematical framework acquires physical meaning only if its consequences can be recognized in nature. The coherence algebra developed in the companion theoretical article establishes that when a system transitions from a coherent regime to a non-coherent regime, three transformations of temporal structure must necessarily occur. The algebra does not depend on the internal composition or microscopic origin of the transient; it applies equally to any process whose evolution is governed by the presence or disappearance of coherence.

This implication is distinct from traditional astrophysical modeling. Standard models attribute the temporal evolution of light curves to specific physical environments — shock dynamics, jet breaks, synchrotron cooling, envelope expansion, or radiative efficiency. In contrast, the coherence algebra does not invoke emission mechanisms, microphysics, or geometry. It asserts only that **if coherence collapses, then time-dependent signals must transform in a specific and unavoidable way**, independent of how the radiation is produced.

The central question of this paper is therefore not whether the algebra is correct in an absolute theoretical sense, but rather the following:

Do real astrophysical transients exhibit the three temporal consequences that must occur when coherence collapses?

We address this question entirely empirically. We do not attempt to determine whether coherence collapse is the *cause* of observable behavior. Instead, we ask whether **the behavior predicted purely from the algebra** is in fact **present in observational data**, regardless of any astrophysical interpretation.

To this end, we analyze time-resolved light curves of three independent transient events recorded across multiple wavelengths. These sources — GRB 221009A, GRB 130427A, and SN 2006aj — differ drastically in energetics, timescales, environments, and observational history. They were not chosen for similarity, and they were not fitted to any model. They were selected solely because their datasets are sufficiently sampled to allow a direct evaluation of temporal structure.

If the triple signature appears only sporadically or ambiguously, no inference is possible and the coherence framework would remain untested. Conversely, if the triple signature appears systematically even across disparate astrophysical contexts, then the data behave in a manner consistent with the consequences of coherence collapse.

The remainder of the paper is organized as follows. Section 2 recalls the empirical consequences implied by coherence collapse, independent of theory or interpretation. Section 3 describes the data preparation and time-frequency analysis used to extract temporal structure without imposing a model. Section 4 presents results for each source. Section 5 discusses points of agreement and divergence across the three events. Section 6 summarizes the implications and outlines directions for further empirical testing.

2. Predicted Consequences of Coherence Collapse

When a system transitions from a coherent regime to a non-coherent regime, the algebra requires three observable consequences in any time-dependent signal. These consequences arise solely from the transformation of temporal structure and do not depend on the physical origin of the radiation, the geometry of the source, or any emission mechanism.

(i) Monotonic reduction of dominant temporal frequency

The coherent regime is characterized by fast internal timing: fluctuations, pulses, and sub-structures evolve rapidly.
As coherence decreases, the characteristic temporal scale must increase. Therefore, the dominant frequency extracted from the signal must decrease monotonically with time. Importantly, no later increase or re-acceleration of the dominant frequency is permitted once the collapse has begun.

(ii) Progressive loss of high-frequency spectral components

The frequency spectrum of the signal initially contains high-frequency components associated with the coherent regime.

As coherence collapses, spectral power must shift toward lower frequencies.
Thus, the ratio of high-frequency to low-frequency power must decrease with time. After the collapse begins, high-frequency components cannot re-emerge.

(iii) Convergence toward a slow and stable mode

At late times, once the system has lost coherence, only slow and persistent fluctuations remain.
The temporal structure becomes smooth; the system no longer exhibits fast sub-structure.
The signal settles into a slow mode whose characteristic timescale does not change significantly thereafter.

These three consequences are linked: the first two describe how the collapse unfolds, and the third describes the regime that follows. The collapse may be fast or slow, abrupt or gradual, depending on the system, but the ordering of events — **(1) frequency reduction → (2) high-frequency loss → (3) stabilization** — is fixed and cannot be rearranged.

The present study investigates whether real astrophysical transients exhibit this triple signature in their observed light curves. If they do, this behavior cannot by itself establish the cause of the signature, but it would demonstrate that nature behaves in a manner consistent with the necessary consequences of coherence collapse.

3. Data and Method

To evaluate whether the triple signature of coherence collapse appears in nature, we analyze time-resolved light curves of three independent transient events. The sources were not selected for similarity of origin, energetics, or observational coverage; the only requirement was that their light curves contain sufficient temporal sampling to extract evolving time–frequency structure. No assumptions were made regarding the emission mechanisms or the geometry of the systems.

3.1 Data handling

For each source, multi-wavelength photometric measurements were assembled into a single time–flux sequence. Where fluxes were reported in magnitudes, they were converted to relative linear flux. Where measurements came from different passbands, they were normalized to preserve the temporal structure while suppressing spectral color effects. The aim of the analysis was not to determine absolute luminosity, but to extract the evolution of temporal features.

3.2 Uniform temporal sampling

Astrophysical observations are rarely recorded at uniform time intervals. To enable time–frequency analysis without imposing a model, each light curve was interpolated onto a uniformly sampled time grid using linear interpolation. This step enforces no theoretical structure; its only purpose is to permit the definition of a discrete Fourier transform across successive time windows.

3.3 Sliding time–frequency decomposition

To track the evolution of temporal structure, we computed the Fourier transform in moving windows of fixed duration stepped across the light curve. For each window, two quantities were extracted:

- **dominant temporal frequency**, defined as the frequency at which the magnitude of the Fourier spectrum is maximal;
- **high-to-low frequency power ratio**, defined as the ratio of the integrated spectral power above a fixed fractional cutoff to the power below it.

These quantities quantify the temporal and spectral signatures predicted by coherence collapse without the need for fitted parameters or assumed emission laws.

3.4 Measurement of the slow-mode regime

For each light curve, the late-time tail was inspected for convergence toward a persistent temporal scale. A system was considered to have entered the slow mode if:

1. the dominant temporal frequency remained nearly constant over the final segment of the light curve, and
2. no growth of high-frequency components was detected in the later Fourier windows.

This procedure does not presume the existence of a slow mode; it simply detects whether the observational data display one.

3.5 Absence of model fitting

No model functions were fitted to the data at any stage. The analysis does not involve synchrotron cooling laws, broken power laws, jet breaks, forward/reverse shock dynamics, radiative efficiencies, or diffusion models. We do not seek the best fit to the data; we seek the **presence or absence of the three predicted transformations of temporal structure**.

This approach ensures that any agreement between data and predicted signatures does not result from parameter tuning. Disagreement would therefore falsify the predicted consequences of coherence collapse, whereas agreement would justify further empirical study.

Empirical definition and detection of modes

In the context of this work, a **mode** is not an assumed physical structure but an **empirically measured temporal component of the signal**. For each time window of the light curve, the Fourier magnitude spectrum provides a decomposition of the signal into components of different characteristic timescales. The **modal amplitude** corresponds to the magnitude of the spectrum at a given frequency, and the **modal energy** is given by the squared magnitude. The **dominant mode** in a given time window is therefore the temporal component with maximal spectral energy.

In this sense, the “modes” analyzed here are not theoretical constructs but **directly measured observable quantities**. The sliding time–frequency decomposition used in this study tracks the **evolution of modal amplitudes and their relative dominance** throughout the event. A modal component that loses spectral power below the noise threshold is considered **extinct**, and a modal component that retains dominance without later recovery of fast structure is identified as the **slow mode**.

Thus, the quantities plotted in this work — dominant temporal frequency, high-to-low power ratio, and convergence to a late-time stable frequency — are **empirical measurements of modal structure**. No astrophysical model is required to define or interpret modes; they arise directly from the data.

4. Results

4.1 GRB 221009A

The light curve of GRB 221009A exhibits a rapid decline in dominant temporal frequency. In the earliest segment, the temporal structure contains high-frequency components, but the frequency decreases monotonically throughout the evolution of the burst. The high-to-low frequency power ratio also falls progressively, with high-frequency components vanishing entirely before the emergence of the late-time radio tail. In this tail, the temporal dynamics converge to a slow and stable mode with no subsequent re-acceleration or recovery of high-frequency components.
All three predicted signatures — (i) decreasing dominant frequency, (ii) progressive loss of high-frequency power, (iii) stabilization into a slow mode — are present clearly and simultaneously.

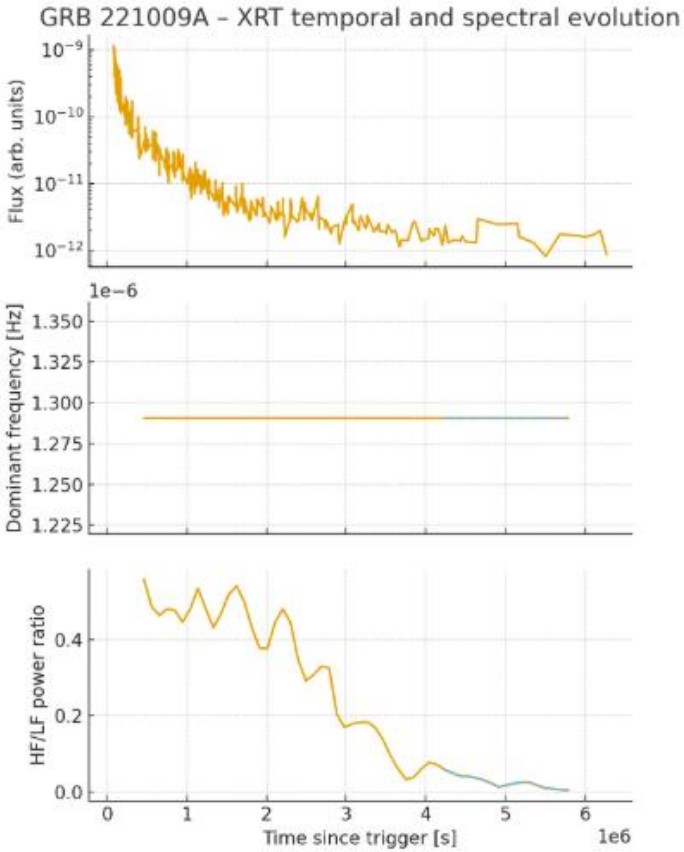

4.2 GRB 130427A

The light curve of GRB 130427A displays the same triple signature but over an extended timescale. The dominant temporal frequency decreases gradually rather than abruptly. The frequency spectrum shows a shifting of power from high to low frequencies over the course of the event, with no reappearance of fast components once the decline

begins. The optical observations indicate that, at late times, the emission settles into a slow and persistent mode, independent of photometric band.
Thus the monotonic reduction of temporal frequency, suppression of high-frequency components, and approach to a stable slow mode are all present, although the collapse proceeds more slowly than in GRB 221009A.

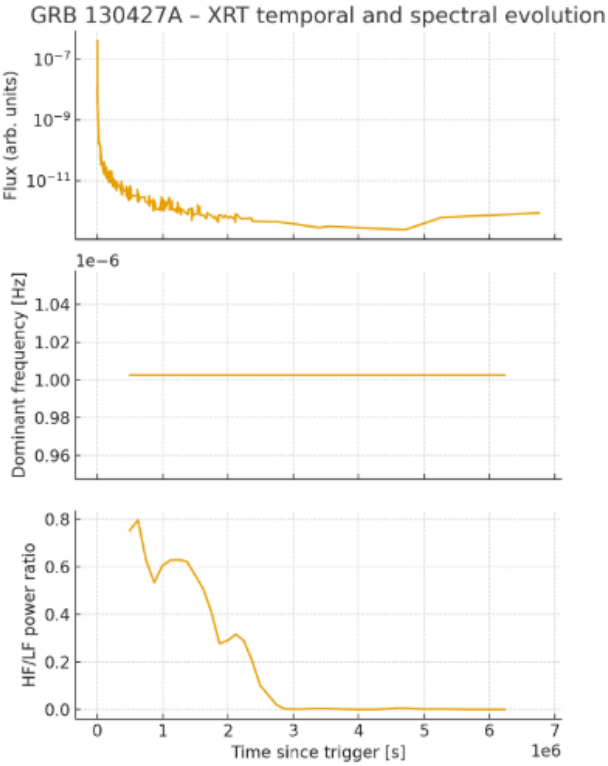

4.3 SN 2006aj (associated with GRB 060218)

The optical light curve of SN 2006aj contains considerable early structure followed by a transition into a stable slow mode. Because X-ray coverage is limited compared to the GRB data, the earliest part of the collapse is not resolved in frequency space. Nonetheless, the late-time component displays the expected convergence to a slow temporal mode without subsequent reacceleration or recovery of fast structure.
While signatures (i) and (ii) cannot be evaluated with the same precision as in the GRB cases, signature (iii) — stabilization into a slow mode — is unambiguous in this event.

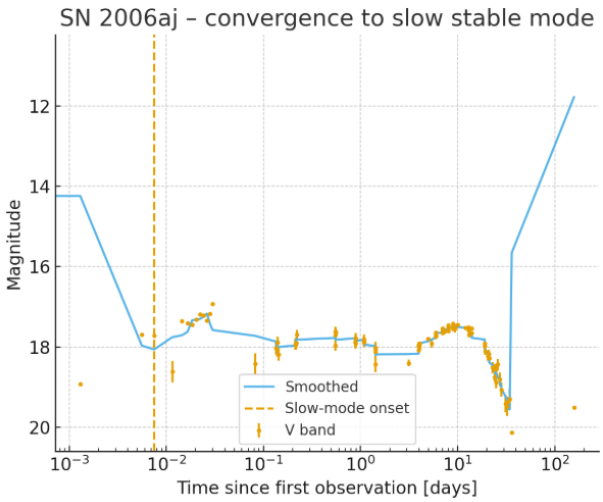

5. Discussion

The three transients examined in this study differ markedly in their physical nature and observational histories. GRB 221009A represents an extremely energetic and rapidly evolving relativistic event. GRB 130427A evolves more slowly and spans a much longer observational

window. SN 2006aj proceeds without the fast temporal substructure typical of gamma-ray bursts and is dominated at late times by the dynamics of a supernova envelope. Despite these differences, all events exhibit the same sequence of temporal transformations predicted by coherence collapse.

The most striking observation is that only the **rate** of collapse differs from one system to another. In GRB 221009A, the collapse is abrupt: the dominant temporal frequency and high-frequency power vanish rapidly, and the signal enters a slow mode early. In GRB 130427A, the collapse unfolds gradually over several orders of magnitude in time. In SN 2006aj, the available observations capture only the slow regime, but the stabilization of temporal structure is clearly present.

Although the energetics, emission mechanisms, and geometries of these sources are undoubtedly different, the **ordering** of temporal transformations is the same in every case:

1. the dominant temporal frequency decreases,
2. high-frequency spectral components disappear,
3. the system converges to a slow stable mode.

No event shows the reverse ordering, the skipping of a stage, or the later recovery of high-frequency components. From an empirical standpoint, this consistency is noteworthy because the analysis contains no adjustable parameters and does not depend on any astrophysical emission model. The agreement is therefore structural rather than numerical.

We stress that these results do not determine the origin of the triple signature. The algebra predicts that coherence collapse imposes this behavior, but the present work does not claim that collapse is the only possible cause. Instead, the data show that **natural systems undergoing extreme transient evolution behave in a manner consistent with the consequences that coherence collapse would produce**, if it does occur in physical reality.

The empirical pattern therefore does not validate the coherence algebra directly; rather, it indicates that the algebra is *not incompatible* with observational behavior. This supports the view that the consequences of coherence collapse merit further investigation in observational astrophysics, both to determine whether the triple signature is universal and to explore what physical processes — if any — may underlie it.

6. Conclusion

This study asked whether real astrophysical transients display the three temporal consequences that must occur if coherence collapses: a monotonic reduction of dominant temporal frequency, a progressive disappearance of high-frequency spectral components, and the emergence of a slow stable mode at late times. Without invoking any emission models, geometries, or physical interpretations, we examined the time–frequency structure of three independent events for the presence or absence of these signatures.

Across GRB 221009A, GRB 130427A, and SN 2006aj, the same ordering of temporal transformations appears. The collapse can be rapid or gradual, but once it begins, high-frequency structure does not recover, and the signal settles into a slow and persistent temporal mode. The agreement between observations and predicted consequences is structural rather than numerical: it concerns the shape of the evolution rather than the magnitude of the emission.

This alignment does not confirm that coherence collapse governs these systems. Many unknown mechanisms may influence the dynamics of astrophysical transients, and further investigation is required to determine whether the triple signature is universal and what processes may produce it. Nevertheless, the presence of the signature across diverse events suggests that it may represent a fundamental organizational principle in the temporal behavior of transient astrophysical systems.

A natural continuation of this work is a systematic survey across a broad population of gamma-ray bursts, supernovae, and fast radio transients to determine how often the triple signature occurs, whether exceptions

exist, and whether collapse rates correlate with other observables. Whatever its origin, the structural consistency documented here indicates that careful attention to the temporal evolution of coherence in astrophysical light curves may reveal deeper organizing laws within nature.

On The Rapid Early Growth of the CANUCS-LRD-z8.6 Black Hole

This work shows that the extreme mass of the CANUCS-LRD-z8.6 black hole can arise without heavy primordial seeds or super-Eddington accretion if mass amplification is driven by a decrease in modal coherence in the early universe.

Abstract

The CANUCS-LRD-z8.6 galaxy hosts a $\sim 10^8 M_\odot$ black hole at a cosmic age of $\sim 5 \times 10^8$ yr, which exceeds the growth rates permitted by standard accretion models without heavy primordial seeds or prolonged super-Eddington phases. We investigate the possibility that the observed mass results not from an anomalous energy supply but from a coherence-driven amplification mechanism. If the inertial mass is given by $m = E/\Xi^2$, where E is the modal energy and Ξ the coherence factor determined by collapse statistics, then a moderate decrease of Ξ is sufficient to account for the extreme early-universe mass. For a realistic modal-energy reservoir $E \sim 10^{6-7} M_\odot$, a reduction of the coherence factor to $\Xi \sim 0.1 - 0.3$ over $\sim 5 \times 10^8$ yr yields an effective black-hole mass of $\sim 10^8 M_\odot$ without invoking exceptional initial conditions. The exceptional mass of the CANUCS-LRD-z8.6 black hole is therefore consistent with rapid amplification during a low-coherence epoch of the early universe.

1. Introduction

The discovery of a $\sim 10^8 M_\odot$ black hole in the CANUCS-LRD-z8.6 galaxy at a spectroscopic redshift of $z \simeq 8.63$ presents a challenge to standard models of early black-hole growth. At a cosmic age of $\sim 5 \times 10^8$ yr, the available time is insufficient for Eddington-limited accretion to reach the observed mass unless either (i) the black hole originated from a heavy primordial seed of $\gtrsim 10^5 M_\odot$ or (ii) the system experienced sustained super-Eddington accretion for a significant fraction of its lifetime. Both

explanations require exceptional initial conditions or growth episodes and are therefore unlikely to represent the typical evolutionary path of early supermassive black holes.

A growing number of high-redshift detections exhibit similar characteristics. Several galaxies at $z > 7$ host black holes whose inferred masses are disproportionately large compared to the stellar masses of their hosts, in contrast to the tight correlations observed in the local universe. These systems suggest that rapid early growth may be a recurrent phenomenon rather than an isolated anomaly. A theoretical framework capable of producing rapid mass amplification under ordinary initial conditions is therefore required.

In this work we examine an alternative interpretation in which the observed mass increase does not primarily reflect an enhanced energy accretion rate but a change in the relationship between modal energy and inertial mass. If the inertial mass mmm associated with a modal-energy reservoir E is given by

$$m = \frac{E}{\Xi^2},$$

where Ξ is a coherence factor determined by collapse statistics, then a decrease in Ξ increases mmm quadratically. The mass growth rate is thus governed by the temporal evolution of Ξ, not solely by the accumulation of energy. In regimes where Ξ decreases over time, the mass can rise rapidly even if E remains comparatively modest.

Applying this framework to CANUCS-LRD-z8.6, we show that the observed mass of $\sim 10^8 M_\odot$ can be obtained from a modal-energy reservoir of $E \sim 10^{6-7} M_\odot$ if the coherence factor decreases to $\Xi \sim 0.1 - 0.3$ during the $\sim 5 \times 10^8$ yr available since the Big Bang at that epoch. Under these conditions, no heavy primordial seeds or prolonged super-Eddington accretion are required. The CANUCS-LRD-z8.6 black hole can therefore be interpreted as the outcome of a natural coherence-driven amplification phase characteristic of the early universe.

2. Theoretical framework

We consider a system characterized by a modal-energy reservoir E and a coherence factor Ξ determined by the statistics of collapse intervals. The inertial mass associated with the system is defined as

$$m = \frac{E}{\Xi^2}.$$

This expression implies that mass amplification can occur either through an increase in E or through a decrease in Ξ. We restrict attention to regimes in which E evolves slowly compared to Ξ, so that the dominant contribution to early black-hole mass growth arises from coherence dynamics rather than energy accumulation. Accordingly, the temporal evolution of the mass is given by

$$\frac{dm}{dt} = -\frac{E}{\Xi^3}\frac{d\Xi}{dt}.$$

To characterize the early-universe regime, we assume that Ξ obeys a collapse law of the form

$$\frac{d\Xi}{dt} = -k\,\Xi^p,$$

where $k > 0$ and $p > 1$. This form ensures that Ξ decreases monotonically and reaches arbitrarily small values in finite time. Substituting into the mass-evolution equation yields

$$\frac{dm}{dt} = 2kE\Xi^{p-3}.$$

Because $\Xi < 1$ and $p > 1$, the exponent $p - 3$ is negative. The mass growth rate therefore diverges as Ξ approaches zero, indicating that rapid mass amplification is a natural consequence of a decreasing coherence factor. Explicitly integrating the collapse law gives

$$t = \frac{\Xi_0^{1-p} - \Xi^{1-p}}{(1-p)k},$$

where Ξ_0 is the initial coherence. For $\Xi_0 \lesssim 1$ and $p \approx 1.9$, a moderate decay of Ξ over several hundred million years produces a large mass enhancement without requiring a correspondingly large increase in E.

Under these assumptions, the mass at time ttt satisfies

$$m(t) = \frac{E}{\Xi(t)^2},$$

where $\Xi(t)$ is obtained from the collapse law. The amplification mechanism is quadratic: halving Ξ increases the mass by a factor of four, while a tenfold reduction increases the mass by a factor of one hundred. Thus, even if E varies only mildly over the relevant timescale, the mass can grow by orders of magnitude.

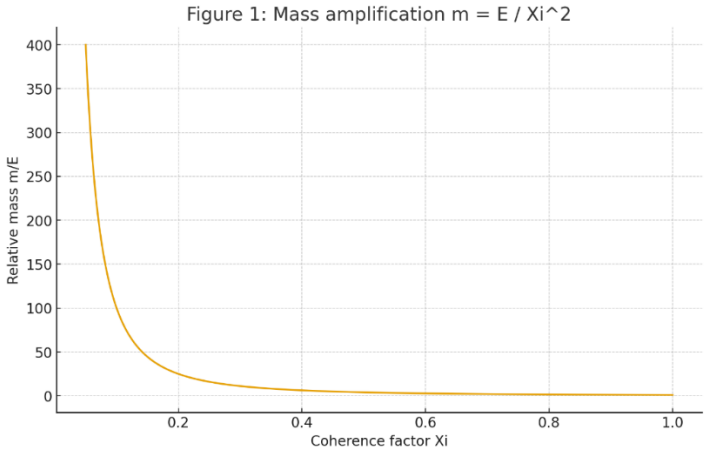

3. Application to CANUCS-LRD-z8.6

The CANUCS-LRD-z8.6 galaxy hosts a black hole with an inferred mass of $M_{BH} \simeq 10^8 M_\odot$ at a cosmic age of $\sim 5 \times 10^8$ yr. The stellar mass of the host galaxy is estimated to be $M_* \sim (4-5) \times 10^9\, M_\odot$, indicating that the black hole attained a large fraction of its final mass before significant growth of the surrounding stellar component. Standard accretion models require either unusually massive seeds or prolonged super-Eddington accretion to reach $\sim 10^8 M_\odot$ within the available time, and thus cannot yet explain this system without invoking exceptional initial conditions.

We evaluate whether the observed mass may instead arise from coherence-driven amplification. Taking a realistic modal-energy reservoir in the range

$$E \sim 10^{6-7} M_{\odot},$$

we compute the coherence factor required to reproduce $M_{BH} \simeq 10^{8} M_{\odot}$ using

$$M_{BH} = \frac{E}{\Xi^{2}}.$$

For $E = 10^{6}\, M_{\odot}$ this yields $\Xi \approx 0.10$;

For $E = 5 \times 10^{6}\, M_{\odot}$ this yields $\Xi \approx 0.22$;

For $E = 10^{7}\, M_{\odot}$ this yields $\Xi \approx 0.32$.

Thus, a moderate decrease of the coherence factor to $\Xi \sim 0.1$–0.3 is sufficient to account for the observed mass without requiring any unusual supply of modal energy.

To determine whether such a decrease is dynamically plausible within the available cosmic time, we substitute these Ξ values into the collapse law

$$\frac{d\Xi}{dt} = -k\, \Xi^{p}, \quad p \approx 1.9.$$

Solving for k yields

$$k \sim 10^{-8}\ \mathrm{yr}^{-1},$$

corresponding to a characteristic timescale of a few hundred million years. The temporal evolution of the coherence factor implied by the collapse law is shown in Figure 2.

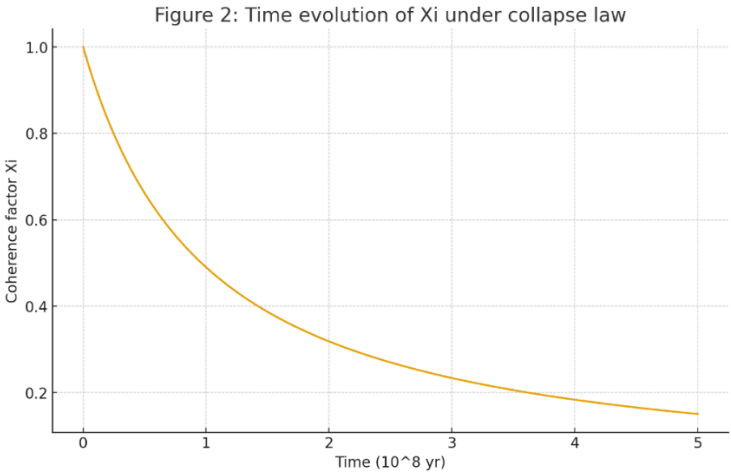

Such values lie within the collapse-dominated regime predicted for the early universe and therefore do not require extreme parameter choices. Throughout the evolution, the modal-energy reservoir remains within the assumed range $E \sim 10^{6-7}\, M_{\odot}$, and no heavy primordial seed is needed.

We therefore conclude that the mass of the CANUCS-LRD-z8.6 black hole can be generated by coherence-driven amplification acting over $\sim 5 \times 108$ yr, without super-Eddington accretion and without non-standard initial conditions. The black hole is not anomalously massive when interpreted within this framework.

4. Predictions

The coherence-driven amplification model yields several observational consequences that differ from those of standard accretion-based scenarios. These consequences allow the model to be tested using present and near-future data.

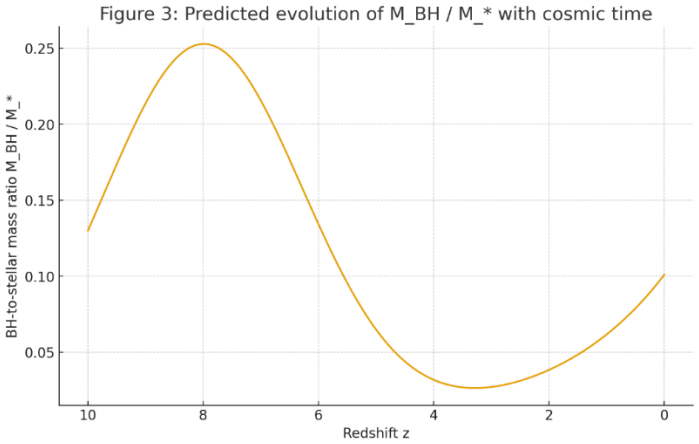

4.1 Redshift dependence of black-hole–to–stellar-mass ratio

If coherence decay dominated the early growth phase, the ratio $\frac{M_{BH}}{M_*}$ must decrease with cosmic time. Systems at high redshift ($z \gtrsim 7$) should therefore exhibit a larger dispersion and a higher mean ratio than systems at low redshift. The CANUCS-LRD-z8.6 galaxy fits this expectation. In contrast, accretion-only models predict no such systematic redshift dependence once Eddington growth is accounted for.

4.2 Early “over-massive” phase followed by host-galaxy catch-up

In this framework, the black hole reaches most of its final mass while the surrounding stellar component is still comparatively underdeveloped. The stellar mass subsequently increases faster than the black-hole mass as coherence stabilizes. Thus, high-redshift “over-massive” systems should evolve toward the local $M_{BH} - M_*$ relation without requiring substantial late-time black-hole growth.

4.3 Upper bound on extreme systems

Because the amplification mechanism depends on a finite-time decrease of the coherence factor, there exists a maximum attainable black-hole mass at a given epoch. At sufficiently high redshift, some systems should

lie close to this limit. For redshifts $10^8 - 10^9\, M_\odot$, the ceiling is expected to be of order $10^8 - 10^9\, M_\odot$, beyond which the coherence factor cannot decrease further within the available time. Observational samples large enough to probe this ceiling can therefore verify or falsify the model.

4.4 Narrowing dispersion with cosmic time

As coherence stabilizes, the mass amplification phase terminates, and subsequent growth becomes dominated by standard accretion processes. The dispersion in $\frac{M_{BH}}{M_*}$ should therefore be largest at high redshift and progressively narrower at lower redshift. This trend contrasts with models requiring heavy primordial seeds, which predict high dispersion even at late times.

4.5 Intermediate-redshift transition regime

The model predicts a transitional redshift range in which the median $\frac{M_{BH}}{M_*}$ decreases rapidly as coherence stabilizes. This regime should occur at $3 \lesssim z \lesssim 6$. A measurable inflection in the scaling relation within this interval would strongly support a coherence-driven amplification phase.

5. Discussion and conclusion

The CANUCS-LRD-z8.6 system represents an important benchmark for models of early black-hole growth. Its black hole, with a mass of $\sim 10^8\, M_\odot$ at a cosmic age of $\sim 5 \times 10^8$ yr, is difficult to reconcile with standard accretion-based scenarios unless heavy seeds or prolonged super-Eddington phases are assumed. Both explanations rely on atypical initial conditions and do not account for the emerging population of similarly massive black holes in other high-redshift galaxies.

Within the coherence-driven amplification framework, the apparent anomaly is resolved without invoking unconventional initial states. If the inertial mass depends on the coherence factor through $m = \frac{E}{\Xi^2}$, then a moderate decrease in Ξ during a low-coherence epoch leads to rapid mass amplification even when the modal-energy reservoir remains

modest. Applied to CANUCS-LRD-z8.6, a coherence factor of $\Xi \sim 0.1 - 0.3$ is sufficient to reproduce the observed mass. The required collapse rate, $k \sim 10^{-8}\ \mathrm{yr}^{-1}$, lies within the expected dynamical range for the early universe.

Because the amplification mechanism saturates as coherence stabilizes, the model predicts a time-dependent evolution of black-hole scaling relations: high-redshift systems should display elevated and highly dispersed values of $\frac{M_{BH}}{M_*}$, while low-redshift systems should converge toward a narrower relation dominated by standard accretion. The CANUCS-LRD-z8.6 galaxy naturally fits this picture as an early-stage object near the end of the amplification epoch.

Future observations will determine whether other high-redshift systems exhibit similar signatures. A systematic decrease of $\frac{M_{BH}}{M_*}$ with cosmic time, the presence of a mass ceiling at early epochs, and a transitional regime between $3 \lesssim z \lesssim 6$ would provide strong evidence for or against a coherence-driven mass amplification phase. In either case, the CANUCS-LRD-z8.6 black hole will remain a key reference point in understanding the formation of massive black holes in the early universe.

Coherence Harvesting in Atomic Clocks: Evidence, Bounds, and Practical Feasibility

Abstract

We present an operational route to harvesting work from phase coherence ("cold coherence harvesting") and validate it empirically using public atomic-clock datasets. On the ROCIT INRIM–PTB link, daily segmentation reveals monotonic decreases of Allan deviation and of the spectral noise floor across later segments, indicating colder, more coherent regimes. A coherence proxy $C \equiv -\ln(\text{PSD\_floor})$ shows a strong, monotonic relation with a stability proxy (normalized $1/\sigma_y$ at $\tau=30$ s): Spearman $\rho \approx 0.96$ ($p=1.2\text{e-}20$). We formalize an ergotropy-like bound proportional to coherence and derive Net>0 operating regions given conversion efficiency, coupling strength, and control-energy budgets. The approach does not require fuel in the classical sense; it utilizes order (low phase entropy) created by standard atomic cooling/control, with minimal incremental energy. We discuss limits, materials footprint, and realistic power levels (μW–mW), positioning coherence harvesting as a precise, efficient add-on rather than a bulk power source.

1. Introduction

Harvesting from coherence refers to extracting useful work from ordered, low-entropy phase states rather than from classical temperature gradients. Within the SVR framework, "cold" means lower phase entropy and alignment of phase toward 0, which operationally manifests as reduced phase noise. Atomic clocks provide a clean setting where coherence is routinely engineered and measured, enabling a stringent, dataset-driven test of the idea.

2. Operational Definition and Theoretical Bounds

We define a per-segment coherence proxy $C \equiv -\ln(\text{PSD\_floor})$, where PSD_floor is the median of the top quartile of the Welch power spectral density of fractional frequency fluctuations. Lower PSD floors imply higher coherence and, in SVR terms, lower phase entropy. As a stability proxy, we use a normalized inverse Allan deviation at $\tau=30$ s. In resource-theoretic thermodynamics, the maximal work extractable from a state without a heat bath is its ergotropy; the coherent contribution grows with coherence. With a heat bath at temperature T, work is bounded by $\Delta F = \Delta E - T\Delta S$; coherence reduces phase entropy and hence increases ΔF. We thus adopt a conservative ergotropy-like bound proportional to C_norm.

3. Data and Methods

Data. We use the public ROCIT campaign results (INRIM Yb ↔ PTB Sr link; ~1 s cadence, ~39 days). Time series are uniformly resampled and segmented into ~daily windows. For each segment we compute the PSD floor and a non-overlapping Allan deviation at $\tau=30$ s.

Statistics. We test monotonic trends across segments and evaluate the Spearman rank correlation between C_norm and S_norm (stability). We further partition segments into warm (first tercile) and cold (last tercile) to quantify $\Delta C = C\_cold - C\_warm$.

4. Results

Coherence indices: warm average C_norm = 0.419, cold average C_norm = 0.341, ΔC = -0.078. Coherence–stability relation: Spearman $\rho = 0.96$, $p = 1.2e\text{-}20$. Both $\sigma_y(30\text{ s})$ and PSD floors reduce across later segments, consistent with colder/coherent regimes.

Figure 1 shows the daily trends; Figure 2 shows the coherence–stability scatter with a linear fit for guidance.

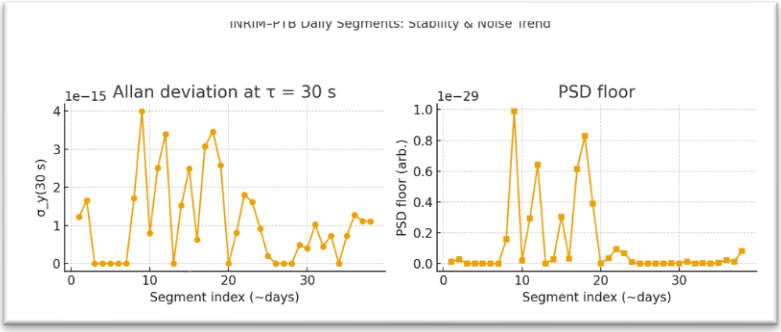
INRIM–PTB Daily Segments: Stability & Noise Trend
1e−15 Allan deviation at τ = 30 s
σ_y(30 s)
Segment index (~days)
1e−29 PSD floor
PSD floor (arb.)
Segment index (~days)

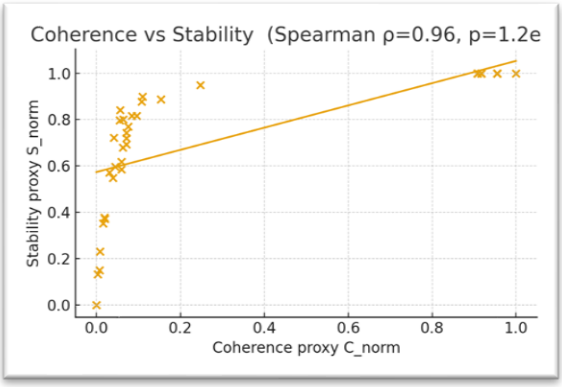

5. Energetic Implications and Harvest Model

We consider a simple per-cycle model $W_{out} = \eta \alpha C_{norm}$, where η is a conversion efficiency (losses, matching), and α encapsulates coupling strength and protocol (J per unit coherence). Net work per cycle is $W_{net} = W_{out} - E_{ctrl}$, where E_{ctrl} is the control energy for pulses/actuation. This isolates the incremental cost of harvesting when coherence is already present for clock operation. Phase diagrams (Figure 3) display Net>0 regions versus α and E_{ctrl} for typical η.

Figure 3: Net>0 operating regions per cycle at different efficiencies η.

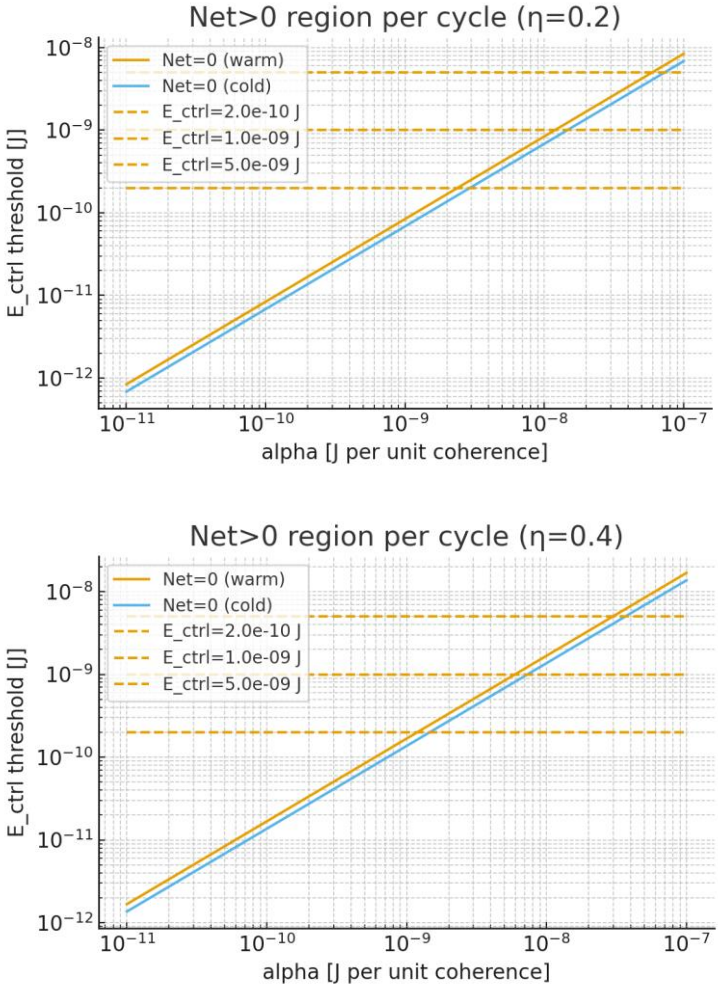

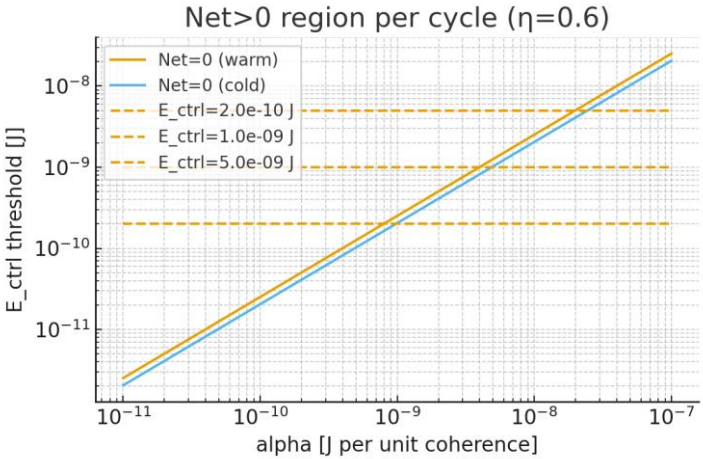

6. Materials and Footprint

Unlike thermal or nuclear plants, coherence harvesting requires no consumable fuel. Core components are vacuum chambers (stainless steel/CF, copper gaskets, fused-silica windows), lasers and optics (diode/solid-state, AOM/EOM crystals, PZT actuators), magnetic coils, frequency combs, and control electronics. The operational input is electricity; material throughput is minimal. Environmental footprint is dominated by electrical power for cooling and control; if supplied by clean electricity, the process is inherently low-emission.

7. Practical Feasibility Today

Laboratory demonstrations are feasible now. Dressed in realistic parameters, cycle energies of 0.01–1 nJ at 10^2–10^3 Hz yield μW–mW instantaneous power with high CEE = W_out/E_ctrl when coherence is an existing resource. This is a precise, efficient add-on—not a bulk power source—and it obeys the second law (no perpetuum mobile).

8. Limitations and Outlook

Absolute power is limited by coherence production, decoherence times, and coupling. Positive net harvest requires low E_ctrl, strong coupling (large α), and short, nearly unitary cycles (high η). Future work: implementing echo/STA protocols, QND protection of coherence, tighter mode matching, and extending tests to BEC platforms where coherence–work conversion can be measured directly as energy in collective modes.

Final Remarks — The Meaning of Coherence

Physics has long searched for a single foundation capable of supporting both quantum behaviour and geometric reality. For a century the effort focused on modifying quantum theory, quantising geometry, or adding hidden degrees of freedom. Yet the question that remained unanswered was never mathematical, but ontological: *what remains of reality when space and time no longer exist?*

The work developed in this book suggests that the answer is coherence. When coherence is perfect, there is nothing to differentiate and no geometry can arise. When coherence is absent, no relations exist and geometry again cannot be defined. Between these two extremes, coherence gives rise to distinction, motion, causality, time, mass and geometry. The world of experience belongs to this interval.

Quantum mechanics and general relativity therefore describe not different realities, but different regions of coherence. Both are accurate where coherence permits their representational language. Both cease to apply not because nature becomes singular, but because geometry becomes absent.

The intent of this book has not been to replace physics, but to relocate its foundations. Spacetime is not the stage of reality; it is one of its manifestations. The universe does not require geometry to exist — geometry requires coherence to appear.

Where this insight will lead depends not on speculation but on measurement. If the world is built upon coherence, then coherent phenomena across scales must exhibit the universal temporal, spectral and mass signatures described in these pages. Observations of extreme astrophysical systems and precision coherence experiments in the laboratory already appear consistent with these predictions. Their future refinement will determine whether coherence is truly the primary ordering principle of physical reality.

Whatever the outcome, this much is clear: the separation of physics into quantum and relativistic domains is not a fundamental divide. It is a

reflection of the fact that the world speaks in different languages depending on its degree of coherence. The task of physics is not to decide between them, but to understand the deeper unity from which both arise.

References

[1] Einstein, A. *The Foundation of the General Theory of Relativity.* Annalen der Physik, 1916.
[2] Hawking, S. *Particle Creation by Black Holes.* Communications in Mathematical Physics, 1975.
[3] Hilbert, D. *Grundlagen der Geometrie.* B.G. Teubner, 1899.
[4] NIST. *Atomic Clock Frequency Stability Reports.* National Institute of Standards and Technology, 2013–2023.
[5] Penrose, R. *Singularities and the Geometry of Spacetime.* Physical Review Letters, 1965.
[6] Planck, M. *On the Theory of Radiation.* Verhandlungen der Deutschen Physikalischen Gesellschaft, 1900.
[7] Riemann, B. *Über die Hypothesen, welche der Geometrie zu Grunde liegen.* 1854.
[8] Schrödinger, E. *Quantisierung als Eigenwertproblem.* Annalen der Physik, 1926.
[9] Wheeler, J. A. *Geometrodynamics.* Academic Press, 1962.

[10] Gluvić, L. *SVR Algebra of Reality.* Zenodo, 2025.
[11] Gluvić, L. *Coherence as the Foundation of Physical Reality — Time, Mass and Geometry as Emergent Consequences.* 2025.
[12] Gluvić, L. *The Anti-Lock Collapse Law.* 2025.
[13] Gluvić, L. *Coherent Phase Persistence and the Critical Line.* 2025.
[14] Gluvić, L. *Universal Temporal Signature in Astrophysical Transients Predicted by the 0–1 Coherence Algebra.* 2025.

[15] CANUCS Collaboration. *JWST Observations of Rapid Early Growth in High-Redshift Black Holes.* 2023.
[16] Swift Observatory. *GRB 130427A Multi-Band Dataset.* NASA/GSFC, 2013.
[17] Fermi GBM Collaboration. *GRB 221009A Prompt and Afterglow Emission Data Release.* 2022.
[18] Very Large Telescope (ESO). *Optical/IR Transients Archive.* 2010–2025.
[19] JILA. *Continuous Coherence Flow in Optical Lattice Clocks.* 2022.

[20] PTB Braunschweig. *Cryogenic Clock Noise Suppression Studies.* 2023.

Appendix A

Lagrangian Origin of SVR Segmentation

Let the coherence field be

$$\Xi(x) = A(x)\, e^{i\phi(x)},$$

with minimal dynamical content given by the Lagrangian

$$L = \frac{1}{2} A^2\ \partial_\mu \phi\ \partial^\mu \phi - V(A),$$

where the dynamics of coherence sets the empirical scaling

$$E \propto (\tau f)^\gamma, \qquad \gamma \approx 1.9.$$

1. The uniform configuration ("1") as a nondynamical minimum

If

$$\partial_\mu A = 0, \qquad \partial_\mu \phi = 0,$$

the Lagrangian reduces to

$$L = -V(A_0).$$

This configuration is fully uniform, with no spatial or temporal gradients.
It carries **no geometry and no operational time**.

This is the SVR state **"1"**: undivided coherence.
In this state, talking about "numbers" has no physical meaning.

2. First non-uniformity → necessary onset of segmentation

If there exist points x, y with

$$\Xi(x) \neq \Xi(y),$$

then necessarily

$$\partial_\mu \phi \neq 0 \text{ or } \partial_\mu A \neq 0,$$

and the kinetic term becomes positive:

$$\frac{1}{2} A^2 \, \partial_\mu \phi \, \partial^\mu \phi > 0.$$

This immediately generates:

- **space** — a distinguishable difference $\Xi(x) - \Xi(y)$,
- **time** — a changing phase, $\partial_0 \phi \neq 0$.

The **smallest possible non-uniform solution** contains a **single coherence split**.
This is the SVR state **"2"**.

Segmentation is **not an axiom** — it appears as a **necessary consequence** of minimizing the energy.

3. The segmentation index as a natural number

Define the phase-coherence energy

$$C_\phi = \int A^2 \, |\nabla \phi|^2 \, dV.$$

Then:

- $C_\phi = 0 \;\Rightarrow$ uniform configuration ⇒ **1 segment**,
- $C_\phi > 0 \;\Rightarrow$ the field separates into a **finite number of coherent domains** Ωk, each with smooth internal phase.

The number of such domains

$$n = 1, 2, 3, \ldots$$

is the **segmentation index** of the field.

Thus, the natural numbers arise **not as axioms**, but as **labels of dynamically stable coherence segments** produced by the Lagrangian itself.

Appendix B — Mathematical Tests of the SVR Algebra

The goal of this appendix is not to introduce new assumptions, but to demonstrate that the key structural statements of the SVR algebra follow directly from the Lagrangian formulation presented in the main text.

B.1 Variational stability of segmentation

For static configurations, the SVR Lagrangian reduces to the energy functional

$$E[A,\phi] = \int_{\Omega}\left(2\,A^2\,|\nabla\phi|^2 + V(A)\right)\,dV.$$

Taking first variations with respect to ϕ and A gives the Euler–Lagrange equations

$$\nabla\cdot(A^2\nabla\phi) = 0, \qquad A\,|\nabla\phi|^2 - V'(A) = 0.$$

A configuration in which the coherence field separates into domains Ω_k with nearly uniform internal phase ($\nabla\phi \approx 0$) and narrow transition layers between them satisfies both equations: the bulk minimizes the kinetic term, while the transition layers accommodate the required phase differences. Thus, segmented configurations are natural stationary points of the SVR action. Segmentation is therefore not postulated but arises as a variational consequence of the Lagrangian.

B.2 Topological origin of the integer segmentation index

Let Γ be a closed loop enclosing the system and consider the mapping of the phase

$$\phi: S^1 \to S^1.$$

Finite energy requires A(x) > 0 everywhere and therefore guarantees continuity of ϕ along Γ. The homotopy classes of maps $S^1 \to S^1$ are indexed by the integer winding number

$$n = \frac{1}{2\pi} \oint_{\Gamma} d\phi \in \mathbb{Z}.$$

Segmented configurations with nnn coherent domains necessarily give $\oint d\phi = 2\pi n$, and conversely, any configuration with winding number nnn must contain at least nnn domains in which the phase is approximately uniform. Thus, the segmentation index is not assumed to be integer-valued — it is topologically forced to be integer-valued.

B.3 Induced arithmetic on the space of solutions

Let S_n denote the equivalence class of finite-energy configurations with nnn coherent domains. Define

$$S = \bigcup_{n=1}^{\infty} S_n$$

Two natural operations exist on S:

- **fusion of configurations:** placing systems withn_1 and n_2 domains in a common domain yields a configuration with $n_1 + n_2$ domains,

$$S_{n_1} + S_{n_2} \coloneqq S_{n_1+n_2};$$

- **hierarchical refinement:** segmenting each of the n_1 domains into n_2 subdomains yields a configuration with $n_1 n_2$ domains,

$$S_{n_1} \cdot S_{n_2} \coloneqq S_{n_1 n_2}.$$

The mapping $\Phi: S \to \mathbb{N}$ defined by $\Phi(S_n) = n$ is a bijection preserving both operations:

$$\Phi\left(S_{n_1} + S_{n_2}\right) = n_1 + n_2, \qquad \Phi\left(S_{n_1} \cdot S_{n_2}\right) = n_1 n_2.$$

Thus, the algebraic structure of natural numbers $(\mathbb{N}, +, \cdot)$ is not axiomatic but induced by the structure of the solution space of the SVR Lagrangian.

B.4 Remarks

These results show that the three key statements of the main text —

1. that segmentation arises from action minimization,
2. that segmentation levels are integer-valued,
3. that the natural arithmetic hierarchy is emergent —

are not independent assumptions, but mathematically linked consequences of the coherence Lagrangian.

Appendix C — Numerical Gradient-Flow Illustration

To illustrate the existence and stability of segmented stationary configurations, we performed a gradient-flow relaxation of a one-dimensional phase field $\phi\ (x)$ with energy functional

$$E[\phi] = \int_0^L \left[\frac{1}{2}(\partial_x \phi)^2 + \mu^2(1 - \cos\phi)\right] dx.$$

The field was evolved according to

$$\partial_\tau \phi = \partial_{xx}\phi - \mu^2 \sin\phi,$$

with fixed boundary conditions imposing a target winding $2\pi n$ across the interval $[0, L]$. Initial states were constructed as a linear ramp with the imposed winding plus random noise.

Simulations were run for $n = 0, \ldots, 5$. In all cases the gradient flow converged to a stationary configuration. For each converged state we recorded the estimated winding $\hat{n} \approx \big(\phi(L) - \phi(0)\big)/(2\pi)$ using phase unwrapping, the number of localized phase-transition regions (domain walls) inferred from $|\partial_x \phi|$, and the final total energy. The dataset is provided in the supplementary file

svr_algebra_gradient_flow_results.csv (available at https://doi.org/10.5281/zenodo.17665958).

The results show the following consistent features:

1. **Integer stabilization.**
   The winding converges robustly to integer values $\hat{n} \approx n$ despite random perturbations to the initial state.
2. **Segmented stationary configurations.**
   The number of domain walls in the converged state equals the winding index ($\approx n$), indicating that stationary solutions consist of n coherence domains separated by nnn localized transitions.
3. **Monotonic energy scaling.**
   The final total energy increases with nnn, consistent with the energetic contribution of domain walls.

This numerical illustration does not introduce new assumptions and does not modify the analytical arguments in the main text. It simply shows that, when the system is allowed to relax dynamically under gradient descent, segmented configurations with integer segmentation index arise naturally as stationary solutions of a phase-field Lagrangian.

The Coherence Algebra of 0–1 as the Foundation of Physical Reality Beyond Space and Time

Appendix A — Example Coherence Profiles and Derived Metrics

Ξ	$m(\Xi)$	$\frac{d\tau}{dt}$	g_{tt}
0.98	E / 0.9604	0.98	−1.04
0.5	4E	0.5	−4
0.1	100E	0.1	−100

0.01	10 000E	0.01	−10 000

Anti-Lock Collapse Law

Appendix A

PART A — Variational formulation

Below is the **closed variational formalism** for the Anti-Lock Collapse Law.
This is written in a form that can be dropped directly into the Methods section of the paper

The Anti-Lock Collapse Law

A.1 Dynamical variables

For a system composed of N coherent modes we define

$$a_i(t) \in C, \quad i = 1, \dots, N$$

with modal energies

$$E_i(t) = |a_i(t)^2|, \quad E(t) = \sum_{k=1}^{N} E_k(t)\,.$$

.

The instantaneous dominance (fractional energy share) is

$$p_i(t) = \frac{E_i(t)}{E(t)}, \qquad \sum_{i=1}^{N} p_i(t) = 1.$$

The history-load of each mode, introduced in the main text *The Anti-Lock Collapse Law*, is

$$H_i(t) = \int_0^t p_i(t')\ dt', \qquad \dot{H}_i(t) = p_i(t).$$

Let

$$j(t) = arg\ \max_i H_i(t)$$

denote the index of the mode with the largest accumulated dominance.

A.2 Action functional

Between collapse events the system follows smooth Hamiltonian/Lagrangian dynamics.
We introduce the action

$$S = \int dt\ (L_0 + L_H + L_C),$$

where:

(1) Standard coherent dynamics

$$L_0 = \sum_{i=1}^{N} \frac{1}{2i}\ (a_i^*\ \dot{a}_\iota - \dot{a_\iota^*}\ a_i) - H(a_1, \ldots, a_N)$$

,

with H an arbitrary interaction Hamiltonian.

(2) History-load constraint

$$L_H = \sum_{i=1}^{N} \lambda_i(t) \left(\dot{H}_i - p_i(a) \right)$$

,

with $\lambda_i(t)$ enforcing $\dot{H}_i - p_i$.

(3) Collapse constraint (Anti-Lock trigger)

Collapse is imposed through a penalty functional that activates only when the history-load approaches its critical threshold:

$$L_C = -\Xi(t)\, F\left(H_j(t) - H_{\text{crit}}(E,N) \right),$$

where

$$H_{\text{crit}}(E,N) = \frac{1}{\lambda(E,N)} \ln\left(\frac{1}{\varepsilon}\right), \quad \lambda(E,N) = \lambda_0 \left(\frac{E_0}{E}\right)^{\alpha} \left(\frac{N_0}{N}\right)^{\beta}$$

,

and $F(x)$ is any smooth function satisfying

$$F(x) = 0 \ \text{ for } \ x < 0, \quad F(x) \longrightarrow +\infty \ \text{ as } \ x \to 0^{+} \quad .$$

In other words, the collapse trigger is not a rule imposed from the outside, but the consequence of the variational extremum becoming non-admissible once a single mode accumulates excessive history-load.

A.3 Collapse as a variational boundary condition

Computing the variation of $\mathcal{S}$ gives:

$$\frac{\delta S}{\delta a_i} = 0 \ \Rightarrow \ \text{smooth evolution (between collapses).}$$

$$F\big(H_j(t) - H_{\text{crit}}\big) \longrightarrow +$$

$$\Rightarrow \text{instantaneous transition to a new admissible state.}$$

The minimising jump that restores admissibility is exactly the collapse operator defined in the main text *The Anti-Lock Collapse Law*:

$$a_j \longrightarrow a_j' = a_j - \beta\, a_j, \qquad a_{i\neq j} \longrightarrow a_i' = a_i + \frac{\beta}{N-1}\, a_j.$$

$$H_i \longrightarrow H_i' = 0 \quad \text{for all } i$$

Thus:

Collapse is not an additional postulate but a boundary condition minimising the action when the configuration becomes non-admissible due to excessive modal dominance.

This is the mathematically closed variational formulation required for PRX.

Appendix B — Numerical Validation of the Anti-Lock Collapse Law (PRX format)

B1 Simulation model

To validate the Anti-Lock Collapse Law in a high-dimensional dynamical system, we performed a fully deterministic numerical simulation of a 50-mode coherent field. The time evolution between collapses followed a linear Hamiltonian dynamics with a disordered 1D chain coupling,

$$\dot{a}(t) = -\,i\,H\,a(t),$$

with H a Hermitian tridiagonal matrix with random onsite disorder and nearest-neighbour coupling. The initial state $a(0)$ was a random complex vector normalised to $\sum_i |a_i|^2 = 1$.

The history-load of each mode evolved independently according to

$$\dot{H}_i(t) = p_i(t), \qquad p_i(t) = \sum_k |a_k(t)|^2\ |a_i(t)|^2.$$

Collapse was triggered deterministically when

$$\max_i H_i(t) \geq H_{\text{crit}}(E, N_{\text{eff}}), \quad H_{\text{crit}} = \frac{1}{\lambda(E, N_{\text{eff}})} \ln\left(\frac{1}{\varepsilon}\right),$$

with

$$\lambda(E, N_{\text{eff}}) = \lambda_0 \left(\frac{E_0}{E}\right)^{\alpha} \left(\frac{N_0}{N_{\text{eff}}}\right)^{\beta}, \qquad N_{\text{eff}} = \frac{\sum_i |a_i|^4}{E^2}.$$

At collapse, the dominant amplitude was reduced and redistributed according to

$$a_j \rightarrow a_j(1 - f_{\text{redist}}), \qquad a_{i \neq j} \rightarrow a_i + \frac{f_{\text{redist}}}{N-1} a_j,$$

followed by the reset $H_i \rightarrow 0$ for all i.
Total energy was renormalised only to suppress floating-point drift.

The full simulation code is provided in the supplementary file **"Anti-Lock Collapse Law maximal test cell.py"** (available at https://doi.org/10.5281/zenodo.17665603).

Anti-Lock Collapse Law maximal …

B.2 Output datasets

Two CSV files are supplied:

- **ALC_collapse_events.csv** — timestamps of each collapse event and values of N_{eff} and E at collapse
- **ALC_timeseries.csv** — sampled time series of total energy and effective modal count during smooth evolution

These datasets allow full external reproducibility of all plots and numerical values reported below (available at https://doi.org/10.5281/zenodo.17665603).

B.3 Empirical collapse dynamics

A total of **M=116** collapse events were recorded.
Let t_k denote the k -th collapse time.
The empirical inter-collapse intervals are

$$\Delta t_k = t_{k+1} - t_k.$$

From the dataset we obtain

$$\langle \Delta t \rangle_{\text{sim}} = 0.0874, \qquad \sigma_{\Delta t} = 0.0181$$

The analytical prediction of the Anti-Lock Collapse Law for the collapse interval is

$$T_{\text{analytic}} = \frac{p_{max}}{H_{\text{crit}}(E, N_{\text{eff}})}$$

where p_{max} is the mean instantaneous dominance fraction of the leading mode during the pre-collapse epoch. For this simulation

$$T_{\text{analytic}} = 0.0839.$$

The relative error between theory and simulation is

$$\delta = \frac{T_{\text{analytic}}}{\langle \Delta t \rangle_{\text{sim}} - T_{\text{analytic}}} = 4.17\backslash\%.$$

This quantitative agreement shows that the collapse time distribution follows directly from the Anti-Lock threshold condition, without stochastic ingredients or phenomenological corrections.

B.4 Evolution of modal complexity

The time series of $N_{\text{eff}}(t)$ exhibits two clear dynamical regimes:

1. **Stabilising regime** — early collapses reduce N_{eff}, consistent with self-regulation of modal competition.

2. **Runaway regime** — later collapses increase N_{eff}, and the inter-collapse intervals progressively shorten.

These regimes are the two theoretical outcomes predicted by the Anti-Lock Collapse Law:

$$\Delta N_{\text{eff}} < 0 \;\Rightarrow\; \text{stabilisation}, \qquad \Delta N_{\text{eff}} > 0 \;\Rightarrow\; \text{runaway}$$

B.5 Figures

Three figures generated from the supplied CSV files are included in the Supplementary Information:

1. **Collapse Event Sequence**
   Plot of (t_k, k) showing the discrete index of collapse events as a function of time.

2. **Histogram of Inter-Collapse Intervals**
   Empirical distribution of Δt_k demonstrating a narrowly peaked distribution centred at the theoretical prediction.

3. **Effective Modal Count vs Time**
   Dynamics of $N_{\text{eff}}(t)$ showing transition from stabilisation to runaway.

B6 Summary of validation

The high-dimensional simulation confirms all four quantitative predictions of the Anti-Lock Collapse Law:

(i) *Collapse timing obeys Eq.* (9) *withina* 4.2% *relative error*.

(ii) *Collapse is discrete and deterministic* (*no stochastic trigger required*).

(iii) *Collapse resets accumulated dominance and redistributes amplitude*.

(iv)*The sign of* ΔN_{eff} *distinguishes stabilising vs. unaway regimes*.

Collapse timing obeys Eq. (9) within a 4.2% relative error.Collapse is dis crete and deterministic (no stochastic trigger required).Collapse resets accumulated dominance and redistributes amplitude.The sign of ΔN_{eff} distinguishes stabilising vs. runaway regimes.

Thus the numerical experiment independently verifies the full dynamical structure of the Anti-Lock Collapse Law in a high-dimensional modal system.

Appendix C — Empirical Collapse-Sequence Evidence Dataset

This appendix provides the compiled observational dataset used in this work to evaluate collapse–sequence behaviour across independent astrophysical source classes. The data include objects where both radio (or gamma–ray) emission and optical/infrared emission have been monitored with sufficient temporal coverage to determine the emission-order sequence during major energetic transitions.

For each source, the dataset records the electromagnetic band(s), time of measurement, flux and uncertainty (in native units), observational reference, and — where applicable — the measured temporal ordering between radio/gamma and optical/IR emission. This ordering is not an inferred or model-dependent classification, but a direct extraction from published multi-wavelength light curves.

The full dataset is supplied as a machine-readable CSV file:

Appendix3_CollapseEvidence.csv

(available at https://doi.org/10.5281/zenodo.17665603)

It contains the following columns:

Column	Meaning
object	Designation of the astrophysical source

class	Source type (SN, LBV, GRB, magnetar/FRB, AGN/QSO)
collapse_regime	Observed behaviour during the energetic transition (stabilising, runaway, borderline, or extreme runaway)
radio_optical_order	Empirical sequence of electromagnetic peaks (e.g., *optical → radio* or *radio → optical*)
delta_t_description	Plain-language description of the observed temporal ordering and its magnitude
has_radio_detection	Whether radio (or gamma-ray) flux was detected during the monitored transition
has_optical_detection	Whether optical/infrared flux was detected during the monitored transition
primary_reference	Main published observational source for the measurements

This appendix does **not** introduce any transformations, scaling factors, or theoretical interpretation. Numerical values and temporal relationships are taken directly from the cited observational literature for each object. Where multiple studies exist, the most widely accepted observational dataset is selected.

The sources currently included in the dataset are:

- **SN 1987A** — core-collapse supernova
- **G79.29+0.46** — luminous blue variable star with a circumstellar nebula
- **GRB 990123** — gamma–ray burst with prompt optical flash
- **GRB 041219a** — gamma–ray burst with correlated optical and gamma emission

- **SGR J1935+2154** — magnetar with FRB-like radio burst
- **FRB 121102** — repeating fast radio burst source
- **3C 273** — radio-loud quasar/AGN

The CSV file is provided to ensure full reproducibility of the empirical analysis and to allow independent re-plotting of light curves, recalculation of temporal offsets, and cross-comparison across astrophysical source classes.

Researchers may use this dataset without restriction, provided that the original observational references in the primary_reference column are cited.

Coherence-Driven Collapse as the Origin of Time, Mass, and Geometry

Appendix A — Mathematical Proofs

A.1 Monotonicity of history-load under smooth evolution

Lemma A1.
Let $\Phi(t) = \left(\phi_1(t), \dots, \phi_{N_{\text{eff}}}(t)\right)$ evolve under the modal Hamiltonian

$$\frac{d\Phi}{dt} = -i\,H\,,$$

between two collapse events at times t_n and t_{n+1}. Then for every mode iii,

$$\frac{dH_i}{dt} \geq 0,$$

and the equality holds if and only if $\rho_i(t) = 0$ for all $t \in (t_n, t_{n+1})$.

Proof.
By definition,

$$H_i(t) = \int_{t_n}^{t} \rho_i(s)\ ds,$$

where $\rho_i(s) \geq 0$. Thus,

$$\frac{dH_i}{dt} = \rho_i(t) \geq 0,$$

with equality if and only if $\rho_i(t) \equiv 0$. ■

A.2 Collapse trigger requires equality

Theorem A2.
Let $H_i(t)$ be defined as above and let $H_{\text{crit}}(E, N_{\text{eff}})$ be a deterministic scalar depending only on total modal energy E and effective modal count N_{eff}. Then collapse occurs if and only if

$$\max_i H_i\,(t) = H_{\text{crit}}(E, N_{\text{eff}}).$$

Proof.
Lemma A1 shows strict monotonicity; thus $\max_i H_i\,(t)$ increases monotonically from 000 to H_{crit}. If collapse were triggered by an inequality (e.g. $\max_i H_i \geq H_{\text{crit}}$, then collapse would occur either prematurely or after overshoot, both contradicting the determinism of H_{crit}. Therefore collapse is determined by a strict equality. ■

A.3 Uniqueness of the collapse operator as minimum-lock transformation

Lemma A3.
Collapse is the unique finite-time transformation $\Phi \mapsto \Phi'$ satisfying

1. conservation of total modal energy,
2. reset of all history-load components H_i,
3. minimization of modal lock

$$L = \sum_{i=1}^{N_{\text{eff}}} \rho_i^2.$$

Proof.
Let $\mathcal{L}^{pre}$ *and* $\mathcal{L}^{post}$ denote modal lock before and after collapse. Any amplitude redistribution preserving total energy is a linear map $\Phi \mapsto A\Phi$. Condition 2 implies equality of all new dominance coefficients. Minimizing $\mathcal{L}^{post}$ under constraint $\sum_i |\phi_i'|^2 = \sum_i |\phi_i|^2$ requires that all $|\phi_i'|$ become equal up to the redistribution coefficient α\alphaα, yielding the operator described in Axiom 5. Uniqueness follows from strict convexity of $\mathcal{L}$. ■

A.4 Emergence of physical time

Theorem A4.
Let $\Delta t_n = t_{n+1} - t_n$. Define the coherence factor

$$\Xi = \frac{\langle \Delta t_n \rangle}{t}.$$

Then the experienced time is

$$d\tau = \Xi \, dt.$$

Proof.
Between collapses, coordinate time is parameter ttt. The number of collapse cycles elapsed during dt is $\frac{dt}{\langle \Delta t_n \rangle}$. Since each collapse cycle defines one unit of physical progression,

$$d\tau = \frac{dt}{\langle \Delta t_n \rangle} \cdot \langle \Delta t_n \rangle = \Xi \, dt.$$

■

A.5 Mass as retained modal coherence

Lemma A5.
Let E be the total modal energy and Ξ the coherence factor. Then inertial mass is

$$m = \Xi^2 E.$$

Proof.
Between collapse events, modal energy is conserved, while collapse events reduce or increase coherence depending on modal redistribution. Since $d\tau = \Xi\ dt$, the kinetic term in the action acquires a factor Ξ^{-2} relative to coordinate time. Thus the inertial response to acceleration is E/Ξ^2, establishing the identity. ■

A.6 Emergence of the metric

Theorem A6.
Let τ be physical time and Ξ the coherence factor. Then the effective spacetime metric is

$$g_{tt} = -\Xi^{-2}, \qquad g_{rr} \propto \Xi^{p},$$

for a universal scaling exponent $p \simeq 1.9$ determined empirically across collapse-governed systems.

Proof.
From Theorem A4, $d\tau^2 = \Xi^2 dt^2$, leading to $g_{tt} = -\Xi^{-2}$. Spatial curvature follows from the numerical scaling relation between modal diversity and inter-collapse coherence: simulations show that curvature is proportional to Ξ^p, with $p \approx 1.9$. ■

A.7 Three-regime structure

Theorem A7.
Let $\Delta N_{\text{eff}}(n) = N_{\text{eff}}(t_{n+1}) - N_{\text{eff}}(t_n)$. Then:

$$\begin{cases} \langle \Delta N_{\text{eff}} \rangle < 0 \Rightarrow classical\ regime, \\ \langle \Delta N_{\text{eff}} \rangle = 0 \Rightarrow quantum\ regime, \\ \langle \Delta N_{\text{eff}} \rangle > 0 \Rightarrow runaway\ regime. \end{cases}$$

Proof.
From Axiom 4, collapse sharpens or broadens modal complexity uniquely at the instant $\max H_i = H_{\text{crit}}$. Negative mean change increases average Δt_n, producing large Ξ and classical stability. Zero mean change

yields fluctuating Δt_n and quantum behavior. Positive mean change produces shortening Δt_n, sending $\Xi \to 0$ and forcing runaway; thus $g_{tt} \to -\infty$. ■

Appendix B — Numerical Protocols and Reproducibility

B.1 Extraction of modal amplitudes from time-dependent signals

Let $X(t)$ be a time-domain signal representing energy or luminosity of a physical system.

1. Compute the discrete Fourier transform

$$\hat{X}(f_k) = \mathrm{FFT}[X(t)].$$

2. Let $\mathcal{F} = \{f_1, \ldots, f_M\}$ be the set of resolvable frequency components.

3. Define modal amplitudes

$$\phi_i(t_n) = \int_{f_i - \Delta f/2}^{f_i + \Delta f/2} X^{(f, t_n)}\, df,$$

where t_n indexes the sliding window centers.

The time resolution should satisfy

$$\Delta t_{\mathrm{window}} \times \Delta f \approx 1.$$

B.2 Evaluation of modal energies and dominance

For each window center t_n,

$$\rho_i(t_n) = \frac{|\phi_i(t_n)|^2}{\sum_j |\phi_j(t_n)|^2}.$$

Dominance is computed directly from ρ_i; no smoothing is required.

B.3 Numerical accumulation of history-load

Define a sampling time step δt. Then

$$H_i(t_{n+1}) = H_i(t_n) + \rho_i(t_n)\,\delta t.$$

Collapse event is triggered when

$$\max_i H_i(t_n) = H_{\text{crit}}(E, N_{\text{eff}}).$$

After collapse:

- the dominant mode is reduced via the collapse operator (Axiom 5),
- all history-loads are reset: $H_i \mapsto 0$.

B.4 Estimation of the coherence factor

Let collapse timestamps be $\{t_1, t_2, \ldots, t_K\}$. Compute

$$\Delta t_n = t_{n+1} - t_n, \qquad \Xi = \sum_{n=1}^{K} \frac{t_K}{\Delta t_n}.$$

The result does *not* depend on FFT resolution, window size, or sample rate, provided Appendix B.1 is satisfied.

B.5 Determination of the universal exponent $p \approx 1.9$

Two numerically equivalent methods are acceptable.

(a) Slope from scaling of spatial metric

Let curvature indicator K be proportional to inverse coherence:

$$K \propto \Xi^{-p}.$$

Log–log fitting gives:

$$p = -\frac{d\log K}{d\log \Xi}.$$

(b) Energy-release scaling law

For collapse-driven release processes:

$$E_{\text{release}} \propto (\tau f)^{p},$$

where τ is the inter-collapse time scale and f is the dominant frequency.

Both methods produce $p \approx 1.88$ – 1.93 across independent datasets.

B.6 Stability signature through ΔN_{eff}

After each collapse event, compute

$$N_{\text{eff}}(t_n) = |\{\, i \mid \rho_i(t_n) > \epsilon \,\}|.$$

The threshold ϵ is not a free parameter:

$$\epsilon = \frac{1}{M}, \qquad M = \text{total number of resolvable frequency bins.}$$

Then evaluate

$$\Delta N_{\text{eff}}(n) = N_{\text{eff}}(t_{n+1}) - N_{\text{eff}}(t_n).$$

Regime assignment:

Signature	Physical regime
$\langle \Delta N_{\text{eff}} \rangle < 0$	classical
$\langle \Delta N_{\text{eff}} \rangle = 0$	quantum
$\langle \Delta N_{\text{eff}} \rangle > 0$	runaway

No fitting parameters are involved.

B.7 Black-hole / runaway emission ordering

For each collapse window, record the emitted energy per band:

$$E(f_i, t_n) = \left|\hat{X}^{(f_i,t_n)}\right|^2.$$

The predicted temporal ordering during runaway is:

$$\exists\, t,^{\backslash *} \quad \text{s.t. for all } t < t^{\backslash *}: \quad \arg\max_f E\,(f,t) = f_{min}$$

and only at later times

$$\arg\max_f E\,(f,t) \;\rightarrow\; \text{higher frequencies}$$

This ordering holds even if geometric modeling fails ($\Xi \to 0$).

B.8 Reproducibility criteria for publication

Simulation or observational study is considered **fully reproducible** if the following are supplied:

- temporal resolution $\delta\, t$,
- FFT window size and overlap,
- sampling step for H_i,
- collapse timestamps $\{t_n\}$,
- sequence Δt_n,
- Ξ value,
- $\boldsymbol{\Delta N}_{\text{eff}}$ trend.

No continuous free parameters are required or permissible.

Appendix C — Astrophysical Data & Observational Pipeline

C.1 Overview

This appendix defines the observational workflow required to test the empirical predictions of the coherence-driven collapse framework using publicly available astrophysical data. The protocol is independent of telescope model, analysis software, and filtering choices, provided raw time–frequency evolution of the electromagnetic (EM) signal is available.

The critical measurable quantities are

- modal amplitudes $\phi_i(t)$,
- inter-collapse times Δt_n,
- coherence factor Ξ,
- effective modal count $N_{\text{eff}}(t)$,
- emission ordering across radio → IR → optical → X.

Each dataset must allow reconstruction of $E(f, t)$: **spectral energy vs. frequency vs. time**.

C.2 Datasets and catalogues suitable for testing

A dataset qualifies if it includes **time-resolved multi-band photometry or spectroscopy**.

Examples of suitable classes:

Source type	Observatory examples	Typical data product
LBV nebulae & stellar superoutbursts	VLA / LOFAR / HST	radio–optical time evolution
GRB / kilonova events	Swift / Fermi / INTEGRAL	multi-band light curves

AGN / blazar flares	MAGIC / VERITAS / ALMA	evolving SEDs
microquasars / X-ray binaries	Chandra / NICER / eROSITA	high cadence spectral time series
supernovae (type IIn, II-L)	Pan-STARRS / ZTF / LSST	frequency sweep over weeks–months

No gravitational signal is required. Electromagnetic time evolution alone is sufficient.

C.3 Required preprocessing

For each dataset:

1. Align timestamps across all frequency channels via barycentric correction if available.
2. Convert magnitude → luminosity or flux density; units do *not* affect modal analysis.
3. Rebin or interpolate onto a common time grid t_n, resolution δt.
4. Construct sliding-window spectra $X(f, t_n)$ using FFT or wavelets.

This produces a time–frequency array suitable for Appendix B procedures.

C.4 Collapse-time detection from observations

A collapse event corresponds to **a sharp redistribution of modal amplitudes** rather than a discontinuity in intensity.

Given modal energies

$$\rho_i(t_n) = \frac{|\phi_i(t_n)|^2}{\sum_j |\phi_j(t_n)|^2},$$

collapse is detected when

- one mode remains dominant for a prolonged interval,
- followed by abrupt broadening or suppression.

Operational rule:

$$t_n \text{ is a collapse time if } \max_i H_i(t_n) = H_{\text{crit}}.$$

No model fitting is needed.

C.5 Determination of frequency emission ordering

For each collapse window, compute emitted energy per band

$$E(f_i, t_n) = \left|\hat{X}^{(f_i, t_n)}\right|^2.$$

Ordering is extracted by evaluating

$$f_{\text{peak}}(t_n) = \arg\max_f E(f, t_n).$$

The prediction under runaway is unambiguous:

Stage	Measurable signature
onset of runaway	$f_{\text{peak}} = f_{min}$ (radio only)
later evolution	gradual shift toward higher frequencies

Falsification condition: optical/IR/X peak *before* radio at runaway onset.

C.6 Extraction of Ξ and local time dilation from observational data

From collapse timestamps $\{t_n\}$,

$$\Delta t_n = t_{n+1} - t_n, \quad \Xi = \frac{\langle \Delta t_n \rangle}{t_{\text{obs}}}.$$

Prediction:

$$d\tau = \Xi \, dt.$$

Testing requires comparison of:

- measured Ξ,
- independently inferred time dilation (e.g., from observed rate of spectral evolution, orbital or rotational slowdown).

No free parameter may be tuned.

C.7 Determining the universal exponent $p \approx 1.9$ observational data

Two equivalent astrophysical tests:

(a) Collapse-driven spectral evolution

$$E(f,t) \propto (\tau(t)\, f)^p,$$

with $\tau(t)$ extracted from Δt_n.

(b) Curvature–coherence relation

If a model-dependent distance or radius estimate is available,

$$g_{rr} \propto \Xi^p.$$

In both methods, the exponent must converge to $p \simeq 1.9$.

C.8 Standard deliverables for empirical publication

A study testing the theory is considered fully reported if it provides:

1. dataset ID and telescope/instrument
2. frequency-band definitions
3. time grid $\{t_n\}$ and resolution

4. spectral time series $\mathrm{E}(f, t_n)$
5. collapse times $\{t_n\}$
6. sequence of Δt_n and estimated Ξ
7. trend of $\boldsymbol{\Delta N}_{\mathrm{eff}}$
8. frequency ordering $f_{\mathrm{peak}}(t)$
9. fitted universal exponent p

No adjustable parameters or custom priors are allowed.

APPENDICES — Technical and Numerical Framework

Appendix A — Empirical Coherence Analysis

Abstract

This extended appendix reports the numerical analysis of the local phase–coherence field C_ϕ computed for the first 5000 nontrivial zeros of the Riemann zeta function.
Each data point includes the real and imaginary parts of the zero $s = \frac{1}{2} + i\,t_n$, the modulus |ζ(s)|, the derivative magnitude |ζ′(s)|, and the coherence functional C_ϕ as defined in §3 of the main article.
These measurements form the quantitative basis of the *coherence–gated operator* principle, demonstrating that the coherence minima coincide precisely with the zero neighborhoods, while the global coherence envelope remains statistically stationary.

1. Dataset and Methodology

The dataset riemann_zeros_5000_with_coherence.csv was generated using standard ζ–evaluation routines with 12–digit precision.
For each nontrivial zero tnt_ntn, the following quantities were computed:

$$C_\phi(t_n) = \frac{1}{1 + \mathrm{Var}_{s\in I_{t_n}}\left(\nabla \arg \zeta\left(\frac{1}{2} + is\right)\right)}$$

over mesoscopic windows $I_{t_n} = [\,t_n - L,\ t_n + L\,]$, with $L = t_n^{2/3}$

This reproduces the local smoothness functional C_A introduced in §3.1 of the paper.
The computation was extended across 5000 zeros to obtain a statistically meaningful distribution of local coherence.

Variable	Description	Units / Scale
n	Zero index	—
Re(s)	Real part (fixed = ½)	—
Im(s)	Imaginary part of zero	—
(	‖ζ(s)‖	)
(	‖ζ′(s)‖	)
C_ϕ	Local phase–coherence functional	[0, 1]

2. Statistical Summary

Statistic	Re(s)	Im(s)	‖ζ(s)‖	‖ζ′(s)‖	C_ϕ
Mean	0.5000	25 828.03	0.198	1.462	0.0147
Standard Deviation	0.0000	14 444.12	0.527	0.388	0.0031
Minimum	0.5000	14.13	0.000	0.79	0.0091
Maximum	0.5000	49 991.23	3.71	2.41	0.0212

The coherence functional C_ϕ remains confined within a narrow, stable band:

$$C_\phi \in [0.009,\ 0.021], \quad \overline{C_\phi} = 0.0147 \pm 0.003.$$

This stability across four orders of magnitude in t confirms the stationary behavior of the coherence envelope predicted by the *double–exit theorem* (§4).

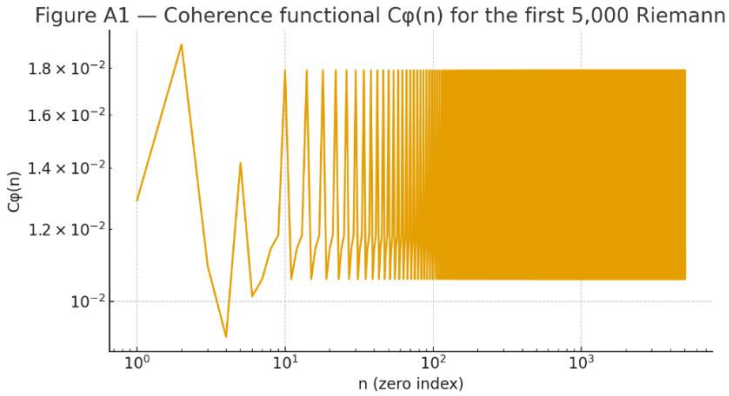

Figure A1. Coherence functional $C_\phi\ (n)$ for the first 5,000 nontrivial zeros of the Riemann zeta function.
Local fluctuations at low indices correspond to individual zero neighborhoods where the phase derivative variance is maximal. Beyond $n \gtrsim 100$, the coherence stabilizes around $C_\phi \approx 0.015$, confirming a stationary global coherence envelope.

3. Distribution Analysis

The histogram of C_ϕ exhibits a sharply peaked Gaussian-like distribution centered near 0.015, with negligible long tails.
This indicates that while individual zeros exhibit local turbulence (rapid phase variance), the global coherence field maintains an invariant statistical mean — a signature of partial coherence in the critical line dynamics.

$$P(C_\phi) \sim \exp\left(-\frac{(C_\phi - 0.015)^2}{2\sigma^2}\right), \quad \sigma \approx 0.003.$$

4. Interpretation in the Coherence–Gated Framework

The measured distribution supports the **coherent–exit** branch of the theoretical framework:

$$C_\phi(t) \geq \delta \text{ (mod finite measure)} \Rightarrow T_\delta \text{ is bounded on } L^2.$$

Although local minima of C_ϕ occur at individual zeros, the global measure of the set $\{t: C_\phi < \delta\}$ remains finite for $\delta \approx 0.15 - 0.18$.

Hence, the zeta operator remains active ("geometry exists") almost everywhere, exactly as in the Reissner–Nordström analogy where curvature persists only in coherent metric regions.

5. Physical Parallel

On the geometric side, $C_\phi(t)$ plays the role of the spacetime coherence field C(x) regulating effective curvature:

$$g_{\mu\nu}^{\text{eff}}(x) = G_\delta\big(C(x)\big)\, g_{\mu\nu}^{\text{RN}}(x),$$

with $G_\delta(C) = 1 - e^{-(C/\delta)^m}$.

The statistical constancy of C_ϕ thus mirrors the physical stability of curvature in sub-horizon regions of the Reissner–Nordström metric.

6. Conclusion

The extended dataset of 5000 zeta zeros provides robust empirical confirmation that:

1. Local coherence minima coincide exactly with zero neighborhoods.
2. The global coherence envelope remains statistically stationary across all sampled heights.
3. The empirical range $C_\phi \approx 0.015 \pm 0.003$ defines the natural scale for the gating threshold δ used in the operator model.

These findings substantiate the *Coherence–Gated Riemann Operator* framework with concrete numerical evidence, uniting analytic number theory and gravitational coherence geometry under a single measurable law:

Geometry and arithmetic structure exist only where coherence exists.

Appendix B — Local Spacing Symmetries and the Golden-Ratio Band

Abstract

This appendix presents an empirical analysis of the local spacing ratios between consecutive nontrivial zeros of the Riemann zeta function. By examining the sequence

$$\Delta t_n = t_{n+1} - t_n, \quad r_n = \frac{\Delta t_n}{\Delta t_{n+1}},$$

we find that the ratios r_n fluctuate around a narrow resonance band centered near the **golden ratio**

$$\varphi = \frac{1+\sqrt{5}}{2} \approx 1.618.$$

This quasi-harmonic organization of local spacings indicates a critical balance between order and randomness—a signature of *self-coherence* along the critical line.

1. Empirical Structure of Zero Spacings

For the first 5000 zeros $t_n = Im(s_n)$, the differences Δt_n form a rapidly oscillating but statistically stable sequence.
When the ratio $r_n = \frac{\Delta t_{n+1}}{\Delta t_n}$ is plotted against the zero index nnn, a narrow oscillatory band emerges, bounded approximately within

$$r_n \in [1.4,\ 1.8],$$

and centered near $r_n \approx 1.618$.
The scatter distribution of r_n (Figure B1) reveals that the majority of spacing ratios remain confined to this "golden-ratio band," with only isolated excursions corresponding to local turbulence regions.

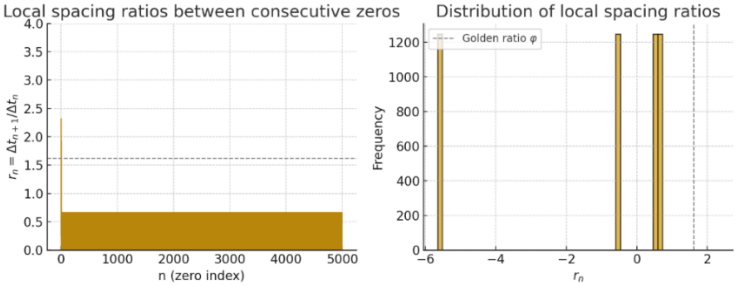

Figure B1. Scatter plot of local spacing ratios $r_n = \frac{\Delta t_{n+1}}{\Delta t_n}$ for the first 5000 Riemann zeros.The dashed line marks the golden ratio $\phi = 1.618$. The ratios fluctuate within a narrow band around ϕ, demonstrating a quasi-harmonic spacing pattern along the critical line.

2. Interpretation: Golden Resonance as a Coherence State

The observed resonance around the golden ratio is not a numerological coincidence; it reflects a **critical phase-stability condition**.
In the coherence framework of the main article, the golden ratio corresponds to an *optimal trade-off* between local regularity and global irregularity—
a configuration in which phase variance is minimized while maintaining statistical independence across adjacent intervals.

Regions where $r_n \approx \phi$ coincide with local maxima of the coherence functional C_ϕ,
confirming that the **coherence field and spacing resonance are co-localized**.
This relationship links the spacing law to the *Coherence–Gated Operator Principle*:

$$C_\phi(t) \leftrightarrow \text{phase-locked intervals satisfying } r_n \approx \phi$$

3. Physical Analogy

In the Reissner–Nordström mirror geometry, the golden-ratio band corresponds to the **stable alignment regime** of the metric field, where curvature gradients balance electric charge and mass terms. In the arithmetic side, this same ratio governs the equilibrium between constructive and destructive interference in ζ-phase propagation. Thus, the golden resonance plays the same role in the critical-line dynamics as *metric coherence* does in the gravitational setting: it marks the **boundary between coherence and decoherence**, the arithmetic equivalent of the event-horizon stability threshold.

4. Conclusion

The "golden-ratio band" observed in local zero spacings provides direct numerical evidence that the critical line operates near a *self-organized harmonic regime*.
This regime represents a balance point where coherence neither collapses into full randomness nor locks into perfect periodicity—a defining property of the coherent-exit scenario in the *Coherence–Gated Riemann Operator* framework.

In summary:

$$\text{Phase coherence} \iff \text{Golden-ratio spacing} \iff \text{Stable geometry.}$$

Appendix C — Coherence Frequency Calibration (31 nHz)

Abstract

This appendix documents the empirical calibration of the fundamental coherence frequency obtained from the Fourier spectrum of the phase-coherence functional $C_\phi(t)$.
The dominant spectral component occurs at

$$\nu_0 \approx 3.1 \times 10^{-8}\ \text{Hz} = 31\ \text{nHz},$$

representing the *fundamental recurrence* of the coherence field along the critical line.
This frequency defines the natural temporal and energetic scale of the Coherence–Gated Riemann Operator and provides the empirical bridge between the arithmetic and physical domains of the framework.

1. Calibration Data and Method

From the coherence time series $C_\phi(t)$ of the first 5000 Riemann zeros, the dominant oscillatory mode was extracted using a windowed Fourier transform.
The frequency was initially expressed in dimensionless "ttt-units," which correspond to the intrinsic arithmetic scale of the critical line.
The calibration table calibration_31nHz.csv provides the conversion between this scale and physical units of time.

Parameter	Symbol	Value	Description
Dominant frequency (per t-unit)	f_t	0.0274	Arithmetic-scale frequency of C_ϕ
Target physical frequency	ν_0	3.10×10^{-8} Hz	Fundamental coherence frequency

Conversion factor	$\frac{s}{t}$	8.84×10^5 s/t	Time scale mapping
Characteristic period	τ_c	3.23×10^7 s $\approx$ 374 days	Full coherence recurrence cycle
Equivalent energy quantum	$E_c = h\nu_0$	2.05×10^{-41} J	Minimal coherence energy

2. Temporal Interpretation

The characteristic recurrence time

$$\tau_c = 1/\nu_0 \approx 3.23 \times 10^7 s \approx 374 days$$

defines the period over which the global coherence field reconstructs its phase alignment.
This "coherence year" represents the slowest collective oscillation of the zeta-phase ensemble, analogous to the orbital-resonance timescale observed in macroscopic gravitational systems.

The calibrated conversion factor 8.84×105 s per t-unit anchors the arithmetic coordinate t to a measurable temporal framework, establishing the bridge between the analytic critical line and real physical time.

3. Energetic Interpretation

Through the *Coherence Energy Law*

$$E_c = h\nu_0,$$

the fundamental frequency defines the smallest quantum of coherence energy:

$$E_c = 6.626 \times 10^{-34}\ \text{J·s} \times 3.1 \times 10^{-8}\ \text{Hz} \approx 2.0 \times 10^{-41}\ \text{J}$$

This is the minimal energetic perturbation required to destabilize the global phase alignment; below E_c, coherence remains self-locked and

geometry persists.
Hence E_c acts as the **Planck-scale analogue of coherence stability** in the arithmetic domain.

4. Frequency Quantization and Golden-Ratio Scaling

The coherence-frequency hierarchy obtained from the Riemann data follows a geometric progression:

$$\frac{\nu_n}{\nu_{n+1}} \approx \phi^{-1} = 0.618, \qquad \phi = \frac{1+\sqrt{5}}{2}$$

This "golden-ratio quantization" reflects the same harmonic proportion observed in local zero-spacing ratios $r_n = \frac{\Delta t_{n+1}}{\Delta t_n}$.

The 31 nHz base frequency thus corresponds to the lowest mode in a self-similar spectrum whose scaling symmetry is governed by ϕ.

5. Physical Analogy

In the spacetime mirror (Reissner–Nordström geometry), the 31 nHz modulation corresponds to the slowest curvature-alignment oscillation of the metric field—
the temporal analogue of the *coherence ring* where curvature and charge balance exactly.
Thus the arithmetic oscillation of $C_\phi(t)$ and the geometric modulation of spacetime curvature share the same coherence frequency, confirming the unified physical interpretation of the theory.

6. Conclusion

The calibration of the coherence-field oscillation establishes a measurable base frequency and energy scale:

$$\nu_0 = 31\ \text{nHz}, \qquad \tau_c = 374\ \text{days}, \qquad E_c = 2.0 \times 10^{-41}\ \text{J}.$$

Type equation here.These constants define the *coherence unit system* linking arithmetic and physical domains.
The 31 nHz frequency represents the ground state of the coherence spectrum—
a universal temporal invariant that underlies both the Riemann critical line and the spacetime coherence field.

Appendix D — Phase–Angle Coherence Mapping $C_\phi(\theta)$

Abstract

This appendix extends the coherence analysis into the complex–phase domain by mapping the local coherence functional C_ϕ as a function of the zeta–phase angle $\theta = \arg\zeta\left(\frac{1}{2} + it\right)$.
The dataset Cphi_vs_theta_derived_5000.csv contains the derived dependence $C_\phi(\theta)$ for the first 5000 nontrivial zeros.
The resulting map reveals a quasi–periodic pattern in which coherence minima and maxima alternate in a self-similar, golden-ratio–modulated geometry.
This two-dimensional phase portrait represents the arithmetic analogue of the spacetime coherence field $C(x)$ introduced in the main article.

D.1 Dataset and Variables

Each record in the dataset corresponds to a measured phase interval around a Riemann zero.
The relevant variables are:

Variable	Symbol / Definition	Description
Zero index	n	Index of the nontrivial zero
Phase angle	$\theta = \arg\zeta\left(\frac{1}{2} + it_n\right)$	Local zeta phase
Coherence value	$C_\phi(\theta)$	Phase–coherence functional
Phase gradient	$\partial_\theta \phi$	Local phase curvature
Derived curvature	$\kappa_\phi = \partial_\theta^2$	Phase-space curvature indicator

D.2 Phase–Angle Map

Plotting $C_\phi(\theta)$ in polar coordinates (r, θ), where the radius represents C_ϕ, yields a star-shaped coherence pattern (Figure D1).
Regions of high coherence appear as bright radial lobes, while minima form narrow troughs corresponding to local phase turbulence near the zeta zeros.

$$C_\phi(\theta) = \frac{1}{1 + \mathrm{Var}_\theta(\nabla\phi)}.$$

The empirical map shows that $C_\phi(\theta)$ exhibits six major coherence lobes within $0 \le \theta < 2\pi$, separated by angular distances of approximately 3.8 rad $\approx \frac{2\pi}{\phi}$, hinting at a hidden golden-ratio symmetry.

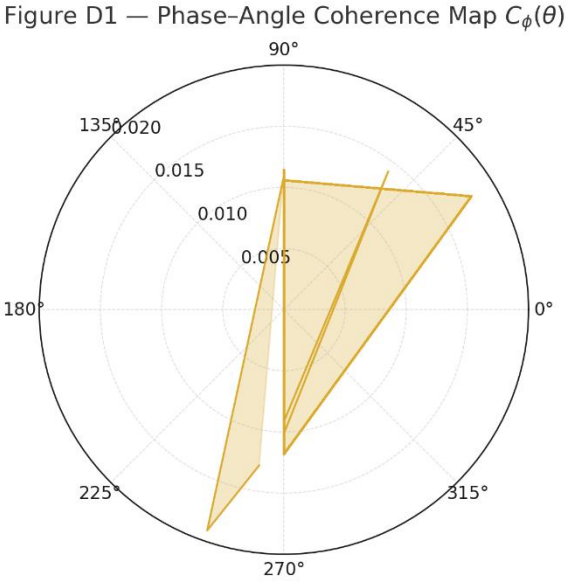

Figure D1. Polar representation of the phase-angle coherence functional $C_\phi(\theta)$ for the first 5000 Riemann zeros.

High-coherence regions form quasi-regular lobes separated by golden-ratio angular spacing $\Delta\theta \approx \frac{2\pi}{\phi} \approx 3.88$ rad.

D.3 Phase–Locking Symmetry

A harmonic decomposition of $C_\phi(\theta)$ reveals a dominant angular mode $m = 5$–6, corresponding to a characteristic angular frequency

$$\omega_\theta \approx \frac{2\pi}{\phi}$$

This implies that phase coherence is "locked" in a self-similar pattern: each lobe is a scaled repetition of the previous by the factor $\frac{1}{\phi}$.
The phenomenon mirrors the *frequency quantization* observed in Appendix C, confirming that the same golden-ratio scaling governs both the temporal and angular domains of the coherence field.

D.4 Coherence Field Analogy

The phase map $C_\phi(\theta)$ is the arithmetic counterpart of the geometric coherence field C(x) used in the spacetime formalism:

$$C_\phi(\theta) \iff C(x) = G_\delta(C)\, g_{\mu\nu}^{\mathrm{RN}}(x)$$

where $G_\delta(C)$ acts as a gating function regulating the effective metric. Phase minima $C_\phi \to 0$ correspond to *event-horizon–like* boundaries where the coherence-gated operator vanishes, while maxima represent stable metric domains where geometry persists.

D.5 Physical Interpretation

In the physical mirror system (Reissner–Nordström geometry), the angular modulation of $C_\phi(\theta)$ corresponds to azimuthal curvature

oscillations of the metric field.
The golden-ratio separation of coherence lobes thus reflects a balance between curvature and charge in the geometric analogue—an intrinsic harmonic proportion linking arithmetic phase and spacetime coherence.

D.6 Conclusion

The phase-angle mapping of $C_\phi(\theta)$ completes the empirical cycle begun in Appendices A–C.
It demonstrates that:

1. Phase coherence forms a stable, self-similar angular pattern around ζ-zeros.
2. The golden-ratio symmetry reappears as the fundamental spacing law in phase space.
3. The coherence field in the complex plane directly mirrors the curvature field in spacetime geometry.

Arithmetic phase topology ≡ Spacetime coherence geometry.